NASA TN D-1300

TECHNICAL NOTE
D-1300

EFFECTS OF SIMULATED RETROROCKETS ON THE AERODYNAMIC CHARACTERISTICS OF A BODY OF REVOLUTION AT MACH NUMBERS FROM 0.25 TO 1.90

By Victor L. Peterson and Robert L. McKenzie

Ames Research Center
Moffett Field, Calif.

NATIONAL AERONAUTICS AND SPACE ADMINISTRATION
WASHINGTON May 1962

NATIONAL AERONAUTICS AND SPACE ADMINISTRATION

TECHNICAL NOTE D-1300

EFFECTS OF SIMULATED RETROROCKETS ON THE AERODYNAMIC CHARACTERISTICS OF A BODY OF REVOLUTION AT MACH NUMBERS FROM 0.25 TO 1.90

By Victor L. Peterson and Robert L. McKenzie

SUMMARY

Force and moment coefficients are presented for a semiellipsoid body shape which had four simulated retrorockets on the forward flat face operating countercurrent to subsonic and supersonic airstreams. Experiments were performed at stream Mach numbers ranging from 0.25 to 1.90 and the retrorockets, which were simulated by expanding cold air through converging-diverging nozzles, were operated over a range of chamber pressures to 1000 psia. Model angle of attack was varied from 0° to 10°.

At all stream Mach numbers the force and moment coefficients exhibited a strong dependence on the ratio of jet to free-stream total pressures. The axial force, exclusive of retrothrust, was of considerably lower magnitude with the jets on than with the jets off. The large effect of the jets on the axial force caused the total decelerating force (drag plus retrothrust) to be nearly equal to the retrothrust alone. The pitching moments underwent erratic variations with changing ratio of jet to free-stream total pressures, but for a wide range of test conditions, they were of smaller magnitude with the jets on than with the jets off. At zero angle of attack and at low supersonic speeds the bow shock wave was observed to be in stable positions close to the model at low values of the jet to free-stream total pressure ratio, far upstream from the model at intermediate values of the pressure ratio, and in intermediate positions at high pressure ratios. The range of pressure ratios for which the bow shock was in the extended position decreased with increasing Mach number until at the highest Mach number the bow shock moved directly from the close position to the intermediate position. It appears that this bow shock phenomenon is peculiar to configurations having several nozzles in close proximity.

INTRODUCTION

The design of a vehicle required to execute a soft landing upon returning from a mission outside the atmosphere introduces a number of problems. Because of the large expenditure of energy required to overcome the earth's gravitational attraction in the launch phase of the

mission, it is imperative that the device used to decelerate and land the vehicle at the termination of a round-trip mission be as light in weight as possible. One such method would be to let aerodynamic drag reduce the velocity as much as possible and then use retrorockets to perform the terminal braking.

Some calculations were made to determine the interrelationships between various parameters of interest, such as fuel weight, velocity, drag coefficient, deceleration, and time of retrorocket operation. The analysis was simplified for this terminal phase by considering only vertical descents with continuous rocket motor operation; no consideration was given to stabilization or control of the vehicle. The vehicle chosen had a ratio of weight to reference area of 150 lb/sq ft prior to firing the retrorocket. The rocket motor had an area ratio corresponding to an exit Mach number of 3.5 and a chamber pressure of 500 psia, and was assumed to burn a fuel with a characteristic velocity of 5000 ft/sec. The results of this simplified analysis with these assumptions were quite sensitive to the value of drag coefficient assumed for the vehicle. For instance, the calculated fuel weights increased by as much as 40 percent as the drag coefficient was reduced from 0.8 to 0. Since the calculations indicated that the landing maneuver could be accomplished with fuel weights ranging from 10 to 20 percent of the initial vehicle weight for a variety of initial conditions, including velocities up to 1000 ft/sec, a further study of the aerodynamic forces and moments experienced by the vehicle during operation of the retrorocket would be of some interest.

A 5 6 8

The purpose of this report is to present measured forces and moments on a model having four simulated retrorockets operating countercurrent to subsonic and supersonic airstreams. The tests conducted in the Ames 6- by 6-Foot Supersonic Wind Tunnel were designed to be exploratory in nature; hence the selection of the configuration was somewhat arbitrary. The tests were performed at Mach numbers from 0.25 to 1.90 and the retrorockets, which were simulated by expanding cold air through converging-diverging nozzles, were operated over a range of chamber pressures to 1000 psia. Model angle of attack was varied from 0° to 10° to determine whether asymmetric flow could lead to stability and control problems when retrorockets are used.

Results of other investigations involving jet flow countercurrent to supersonic streams are presented in references 1 and 2.

SYMBOLS

A_e nozzle exit area

A_{ref} coefficient reference area, $\frac{\pi D^2}{4}$

C_A axial force coefficient, $\frac{\text{axial force}}{q_\infty A_{ref}}$

C_D drag coefficient, $\frac{\text{drag}}{q_\infty A_{ref}}$

C_m pitching-moment coefficient referred to center of model face, $\frac{\text{pitching-moment}}{q_\infty L A_{ref}}$

C_N normal-force coefficient, $\frac{\text{normal force}}{q_\infty A_{ref}}$

C_p pressure coefficient, $\frac{p - p_\infty}{q_\infty}$

C_T retrothrust coefficient, $\frac{\text{jet retrothrust}}{q_\infty A_{ref}}$

D model maximum diameter

L length of body including portion deleted by sting mounting

M Mach number

p static pressure

p_t total pressure

q dynamic pressure, $\frac{\gamma}{2} pM^2$

R radius of model face

x,r,θ cylindrical coordinates defined by figure 1(b)

α model angle of attack

γ ratio of specific heats

Subscripts

b model afterbody

e nozzle exit

f model face

j	jet
∞	free stream
2	pressure after exit from a normal shock

MODEL AND APPARATUS

Model Description

The model shape was a semiellipsoid with the 5.0-inch-diameter flat face forward. The semimajor axis of the model was 7.5 inches. Four nozzles in the model face were spaced 90° apart on a 2.12-inch-diameter circle. Each nozzle had a throat diameter of 0.20 inch, a conical converging section with a semivertex angle of 30°, and a conical diverging section with a semivertex angle of 15°. The exhaust cones were extended to a length sufficient for a nozzle-exit Mach number of 3.0 based upon one-dimensional flow considerations. All nozzles were connected to a common plenum chamber located within the model. The model was sting mounted in the wind tunnel in the manner shown in figure 1(a). A dimensional sketch of the complete model is presented in figure 1(b), and details of the nozzles are presented in figure 1(c).

Pressure orifices of 0.030-inch diameter were installed flush with the model surface at 87 positions on the model face and at 62 positions on the body. The exact locations of the orifices are tabulated in figure 1(b).

The model used in this investigation was intended to represent a reentry vehicle that would employ rocket braking for terminal recovery after aerodynamic braking had slowed the descent to low supersonic speeds. Rather arbitrary choices were made, however, regarding the details of the configuration. Multiple nozzles were used with a ratio of nozzle throat to vehicle reference area of 0.0064 which was considered representative of a possible full-scale vehicle. In terms of a vehicle weighing 10,000 pounds with a reference diameter of 8 feet, this area ratio corresponds to maximum values of retrothrust ranging from 35,000 to 70,000 pounds for motor chamber pressures ranging from 500 to 1,000 psia, respectively.

Apparatus and Instrumentation

The simulated retrorockets were supplied by a high-pressure source of dry air which was controlled by two remotely operated pneumatic valves. Air was piped to the model plenum chamber through a hollow streamlined strut and sting as shown in figure 1(a). Pressure in the plenum chamber was measured by a probe (see fig. 1(b)) connected to two high-accuracy

Bourdon-tube dial gages of different pressure ranges. Plenum chamber temperature was measured by an iron-constantan thermocouple (see fig. 1(b)) connected to an automatic recording potentiometer. Model surface pressure orifices were connected to manometer tubes filled with tetrabromoethane (specific gravity = 2.92 at 80° F). Liquid column heights were photographically recorded. Shadowgraph apparatus was used to provide photographs of the flow field in the vicinity of the model.

TESTS AND PROCEDURE

Ranges of Test Variables

Tests were conducted at free-stream Mach numbers of 0.25, 0.65, 0.80, 1.50, 1.70, and 1.90. Free-stream total pressure was set at 12, 14, and 16 psia for $M_\infty = 0.25$ and at 5, 7, and 9 psia for all other free-stream Mach numbers. Free-stream Reynolds numbers varied from 1.3 to 2.6 million per foot for these ranges of pressures and Mach numbers. At Mach numbers of 0.65 and 1.70 the model was positioned only at zero angle of attack but for all other Mach numbers the angles of attack were 0°, 5°, and 10°. For each set of free-stream conditions and model attitude the nozzle plenum chamber pressure was varied up to 1000 psia. Operation over this pressure range resulted in combined weight flows through the four nozzles of between 0 and about 3.1 pounds per second. Shadowgraphs were taken at every data point. A special series of shadowgraphs was made, without accompanying model pressure distribution data, at free-stream Mach numbers of 1.28, 1.50, and 1.70 to investigate more thoroughly the flow field around the model.

Data Reduction

Pressure coefficients were computed from the individual pressure measurements made on the model surface. Force and moment coefficients for the model face were obtained from integrations of the pressure coefficients over the model face excluding the nozzle exits. For the model body, the force and moment coefficients were obtained from integrations of the pressure coefficients over all the body except that portion deleted by the sting mounting (see fig. 1(b)). The total force and moment coefficients for the model were then obtained from a summation of the face and body contributions. To perform the various integrations it was necessary to extrapolate certain quantities; for example, because of physical limitations, no orifices could be located on the model face at values of $r_f/R = 1.0$. Therefore, to provide consistent results for the integrated coefficients, the necessary values of pressure coefficient were obtained mathematically by passing a second degree curve through the three experimental data points nearest the unknown value and extrapolating to the desired model location.

The retrothrust coefficient, C_T, was based on free-stream dynamic pressure and model reference area to allow direct magnitude comparisons with other force coefficients. Retrothrust coefficients were calculated by means of the following equation:

$$C_T = \frac{4\left(\frac{A_e}{A_{ref}}\right)\left[\left(\frac{p_{t_j}}{p_{t_\infty}}\right)\left(\frac{p_e}{p_{t_j}}\right)\left(1 + \gamma_j M_j^2\right) - \frac{p_\infty}{p_{t_\infty}}\right]}{\left(\frac{q_\infty}{p_{t_\infty}}\right)}$$

A5688

The ratio (p_e/p_{t_j}) and the jet Mach number M_j appearing in the above equation were determined from equations based on the assumption of one-dimensional isentropic flow.

Accuracy

The free-stream Mach numbers quoted are nominal values and are accurate within ± 0.04. However, each set of data at a given Mach number, angle of attack, and free-stream pressure is consistent in Mach number within ± 0.02. Pressure measurements on the model surface are accurate within ± 0.02 psia. With the jets off, a comparison of the pressure coefficients at the center of the model face with those calculated for free-stream stagnation conditions showed differences amounting to 8.0 percent at the lowest Mach number ($M_\infty = 1.25$) diminishing to 1.3 percent at the highest Mach number ($M_\infty = 1.90$). This relatively large error at the lower Mach numbers, where small differences between total and static pressures must be measured, was much greater than the scatter in values of local coefficient. The gage used to indicate the pressure measured by the probe within the nozzle plenum chamber was accurate to ± 1.5 percent throughout the pressure range. Nozzle exit Mach number was measured and found to vary between 3.04 and 3.06 across the exit planes. Boundary-layer thicknesses inside the nozzles at the exits were negligible compared to the exit diameter. No adjustments of model angle of attack or angle of sideslip were made for wind-tunnel stream inclinations which are known not to exceed $\pm 0.3^\circ$. Body force errors due to the presence of the sting were found from pressure measurements to be negligible compared to other model forces.

RESULTS AND DISCUSSION

A cursory examination of the force and moment coefficients for the model at zero angle of attack showed abrupt and seemingly erratic variations of these parameters with the ratio of jet to free-stream total pressure. This effect was particularly evident at supersonic free-stream Mach numbers. Further study showed that rapid changes in certain coefficients appeared to be linked with the behavior of the bow shock wave and mutual interactions of the jets observed in shadowgraphs taken throughout the tests. Therefore, since the flow over the model was dictated to some extent by interactions between the jets themselves and the jets and free stream, the flow phenomena ahead of the model are described prior to interpretation of the resulting pressure and integrated force and moment coefficients.

Bow Shock and Interference Phenomena

Tests of the model at zero angle of attack and at some supersonic Mach numbers revealed abrupt changes in the bow shock standoff distance at certain jet pressures. Shadowgraphs of this phenomenon are presented in figure 2 for the model at zero angle of attack and for a free-stream Mach number of 1.50. The photographs of figure 2 show that the bow shock assumed a position close to the model at low jet pressures, moved far upstream from the model at intermediate jet pressures, and then returned to an intermediate position at high jet pressures. For these particular free-stream conditions ($M_\infty = 1.50$, $p_{t_\infty} = 7$ psia) the ratio of jet to free-stream total pressures at which the bow shock moved abruptly away from the model was about 57.2 This is evidenced by figures 2(d) and 2(e) which show the bow shock at two different positions for this jet pressure. Measurements, obtained from shadowgraphs, of the variation of bow-shock position with jet to free-stream total pressure ratio are presented in figure 3 for free-stream Mach numbers of 1.50, 1.70, and 1.90. These results show that at the highest free-stream Mach number the bow shock moved directly from the close to the intermediate position. The results in figure 3 also indicate that bow shock standoff distance was a function of the total pressure ratio, p_{t_j}/p_{t_∞}, rather than individual pressure magnitudes.

A detailed analysis of the circumstances believed to be responsible for the unusual behavior of the bow shock wave is presented in the appendix. Also included therein are results of calculations made using theory for free jets exhausting into still air to obtain a correlation with the data of this investigation.

Pressures on the Model Surface

The force and moment coefficients obtained from integrations of the pressures on the model surface are of primary interest. For this reason, only representative samples of the distributions of pressure on the model with and without the simulated retrorockets operating are presented.

The effects of the retrojets on the model pressure coefficients at subsonic speeds are typically illustrated in figure 4 for a Mach number of 0.65 and an angle of attack of 0°. The data of figure 4 show a large difference between the jet-off and jet-on distributions of pressures, but the pressures on the model were relatively independent of jet total pressure for total pressures between 300 and 1000 psia. The results of figure 4(a) show that the jets prevented attainment of free-stream stagnation pressure on the model face; in fact, the pressures on the model face with the jets on were quite near free-stream static pressure. For the model body (fig. 4(b)), with the jets off, the pressure distributions were indicative of separated flow. This observation was substantiated by shadowgraphs. With the jets on, however, the pressures at the rear of the body recovered to near free-stream static pressure and there was no evidence of flow separation in the shadowgraphs. It might be conjectured that the highly turbulent mixture of tunnel flow and turned jet flow was attached over the rearward portion of the body.

Typical effects of the retrojets on the model pressure coefficients at supersonic speeds are illustrated in figure 5 for a Mach number of 1.70 and an angle of attack of 0°. The data of figure 5 show dependence on jet total pressure, over a wider range, than did the subsonic results of figure 4. The dependence of model face pressure distributions on jet total pressure shown in figure 5(a) results primarily from the effects of total pressure ratio p_{t_j}/p_{t_∞} on the position of the bow shock wave which are discussed in the appendix. On the model body, effects of the jets on the pressure distributions at supersonic speeds (fig. 5(b)) were encountered with the bow shock wave in the extended position. The flow over the model body apparently was quite similar with the jets on or off, though, since the pressures were nearly the same in magnitude and distribution. Shadowgraphs for these conditions indicated attached flow over most of the body.

Force and Moment Coefficients

All of the force and moment coefficients were obtained from integrations of the pressure coefficients and thus exclude effects due to frictional forces acting on the model surface. It should also be remembered that retrothrust from the simulated rockets contributed to these coefficients only to the extent that the presence of the jets altered the pressures over the model surface.

The coefficients of axial force are presented in figure 6 as a function of the jet to free-stream total pressure ratio. The contributions of the model face and model body are presented separately in figures 6(a) and 6(b), respectively, and the sum of the two contributing model components is presented in figure 6(c). The results of figure 6(a) for the model face show the values of the coefficient obtained with the nozzles operating to be considerably lower than those obtained with no nozzle flow. In fact, negative values of C_{A_f} prevailed for a wide range of test conditions. Values of this coefficient were somewhat higher over the ranges of total pressure ratio for which the bow shock wave was in the extended position; for example, at $M_\infty = 1.50$, $\alpha = 0^\circ$, $65 < p_{t_j}/p_{t_\infty} < 110$. The component of axial force coefficient contributed by the model body showed more dependence on jet operation at subsonic Mach numbers than at supersonic Mach numbers (see fig. 6(b)). Also, it is shown that movement of the bow shock to the extended position caused the body axial force coefficient to be reduced. This contrasts with the increase in axial force coefficient of the model face measured for the same conditions; for example, compare results of figures 6(a) and 6(b) for $M_\infty = 1.50$. The axial force coefficients for the complete model (fig. 6(c)) generally follow the trends with pressure ratio established by the model face.

The normal-force coefficients, which are simply the pressure loads on the model body, are presented in figure 7 as a function of the jet to free-stream total pressure ratio. These coefficients displayed erratic variations with pressure ratio and angle of attack. However, it is noted that while the normal forces were positive at positive angles of attack for $M_\infty = 0.80$, they were predominantly negative at supersonic Mach numbers. It is believed that the negative normal forces at supersonic speeds probably resulted from longer runs of attached flow on the lower surface of the body than on the upper surface when the model was at angle of attack. Shadowgraphs for the jet-off conditions substantiate this.

The pitching-moment coefficients resulting from pressure loads on the model are presented in figure 8 as a function of the jet to free-stream total pressure ratio. The pitching-moment coefficients for the model face (fig. 8(a)) arise from asymmetric axial loading. Thus, they are independent of the model moment reference center, provided it lies on the longitudinal axis of the model. A measure of the symmetry of the model face and of the nozzle flows is afforded by the insignificant pitching moments of the model face at zero angle of attack. The variation of pitching moment of the model face with angle of attack was positive (static instability) at all Mach numbers with the jets both off and on. Turning the jets on to low values of the pressure ratio p_{t_j}/p_{t_∞} resulted in large destabilizing effects. At subsonic speeds, these large effects persisted throughout the entire range of pressure ratios. However, at supersonic speeds they diminished with increasing pressure ratio until at the highest pressure ratios small stabilizing effects existed. The pitching-moment coefficients for the model body are presented in figure 8(b). In most cases these pitching-moment results reflected trends consistent with the normal-force results; however, in some cases the

asymmetric axial loading predominated. The total pitching-moment coefficients for the model are presented in figure 8(c). The variations of this parameter with pressure ratio were quite erratic but were repeatable at any given set of conditions. In general, these results show that the nozzles could be operated over a wide range of pressure ratios without the pitching-moment coefficients exceeding values for jets-off conditions.

The total decelerating force consists of model drag plus retrothrust. This quantity could not be measured directly but an indication of its magnitude, exclusive of skin-friction drag, was obtained by adding drag coefficients due to integrated pressure loads to calculated retrothrust coefficients based on free-stream dynamic pressure and model reference area. Curves showing the dependence of the calculated retrothrust coefficient on free-stream Mach number and jet to free-stream total pressure ratio are presented in figure 9 for the model of this investigation. Of note is the fact that for a given total pressure ratio the retrothrust coefficient is very large at low subsonic speeds and relatively small at supersonic speeds. The total decelerating force coefficients are presented as a function of retrothrust coefficient in figure 10 for zero angle of attack. The total decelerating force was nearly always less than the jets-off drag of the model for values of retrothrust coefficient smaller than the jets-off drag coefficient. Thus, if the purpose of the retrorockets were to slow the descent of the vehicle it would not be practical to operate the rockets at these low retrothrust coefficients. For values of retrothrust coefficient above the jets-off drag coefficient the results of figure 10 indicate that the total retarding force was very nearly equal to the retrothrust itself. This trend was to be expected because of the previously discussed effects of the jets on the axial force coefficients.

A 5 6 8

CONCLUSIONS

An experimental investigation directed toward the determination of the effects of simulated retrorockets on the aerodynamic characteristics of a body of revolution showed that:

1. Force and moment coefficients exhibited a dependence on the ratio of jet to free-stream total pressures.

2. The axial forces, exclusive of retrothrust, were of considerably lower magnitude when the jets were on than when they were off; in fact, they were negative for some test conditions. Thus, the total decelerating force (drag plus retrothrust) was generally less than the jets-off drag for values of retrothrust less than the jets-off drag and approximately equal to the thrust for higher values.

3. The pitching moments underwent erratic variations with changing ratio of jet to free-stream total pressures, but for a wide range of test conditions, they were of smaller magnitude with the jets on than with the jets off.

4. At zero angle of attack and at some supersonic speeds the bow shock wave was observed to be in stable positions close to the model at low values of the jet to free-stream total pressure ratio, far upstream from the model at intermediate values of the pressure ratio, and in intermediate positions at high pressure ratios. It appears that this bow shock phenomenon is peculiar to configurations that have several nozzles in close proximity.

Ames Research Center
National Aeronautics and Space Administration
Moffett Field, Calif., Feb. 2, 1962

APPENDIX

ANALYSIS OF BOW SHOCK AND JET INTERFERENCE PHENOMENA

For the purpose of directing attention to pertinent circumstances affecting the flow field between the bow shock and model, a series of sketches made from a study of enlargements of the shadowgraphs of figure 2 is presented in figure 11. These sketches illustrate the sequence of events that gave rise to the unusual behavior of the bow shock. With the nozzles operating at relatively low total pressure the initial portions of the jets were separated, were free of normal shocks, and displayed an expansion and contraction cycle similar to the first of multiple cycles common to free jets. This type of flow field, which is sketched in figure 11(a), was observed to occur for values of the pressure ratio p_{t_j}/p_{t_∞} between 22, the lowest at which the jets were operated, and 28 at $M_\infty = 1.50$. Within this range the total pressures of the jet and free-stream flows were apparently matched by viscous losses and a series of weak shock waves in the jets. Increasing the pressure ratio from 22 to 28 caused the bow shock to move from about 1.0 to 1.3 model diameters ahead of the model face as shown by the results of figure 3.

Concurrent with the upstream movement of the bow shock was an expansion of the boundaries of each jet. The maximum cross-sectional area of each jet increased as a result of this expansion and reached a value for which the local Mach number at the maximum area, in combination with existing pressures, was sufficient to support a normal shock in the first cycle of each jet. The flow field then took the form sketched in figure 11(b). This type of flow field occurred for total pressure ratios between 28 and 57 to 65, depending upon free-stream pressure, at $M_\infty = 1.50$. The presence of the normal shock in each jet nearly arrested the movement of the bow shock with changing total pressure ratio in this range as shown in figure 3. The continued expansion of the jet boundaries with increasing jet pressure in this range caused the boundaries of the jet from each nozzle to interfere physically with one another as shown in figure 11(c). The jet interference became more pronounced as pressure ratio continued to increase until no further inward expansion was possible. At this point the flow field was observed to appear like that sketched in figure 11(d).

Raising total pressure ratio above about 60 at $M_\infty = 1.50$ increased the difference between $p_{t_{\infty_2}}$ and p_{t_j} to the extent that normal shocks in the jets in conjunction with viscous losses could no longer match $p_{t_{\infty_2}}$ and p_{t_j}. The normal shock disappeared and jet interference abruptly terminated. Each jet then developed at least one full expansion-contraction cycle which extended the high pressure region of the jets further upstream

from the model and thereby moved the bow shock upstream. Further increase in total pressure ratio increased the number of expansion-contraction cycles in the jets and caused the bow shock to move even farther upstream. A qualitative sketch of this type of flow field is shown in figure 11(e). The flow field in which the bow-shock position was extended existed between the values of p_{t_j}/p_{t_∞} of about 60 and 110 for $M_\infty = 1.50$ as shown by figure 3.

At the onset of the fully developed cyclic jet flow the jets were distinctly separated but as the ratio of jet to free-stream total pressure was further increased, the jets were forced to expand again and finally interfere for the second time. This time an oblique shock wave formed in the jets at the contact point and deflected them away from the center line of the model. The extended high pressure region ahead of the model was destroyed and the bow shock moved abruptly to a position several model diameters closer to the model face. A sketch of this flow condition is shown in figure 11(f). Further increase in pressure ratio only enlarged the flow pattern shown in figure 11(f) which, in turn, resulted in the gradual upstream movement of the bow shock shown for $p_{t_j}/p_{t_\infty} > 112$ in figure 3. It is conceivable that the entire cycle of normal shocks forming in the jets, jet mutual interference, and bow shock extension and return could repeat itself at higher jet pressures with retention of the oblique shock at the point of mutual jet interference. However, pressure ratios of a higher magnitude were not obtainable to substantiate this.

The abrupt upstream movement of the bow shock and its subsequent movement back toward the model might be expected to be accompanied by similarly abrupt variations in the pressure coefficient on the model, especially the model face. A typical comparison of pressure coefficient on the model face and bow shock standoff distance as a function of the total pressure ratio is made in figure 12 for a free-stream Mach number of 1.50. The pressure coefficients measured at r_f/R of 0.5 and four values of θ_f, $\pm 22.5^\circ$ and $\pm 67.5^\circ$, were averaged to provide a mean value of pressure coefficient between the nozzle exits for this comparison. This comparison shows that as the total pressure ratio was increased to about 60 the pressure coefficient varied smoothly from stagnation to a negative value. Then, as the bow shock moved upstream, pressure coefficient jumped to a small positive value. At total pressure ratio above about 112 the pressure coefficient became negative.

In an attempt to gain further insight into the flow phenomena, an interesting correlation was found to exist between the data of this investigation and calculations made using theory for free jets exhausting into still air. As noted previously, the apparent sequence of events based on shadowgraphs lead to the conclusion that just prior to the movement of the bow shock to the extended position, the jets were expanded to the longitudinal center line of the model and each jet contained a normal shock at its maximum area. The assumptions that (a) a normal shock exists at the maximum area of the first cycle of a free jet, (b) the

maximum jet radius is equal to the distance between the nozzle center line and the model longitudinal center line, and (c) the jet total pressure behind the jet normal shock is equal to the free-stream total pressure behind a normal bow shock (i.e., $p_{t_{j_2}} = p_{t_{\infty_2}}$), made it possible to use the results of reference 3 to calculate the total pressure ratio necessary to satisfy the given conditions. These calculations describe the ratios of total pressures as a function of free-stream Mach number at which the bow shock would move abruptly upstream.

The total pressure ratios, as a function of M_∞, for which the bow shock should move back toward the model were also calculated. A correlation of the shadowgraphs and the pressure coefficients measured on the model face near the nozzle exits showed that after the bow shock returned from its extended position, the pressure coefficient was between about -0.1 and -0.3. Also, as pointed out previously, at the time of the bow shock return the jets had again expanded sufficiently to interfere mutually. Thus, the assumptions that the pressure coefficient measured on the model face near the nozzle exits was indicative of the pressure coefficient along the jet boundaries and that the maximum jet radius was equal to the distance between the nozzle center line and the model center line, made it possible again to use the results of reference 3 to obtain the ratio of total pressure necessary to satisfy these conditions.

The results of both of the aforementioned calculations are presented in figure 13 wherein the experimental data are also shown for comparison. The experimental and calculated pressure ratios for which the bow shock moves to the extended position are in nearly perfect agreement. The experimentally measured trend showing the range of total pressure ratios for which the bow shock was in the extended position to diminish and disappear with increasing free-stream Mach number is also predicted by the calculations.

It should be emphasized that even though the calculations agree quite well with the experimental measurements, it remains to be proven whether or not this semiempirical analysis would apply to other multijet configurations.

REFERENCES

1. Charczenko, Nickolai, and Hennessey, Katherine W.: Investigation of a Retrorocket Exhausting From the Nose of a Blunt Body into a Supersonic Free Stream. NASA TN D-751, 1961.

2. Hayman, Lovick O., Jr., and McDearmon, Russell W.: Jet Effects on Cylindrical Afterbodies Housing Sonic and Supersonic Nozzles Which Exhaust Against a Supersonic Stream at Angles of Attack From 90° to 180°. NASA TN D-1016, 1962.

3. Love, Eugene S., Grigsby, Carl E., Lee, Louise P., and Woodling, Mildred J.: Experimental and Theoretical Studies of Axisymmetric Free Jets. NASA TR R-6, 1959.

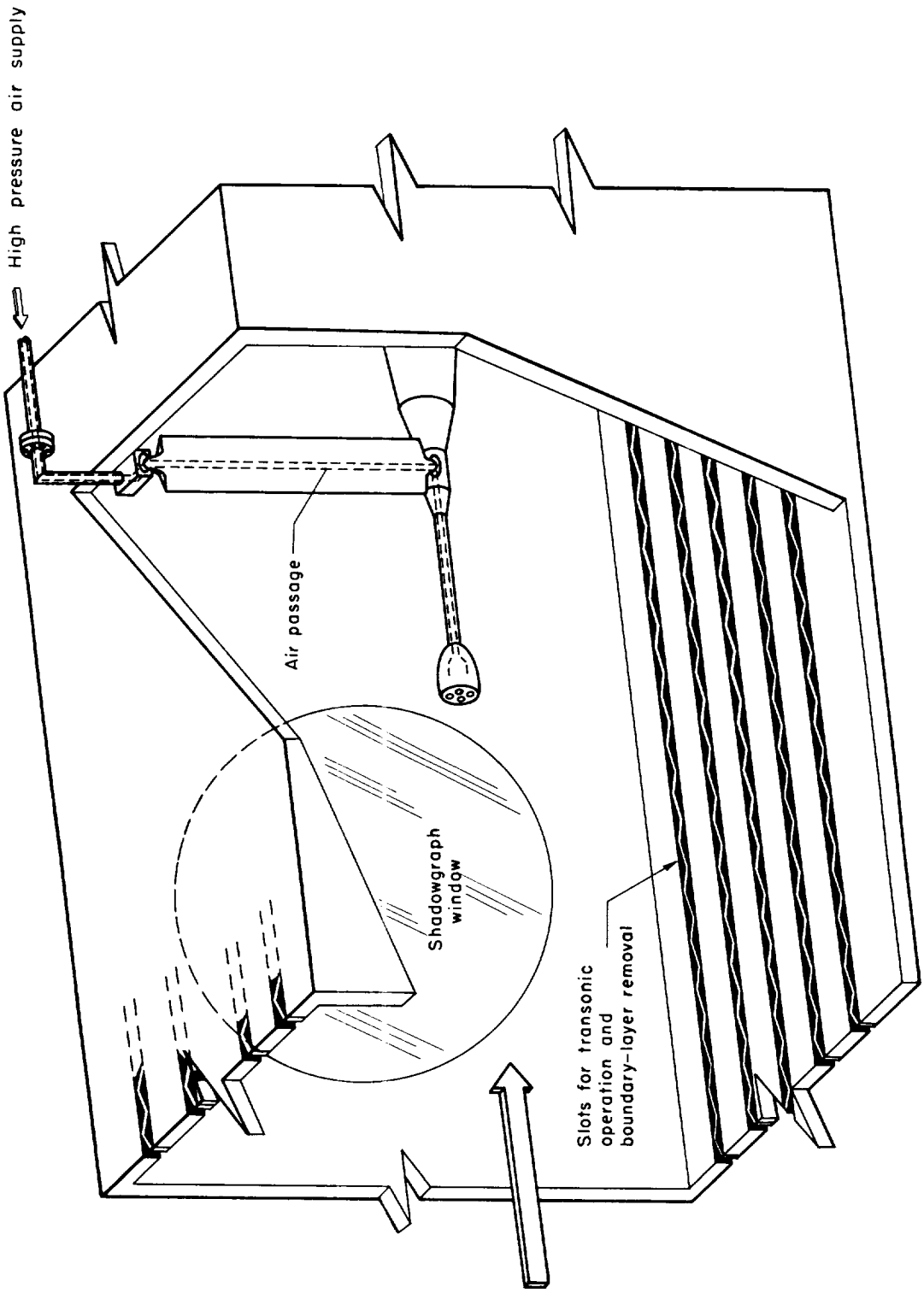

(a) Schematic drawing of model installed in wind tunnel.

Figure 1.- Wind-tunnel installation and model sketches.

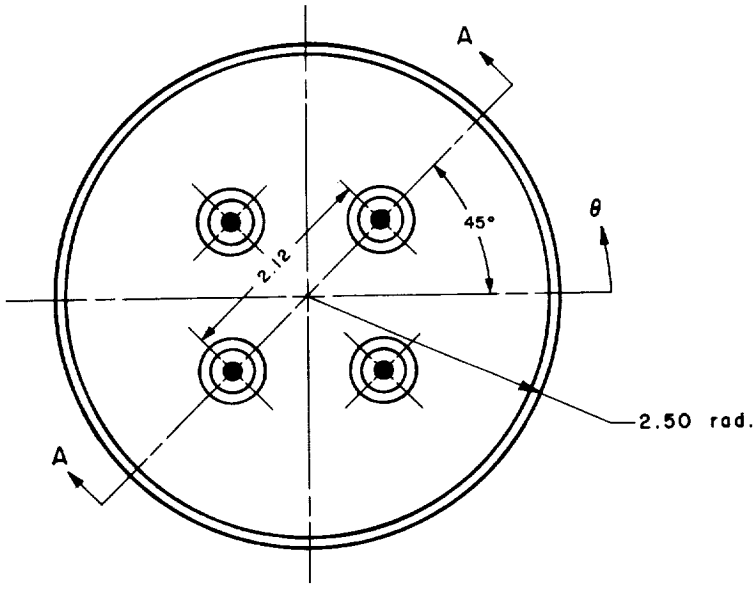

MODEL FACE

Body orifice locations								
	θ_b, deg							
	-90.0	-60.0	-30.0	0	30.0	60.0	90.0	180.0
$-\frac{x}{L}$	0.05	0.05	0.05	0.05	0.05	0.05	0.05	0.05
	.10	.10	.10	.10	.10	.10	.10	.10
	.20	.20	.20	.20	.20	.20	.20	.20
	.40	.40	.40	.40	.40	.40	.40	.40
	.60	.60	.60	.60	.60	.60	.60	.60
	.70	.70	.70	.70	.70	.70	.70	.70
	.80	.80	.80	.80	.80	.80	.80	.80
		.90	.90	.90		.90	.90	.90

Face orifice locations										
	θ_f, deg									
	-90.0	-67.5	-45.0	-22.5	0	22.5	45.0	67.5	90.0	180.0
$\frac{r_f}{R}$	0.	0.	0.	0.	0.	0.	0.	0.	0.	0.
	.10	.10	.10	.10	.10	.10	.10	.10	.10	.10
	.20	.20	.20	.20	.20	.20	.20	.20	.20	.20
	.30	.30	.25	.30	.30	.30	.25	.30	.30	.30
	.40	.40	.60	.40	.40	.40	.60	.40	.40	.40
	.50	.50	.70	.50	.50	.50	.70	.50	.50	.50
	.60	.60	.80	.60	.60	.60	.80	.60	.60	.60
	.70	.70	.90	.70	.70	.70	.90	.70	.70	.70
	.80	.80		.80	.80	.80		.80	.80	.80
	.90	.90		.90	.90	.90		.90	.90	.90

(b) Model details and dimensions.

Figure 1.- Continued.

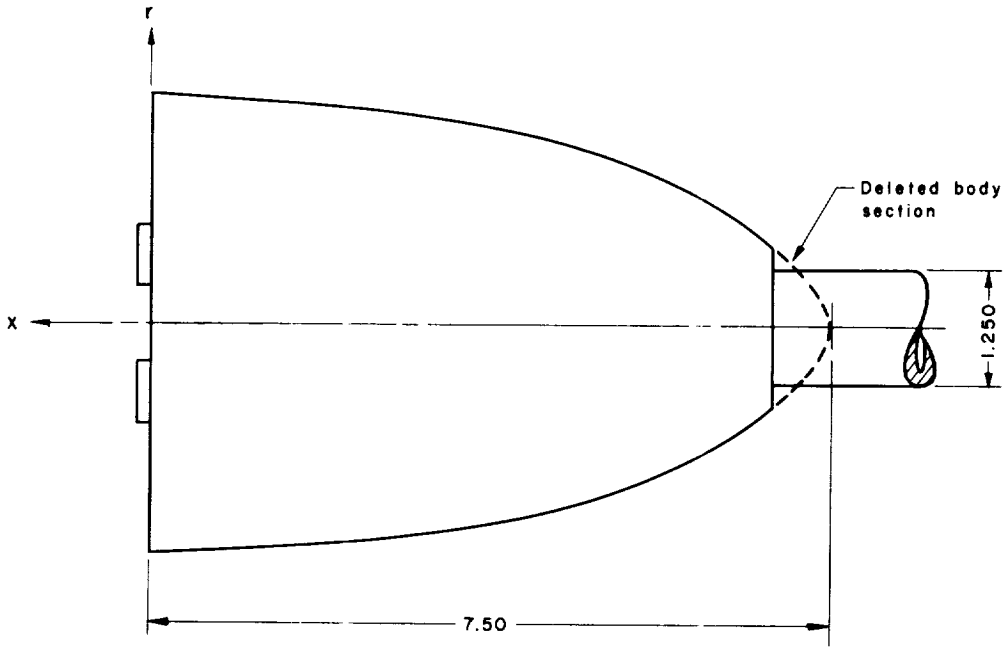

MODEL AFTERBODY AND STING

Note: all dimensions in inches unless otherwise noted

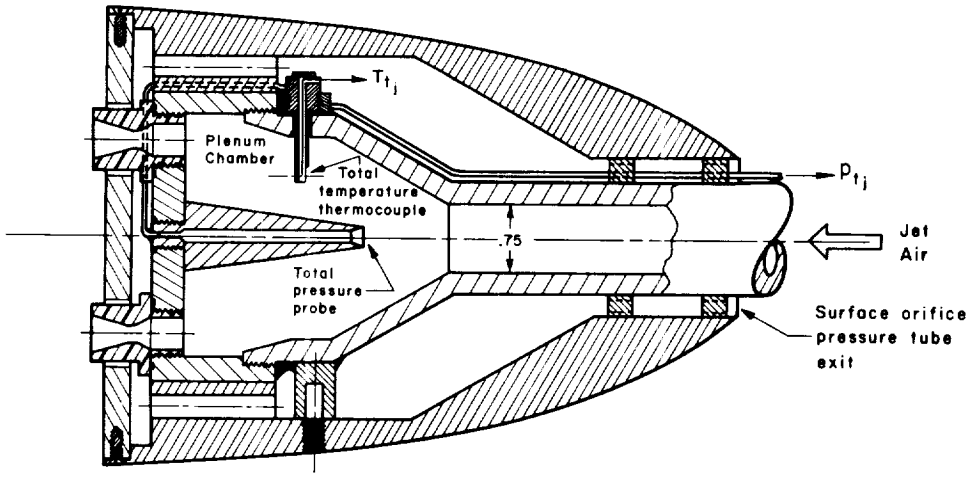

SECTION A-A

MODEL INTERNAL CONFIGURATION

(Surface pressure orifices not shown)

(b) Model details and dimensions - Concluded.

Figure 1.- Continued.

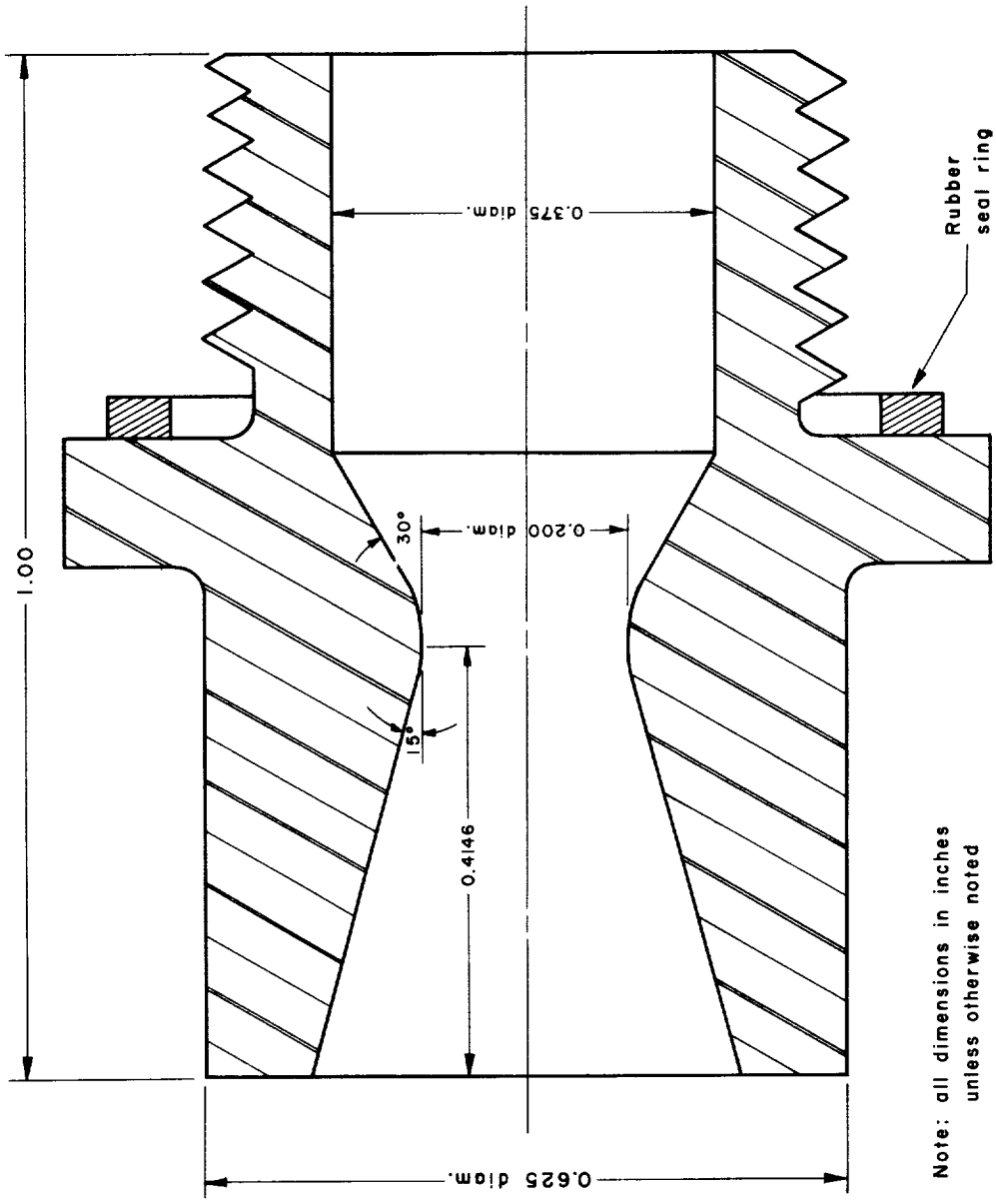

(c) Details of jet nozzles.

Figure 1.- Concluded.

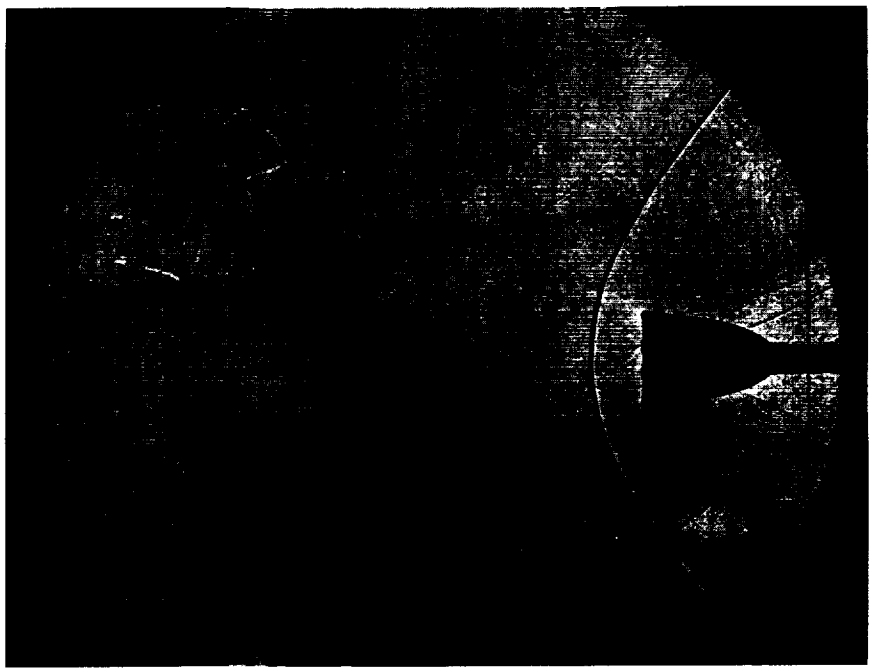

(a) Jets off.

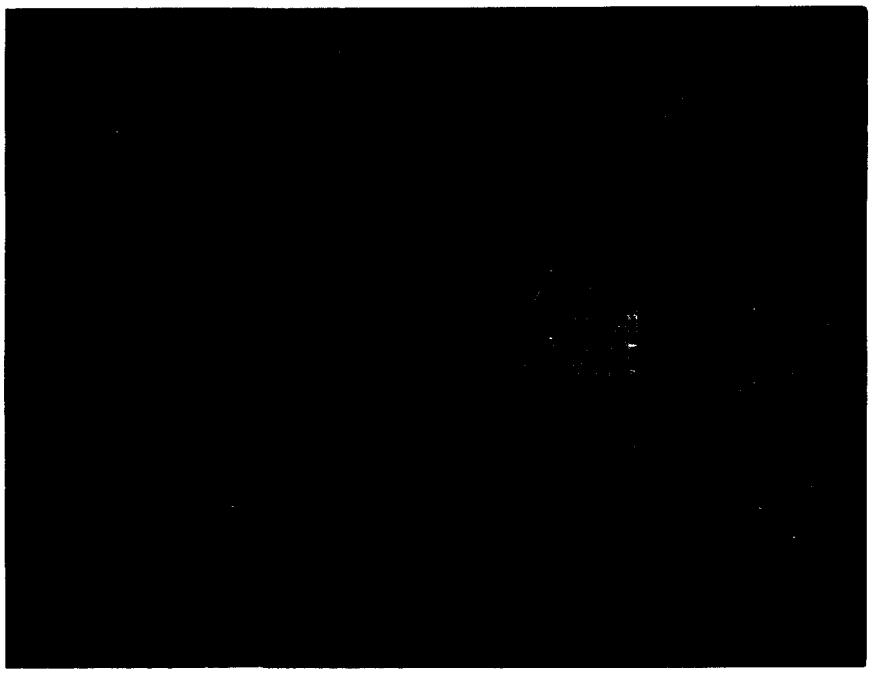

(b) $p_{t_j}/p_{t_\infty} = 28.6$

Figure 2.- Shadowgraphs illustrating effect of jet to free-stream total pressure ratio on bow shock position; $M = 1.50$, $p_{t_\infty} = 7$ psia, $\alpha = 0^\circ$.

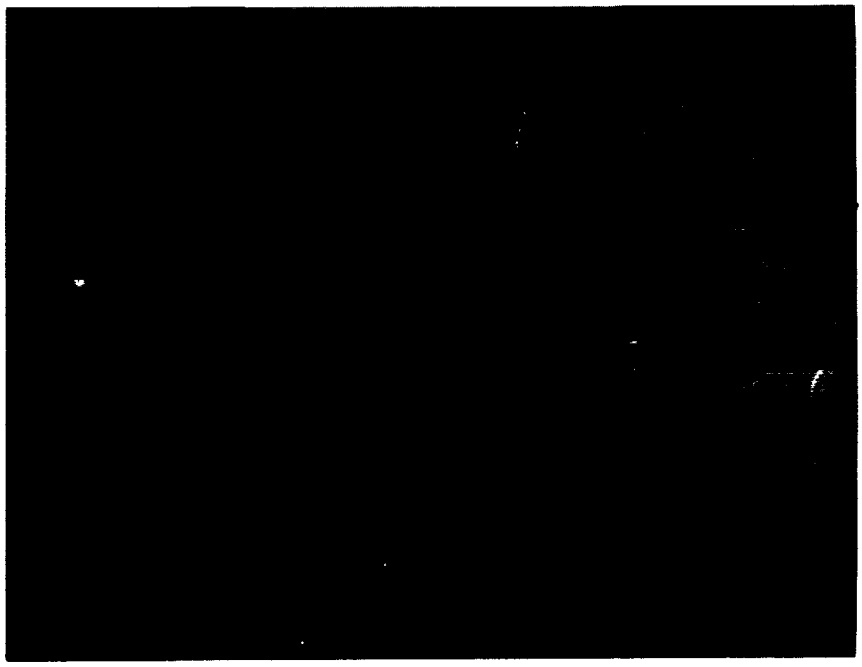

(c) $p_{t_j}/p_{t_\infty} = 42.9$

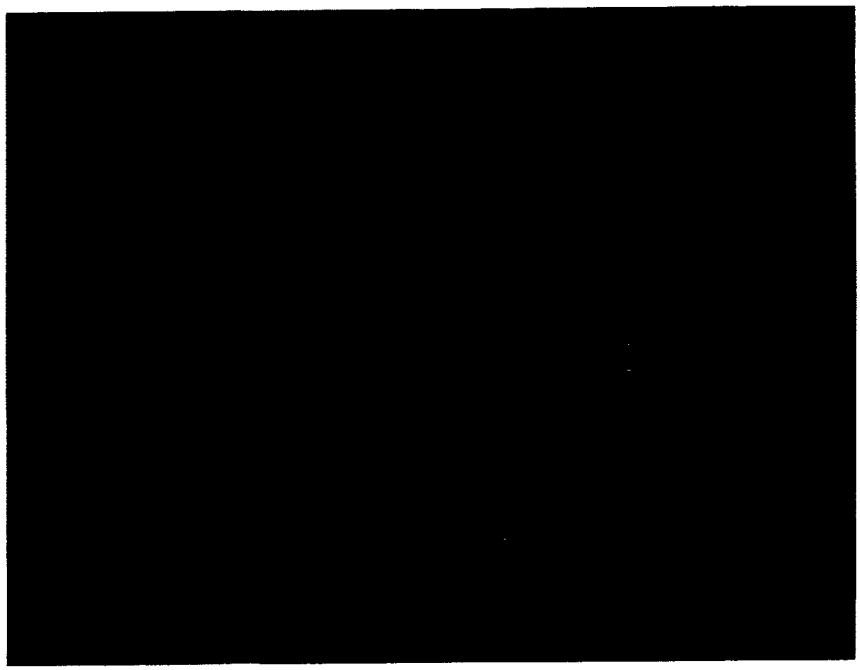

(d) $p_{t_j}/p_{t_\infty} = 57.2$

Figure 2.- Continued.

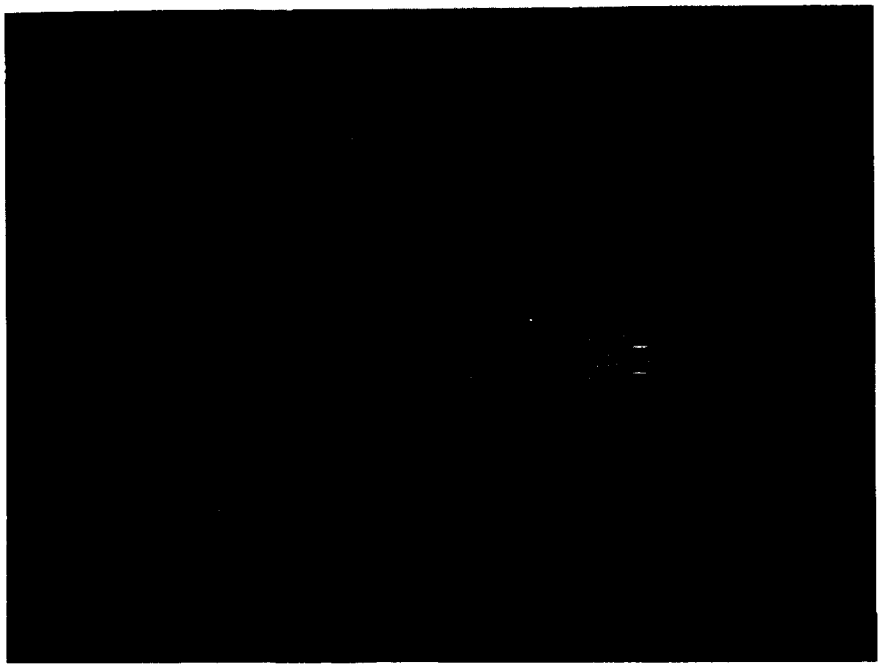

(e) $p_{t_j}/p_{t_\infty} = 57.2$

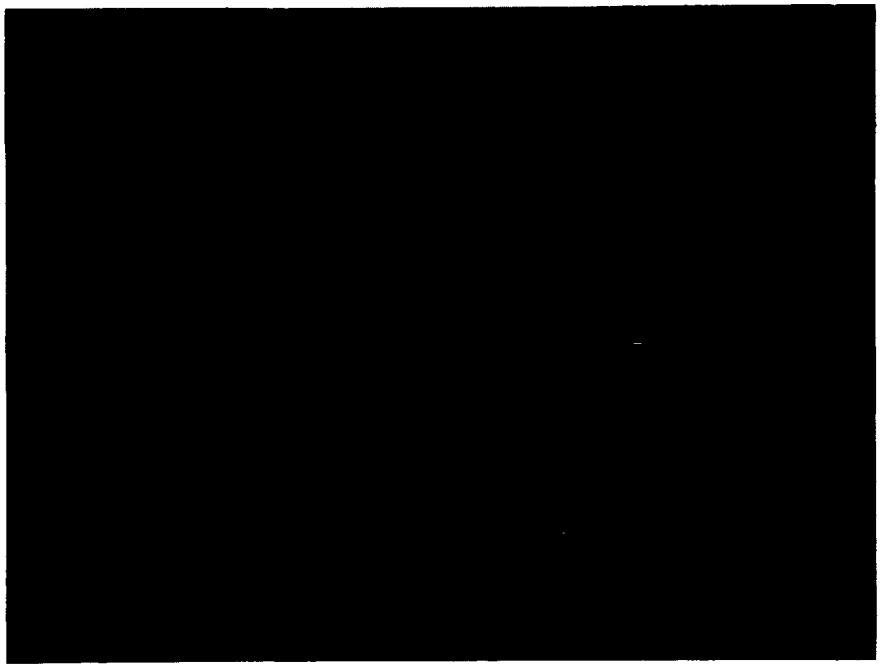

(f) $p_{t_j}/p_{t_\infty} = 71.4$

Figure 2.- Continued.

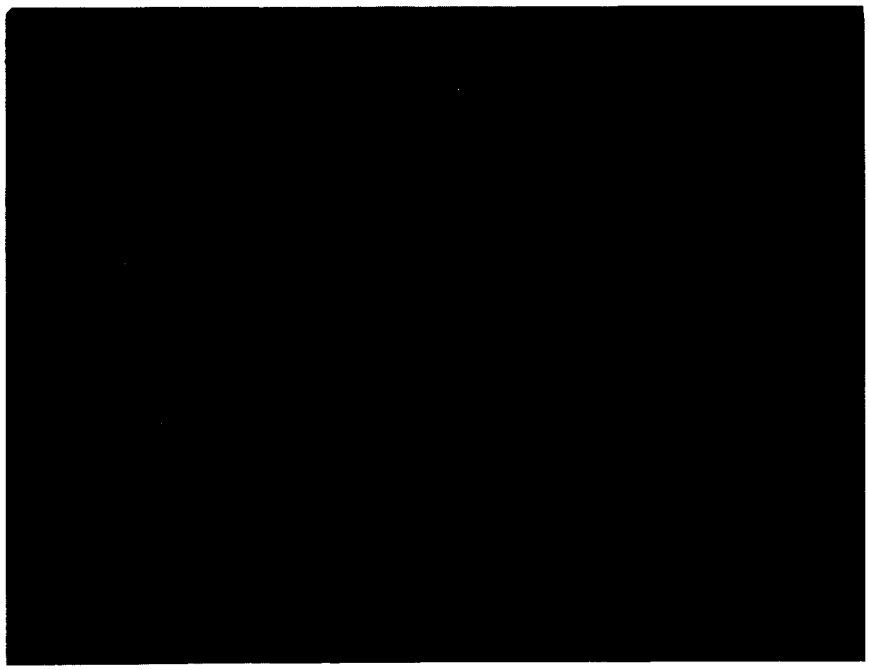

(g) $p_{t_j}/p_{t_\infty} = 85.7$

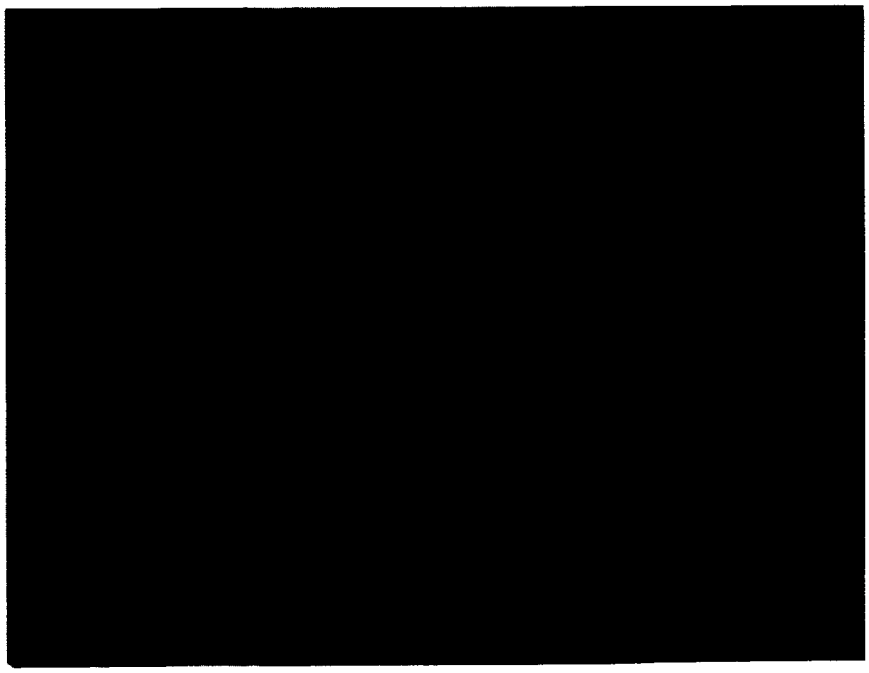

(h) $p_{t_j}/p_{t_\infty} = 100.0$

Figure 2.- Continued.

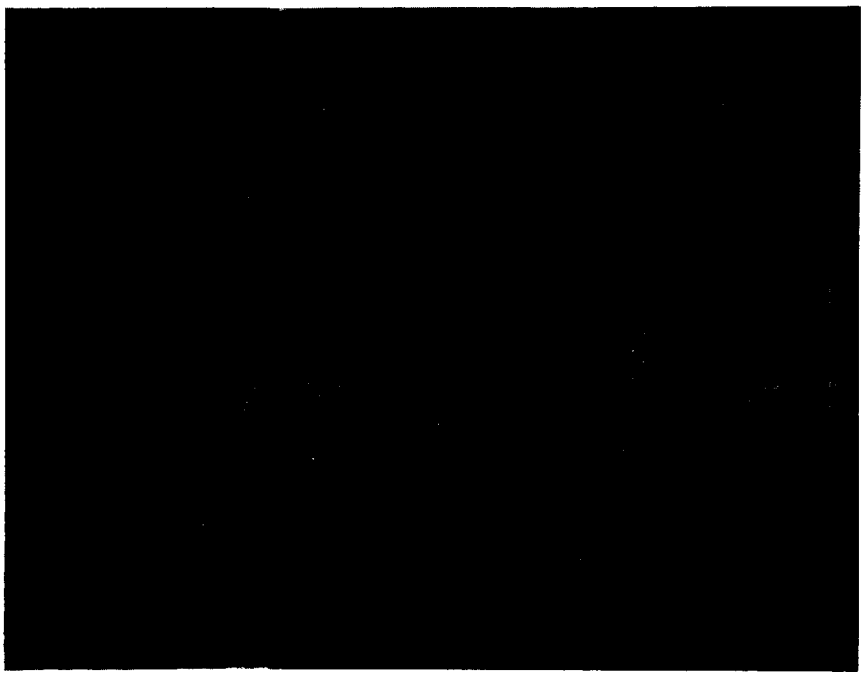

(i) $p_{t_j}/p_{t_\infty} = 114.3$

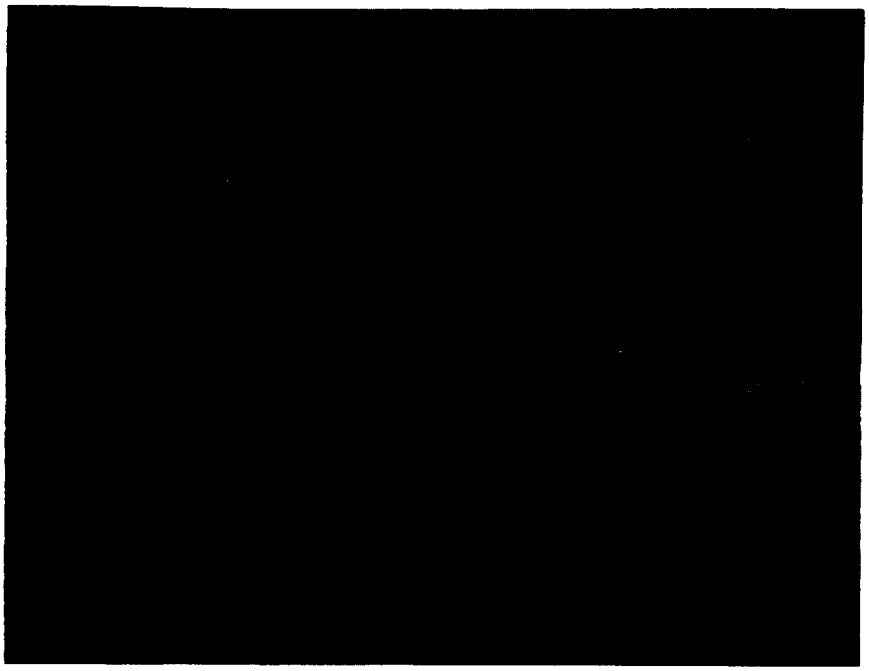

(j) $p_{t_j}/p_{t_\infty} = 128.6$

Figure 2.- Continued.

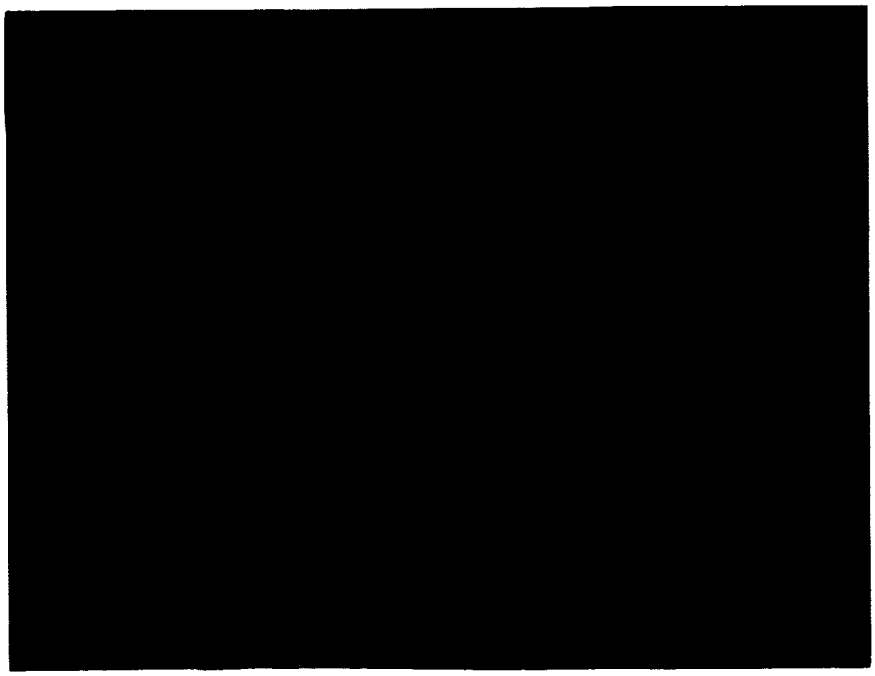

(k) $p_{t_j}/p_{t_\infty} = 142.9$

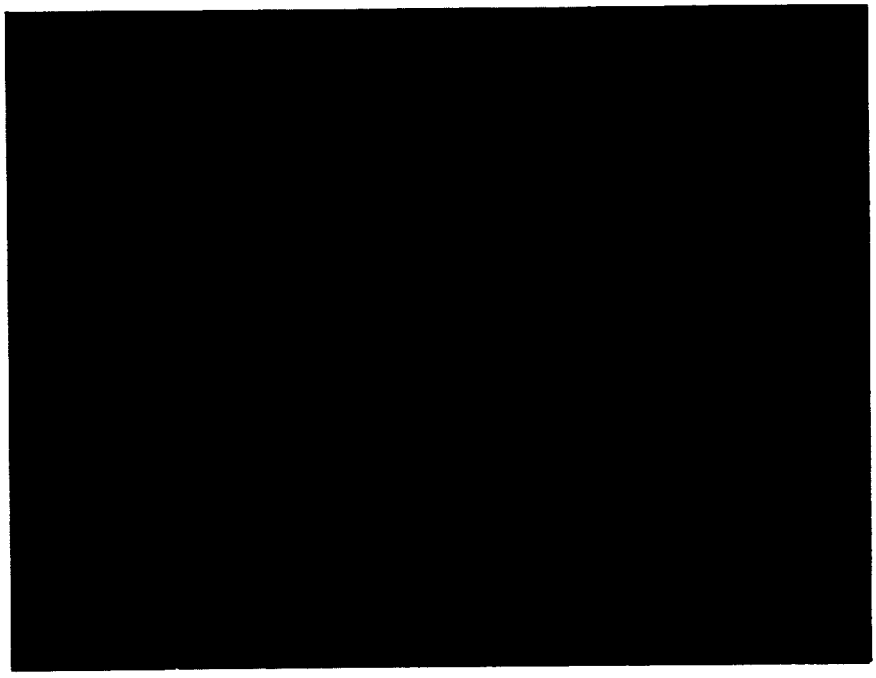

(l) $p_{t_j}/p_{t_\infty} = 157.3$

Figure 2.- Concluded.

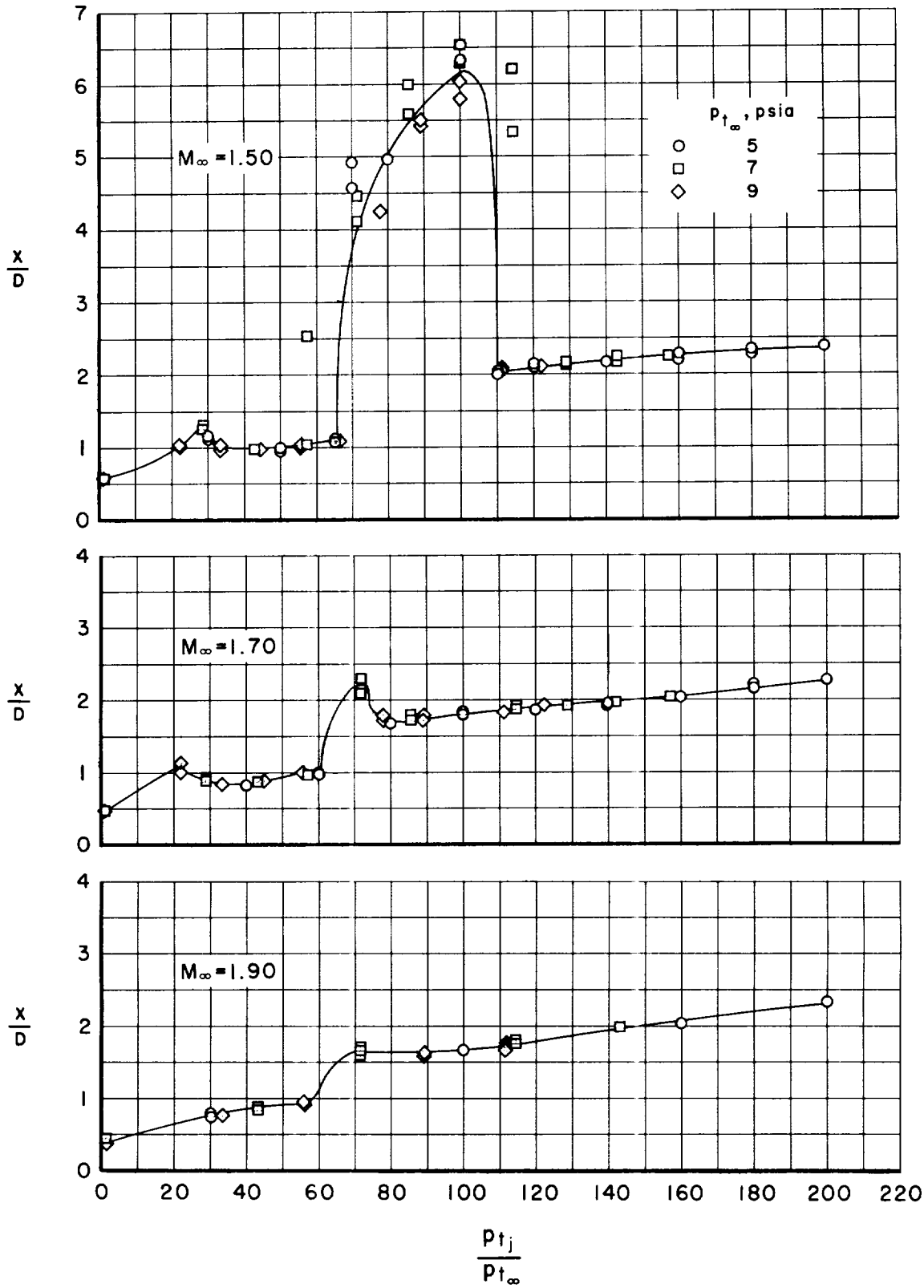

Figure 3.- Effects of jet to free-stream total pressure ratio on bow shock standoff distance; $\alpha = 0^\circ$.

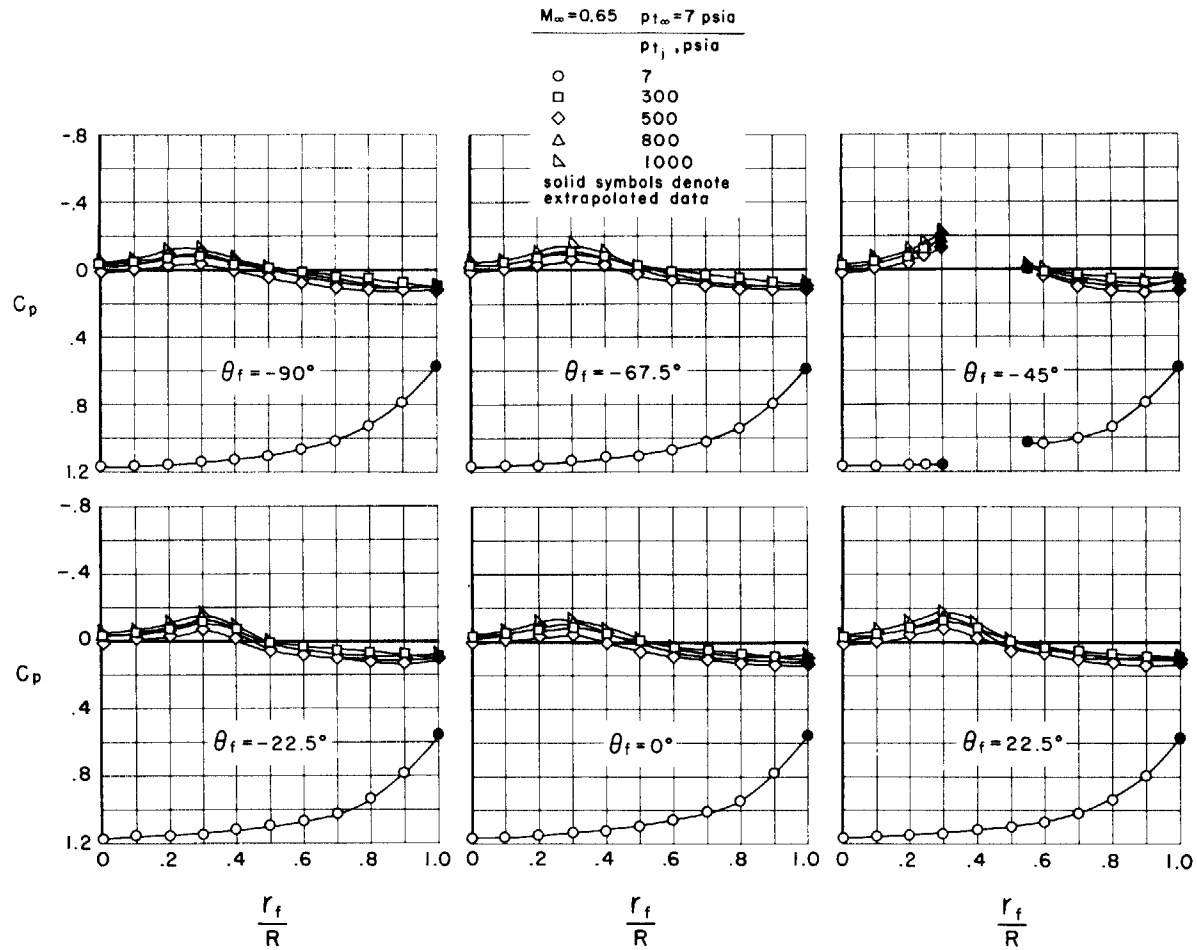

(a) Pressure coefficients on model face.

Figure 4.- Typical effects of the retrojets on the model pressure distributions at subsonic free-stream Mach numbers; $\alpha = 0^\circ$.

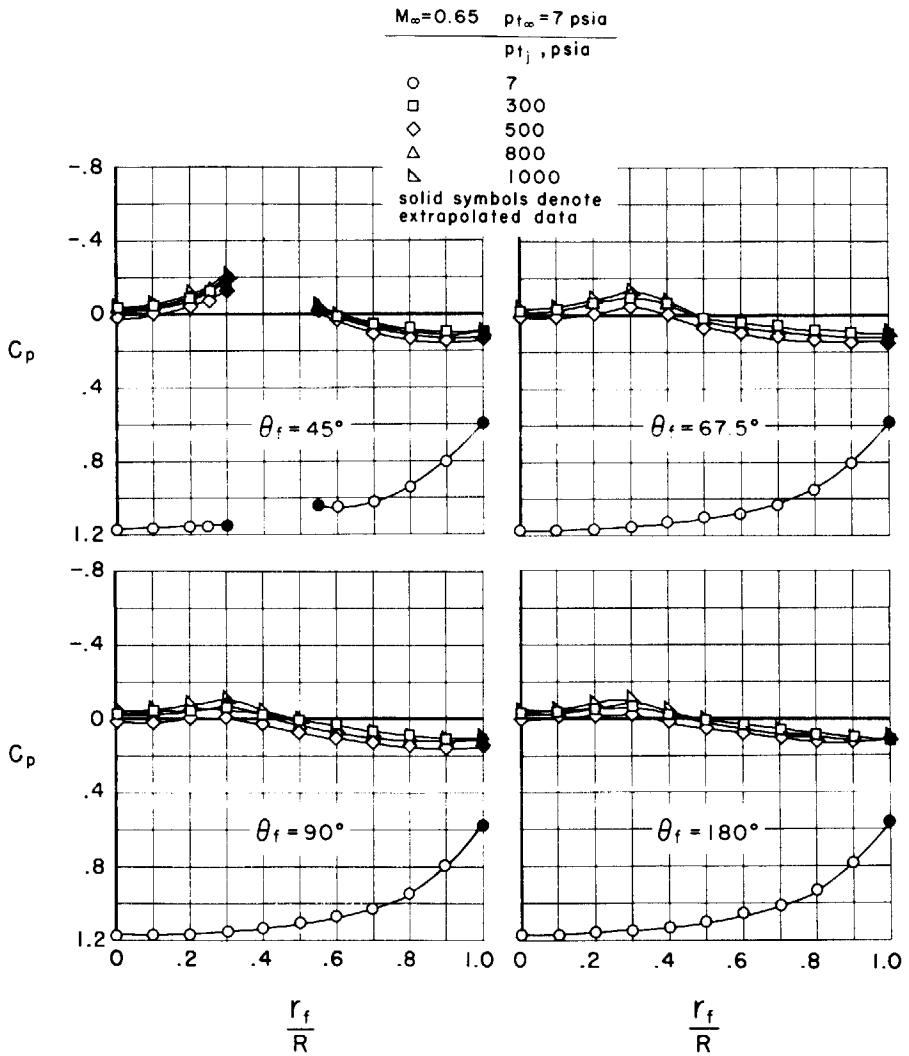

(a) Pressure coefficients on model face - Concluded.

Figure 4.- Continued.

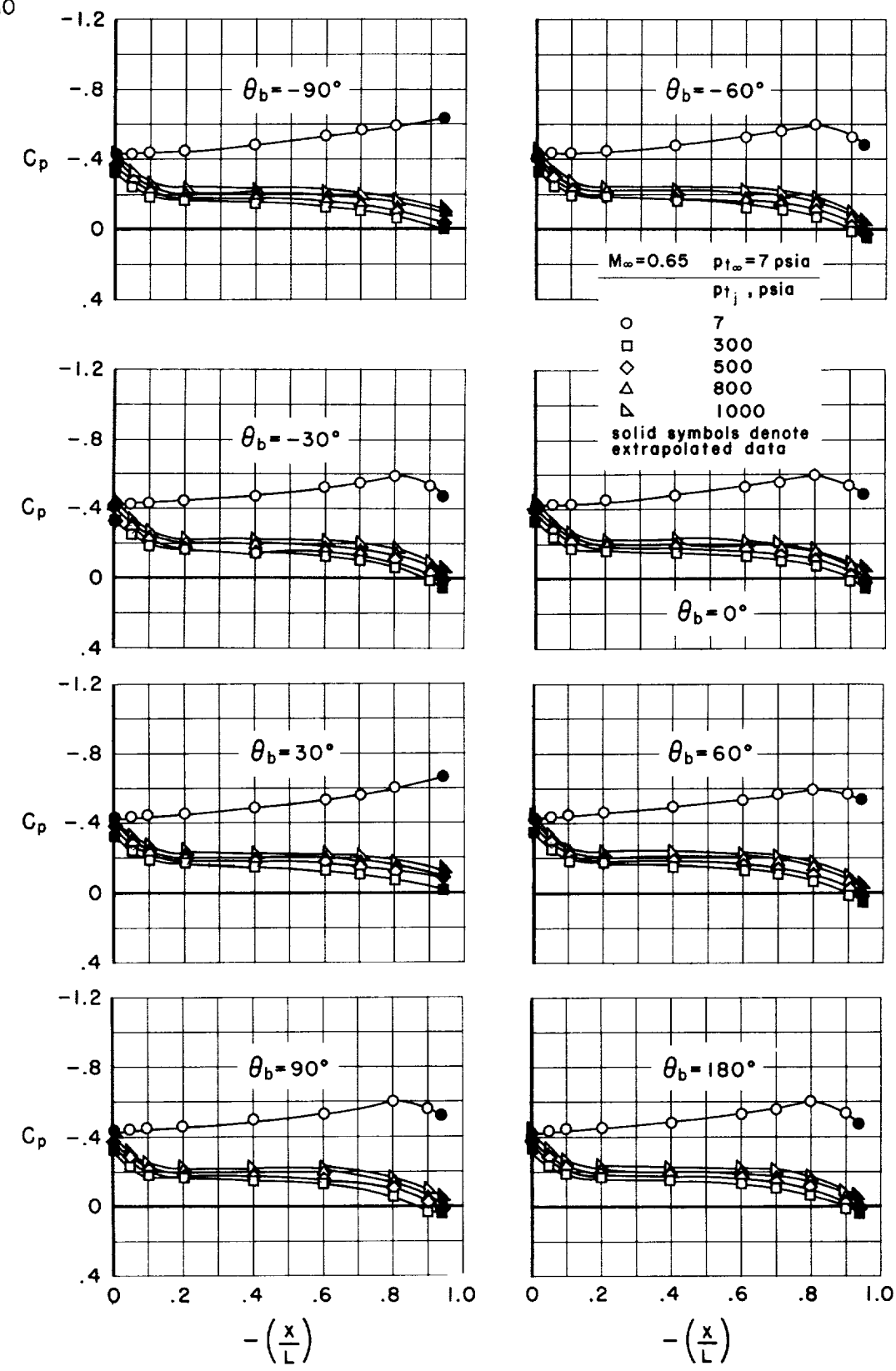

(b) Pressure coefficients on model body.

Figure 4.- Concluded.

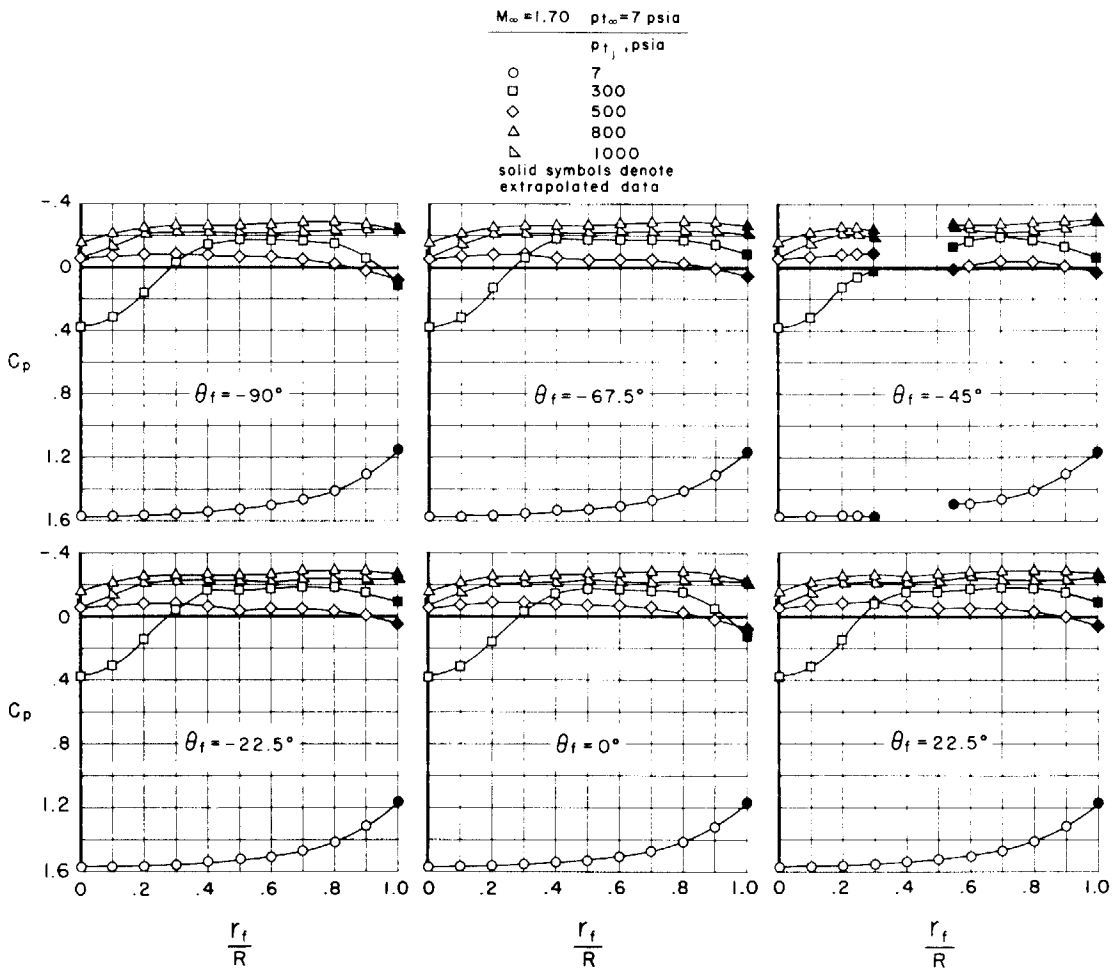

(a) Pressure coefficients on model face.

Figure 5.- Typical effects of the retrojets on the model pressure distributions at supersonic free-stream Mach numbers; $\alpha = 0^o$.

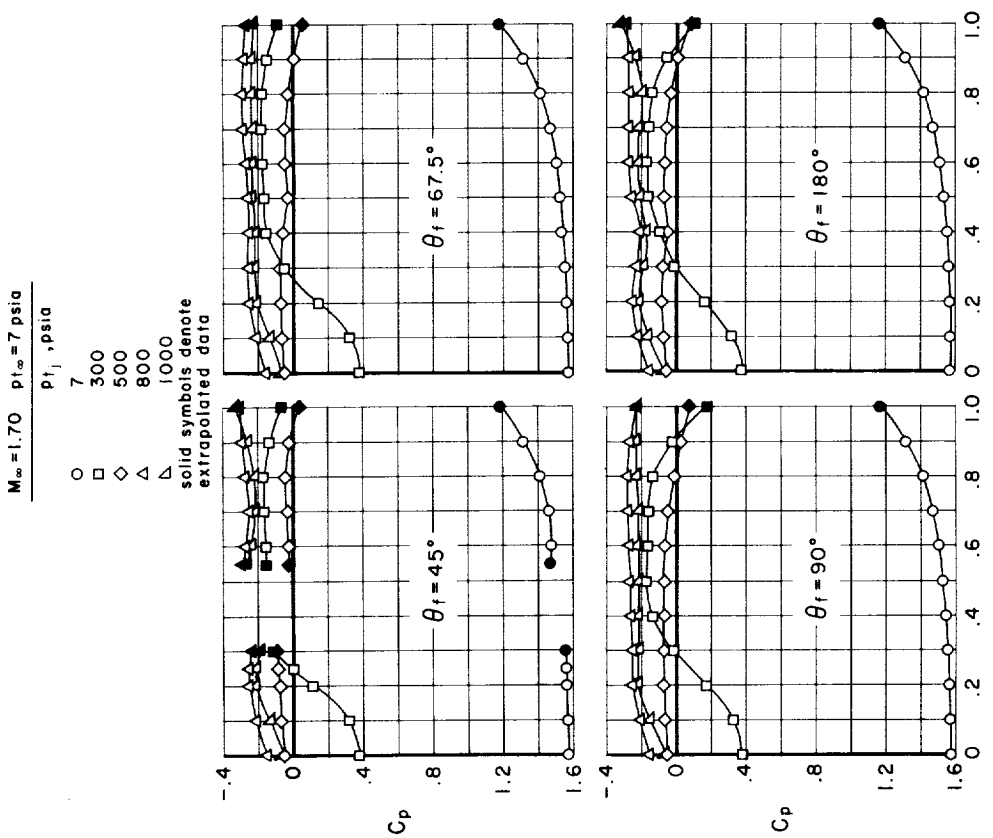

(a) Pressure coefficients on model face - Concluded.

Figure 5.- Continued.

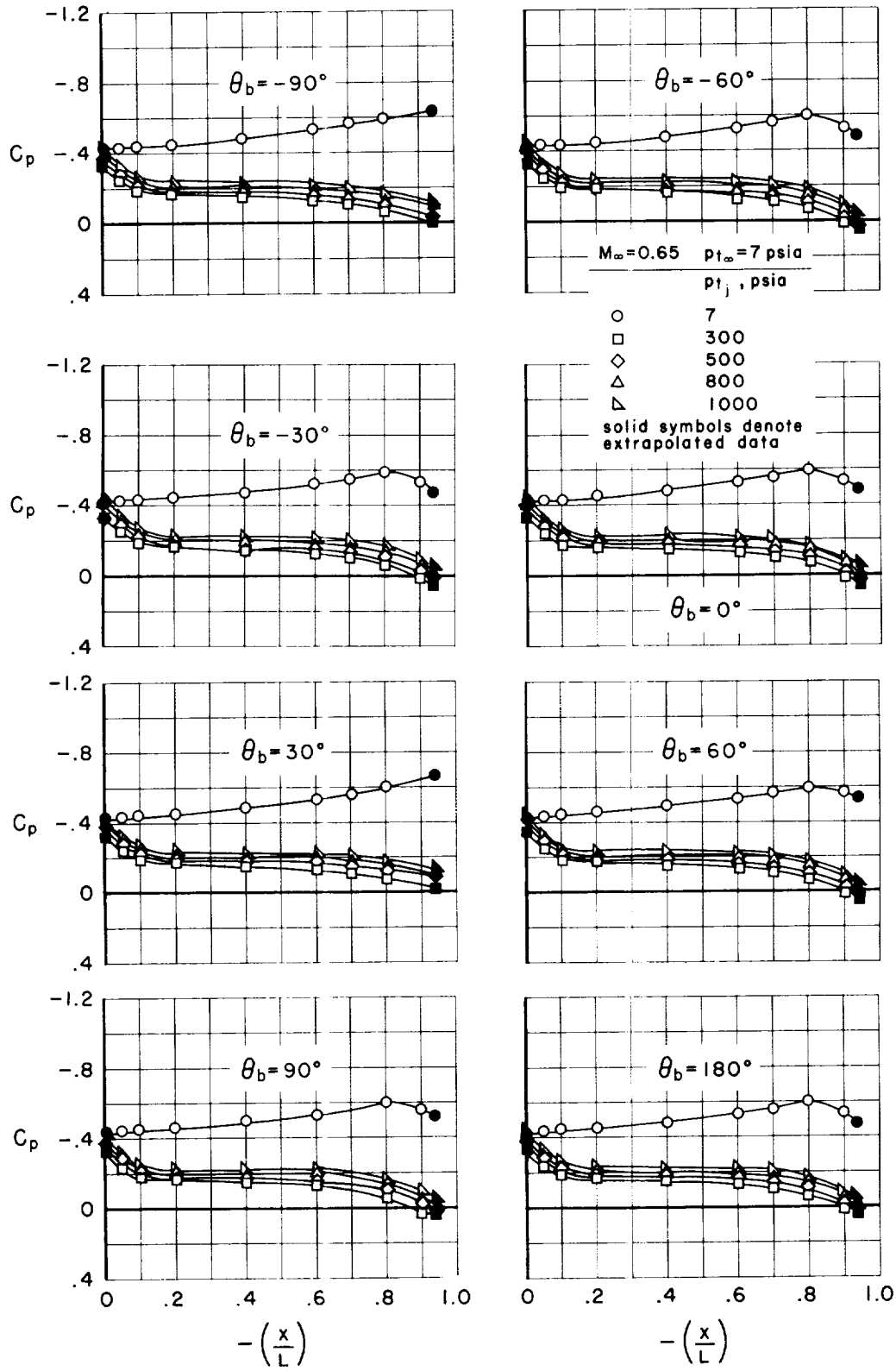

(b) Pressure coefficients on model body.

Figure 5.- Concluded.

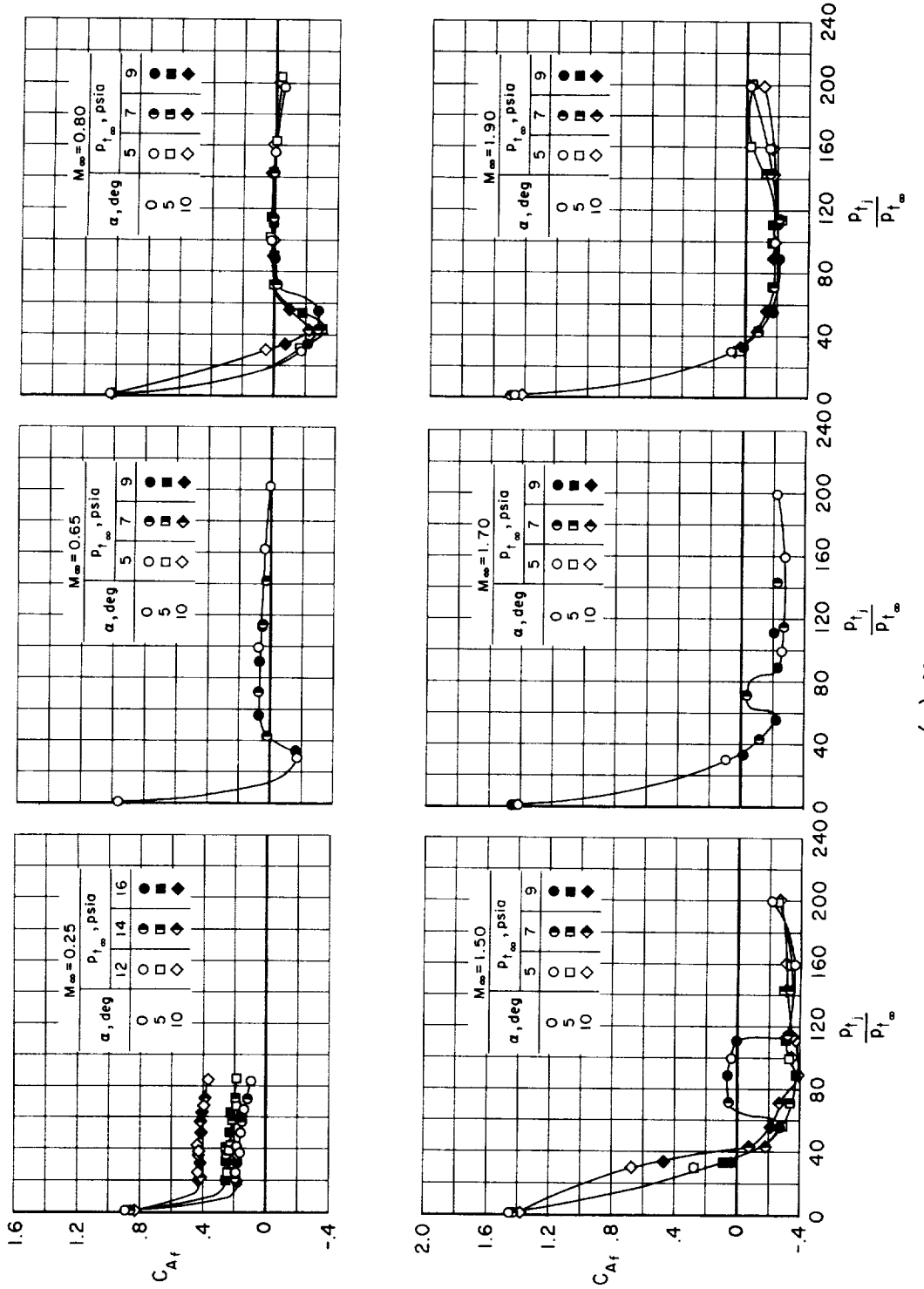

(a) Model face.

Figure 6.- Effects of the retrojets on coefficients of axial force exclusive of retrothrust.

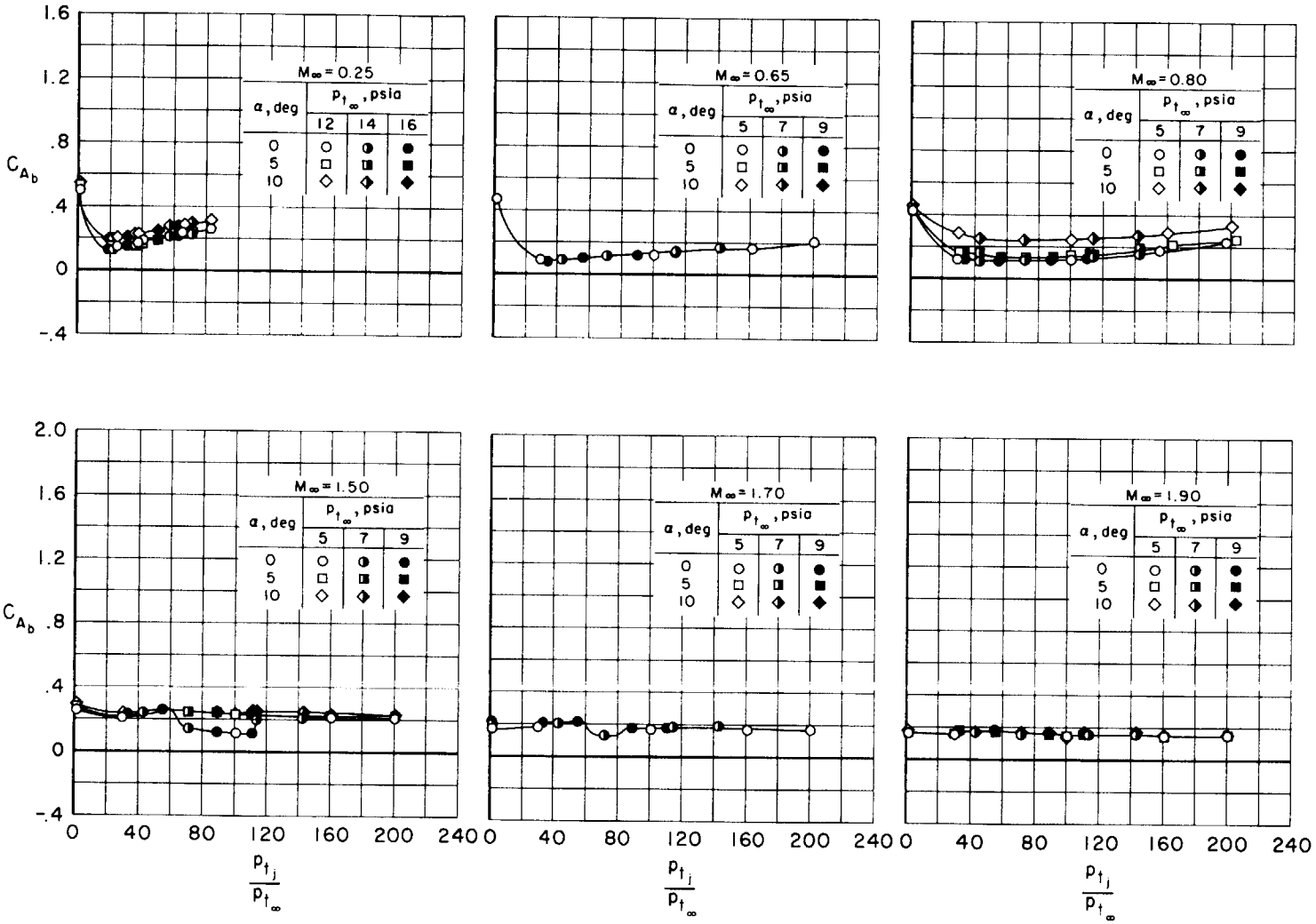

(b) Model body.

Figure 6.- Continued.

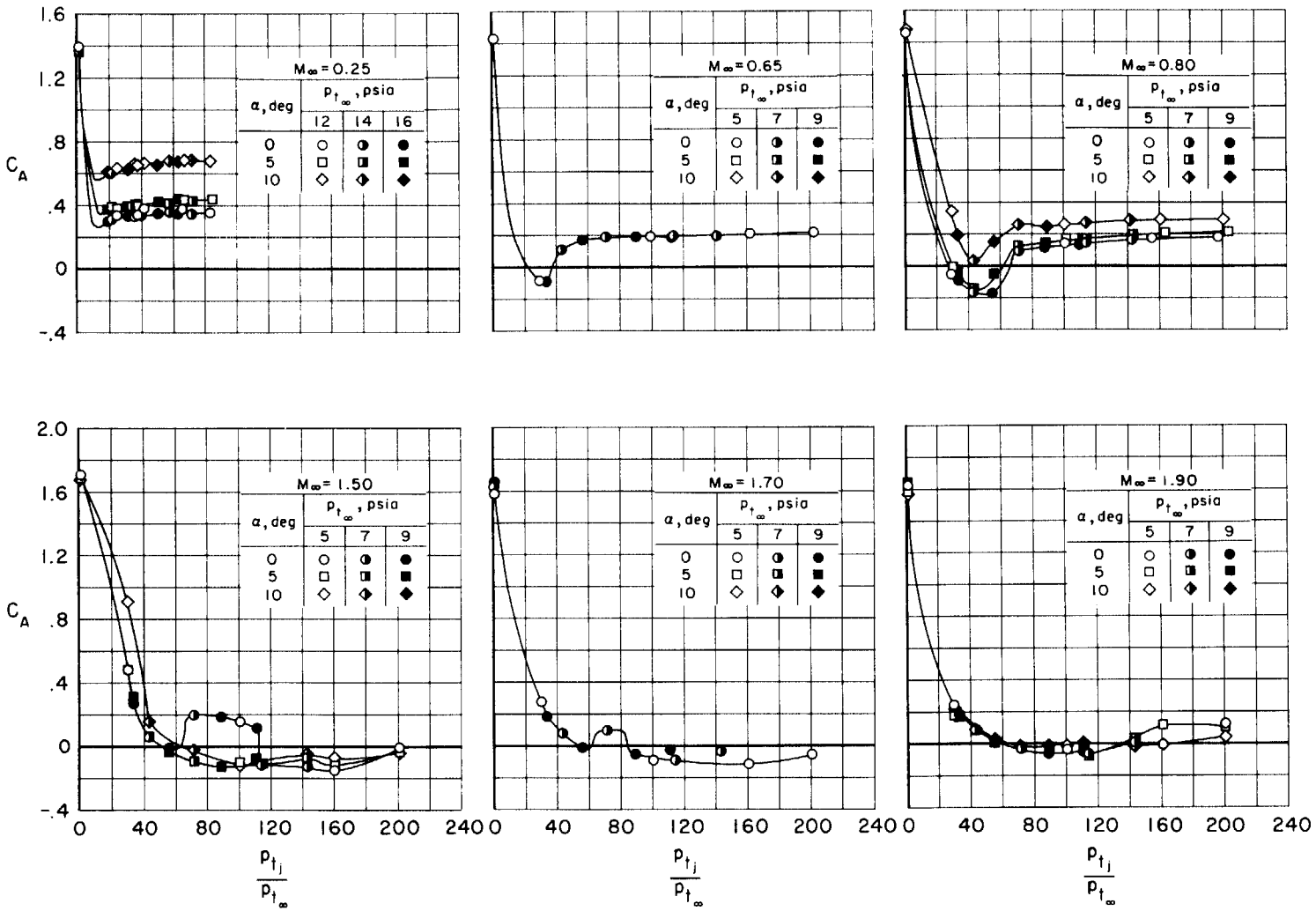

(c) Complete model.

Figure 6.- Concluded.

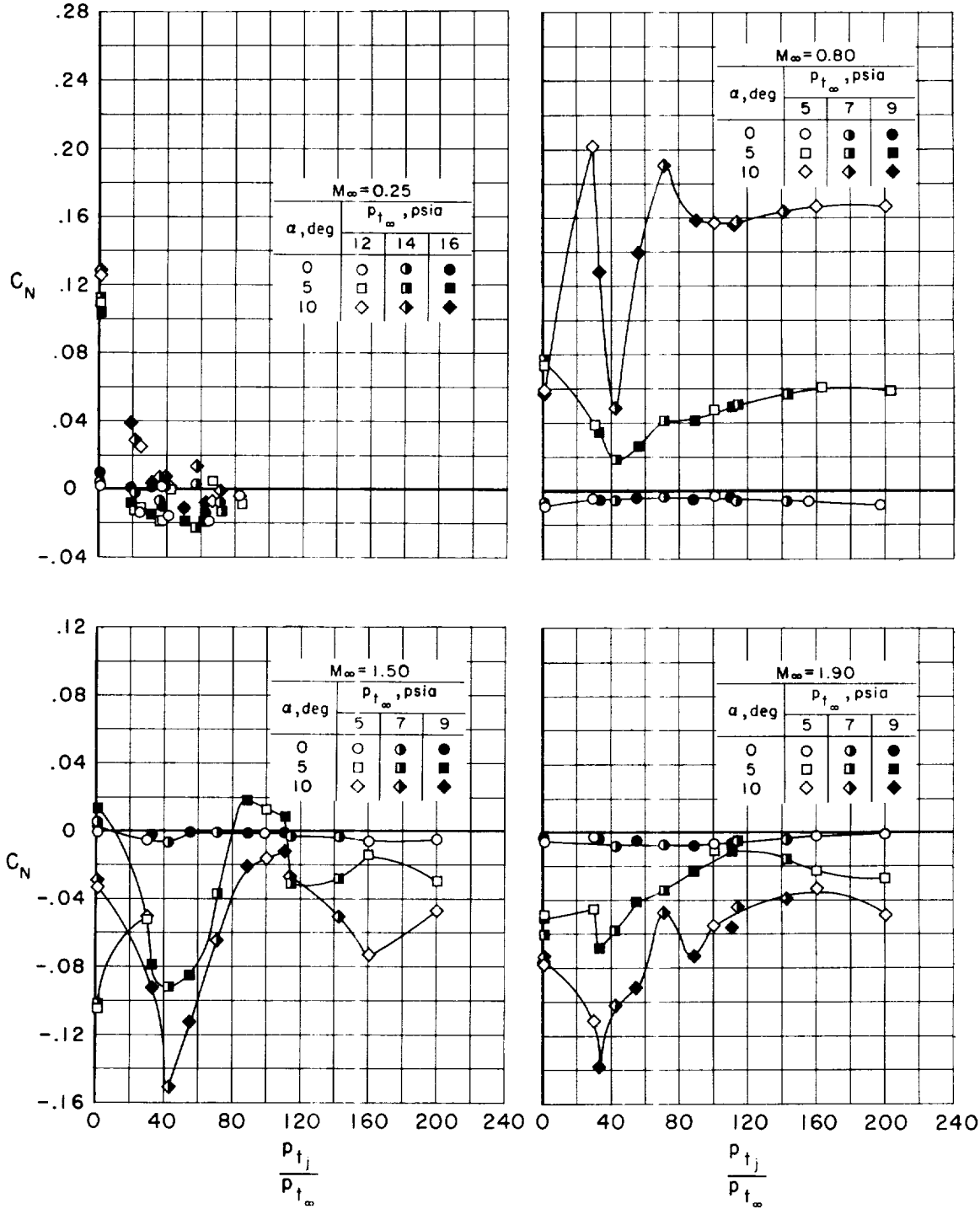

Figure 7.- Effects of the retrojets on coefficients of normal force.

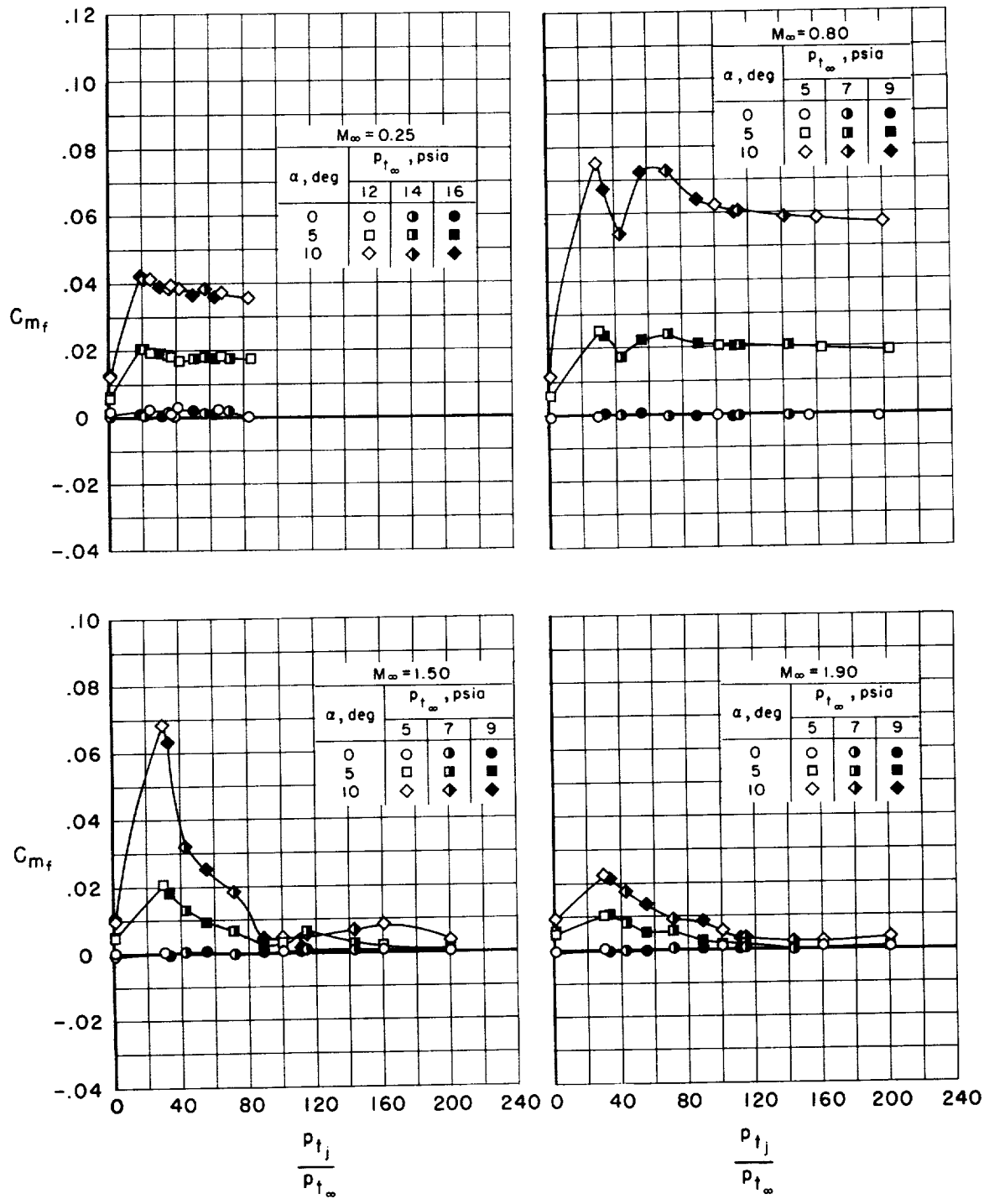

(a) Model face.

Figure 8.- Effects of the retrojets on pitching-moment coefficients.

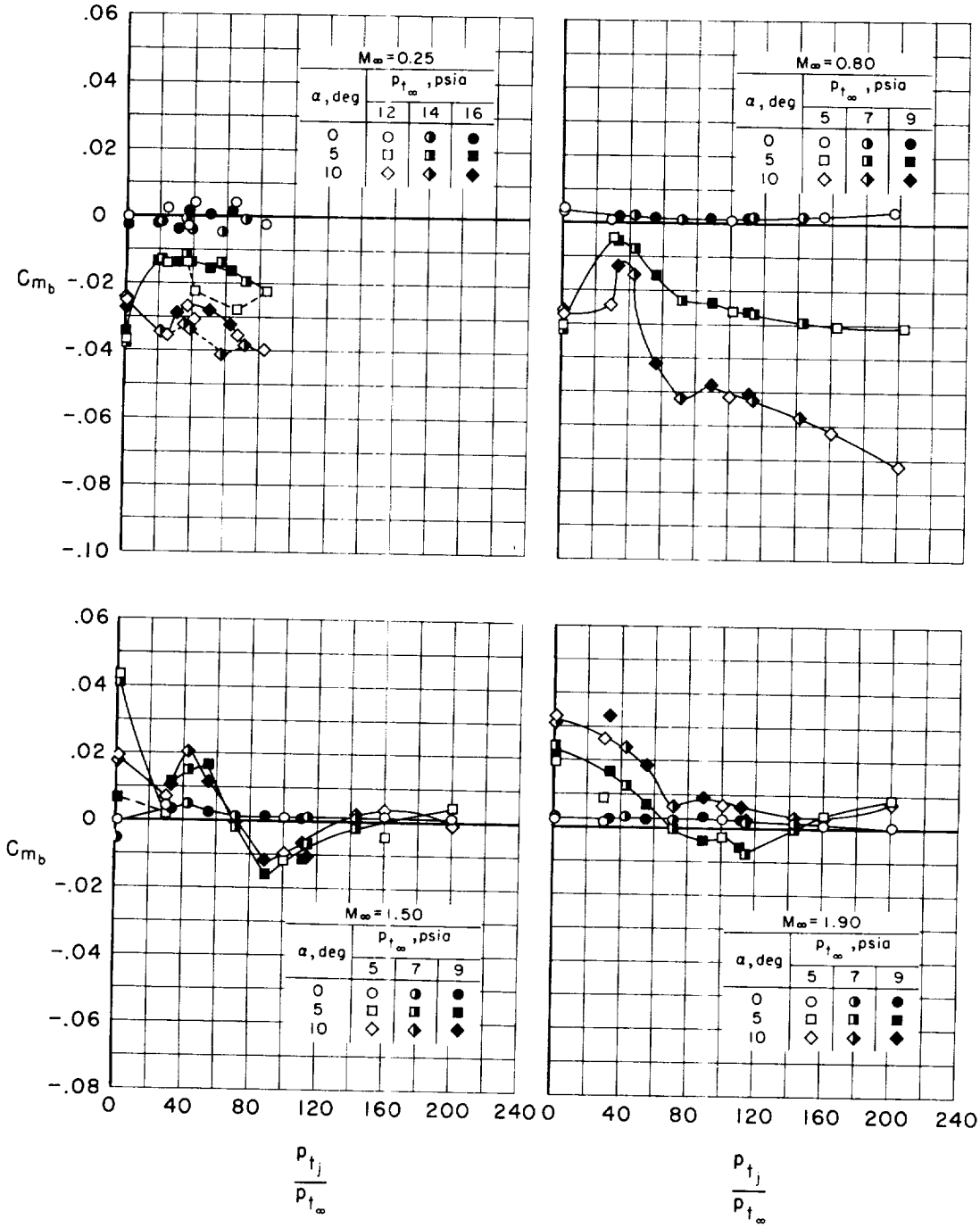

(b) Model body.

Figure 8.- Continued.

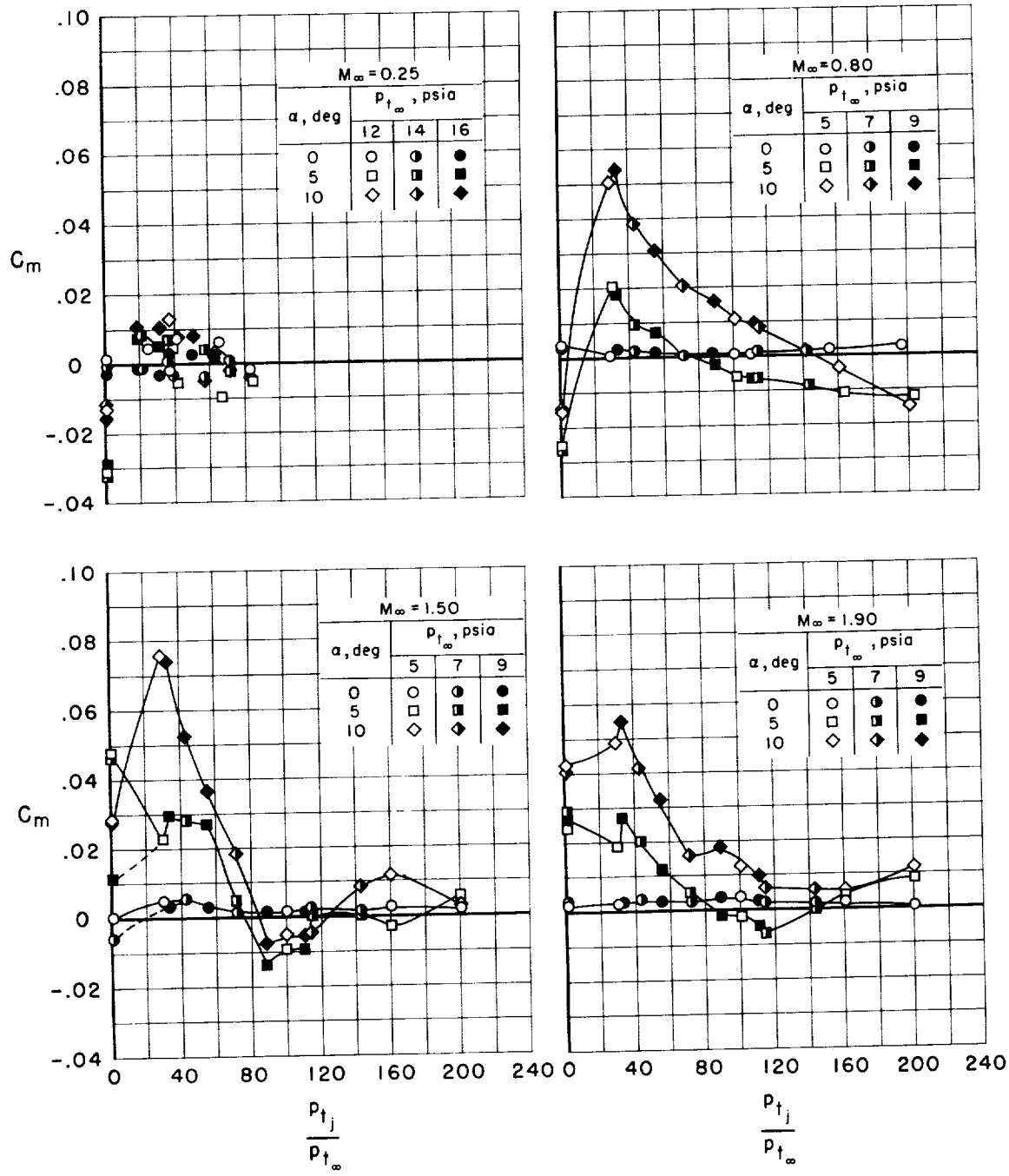

(c) Complete model.

Figure 8.- Concluded.

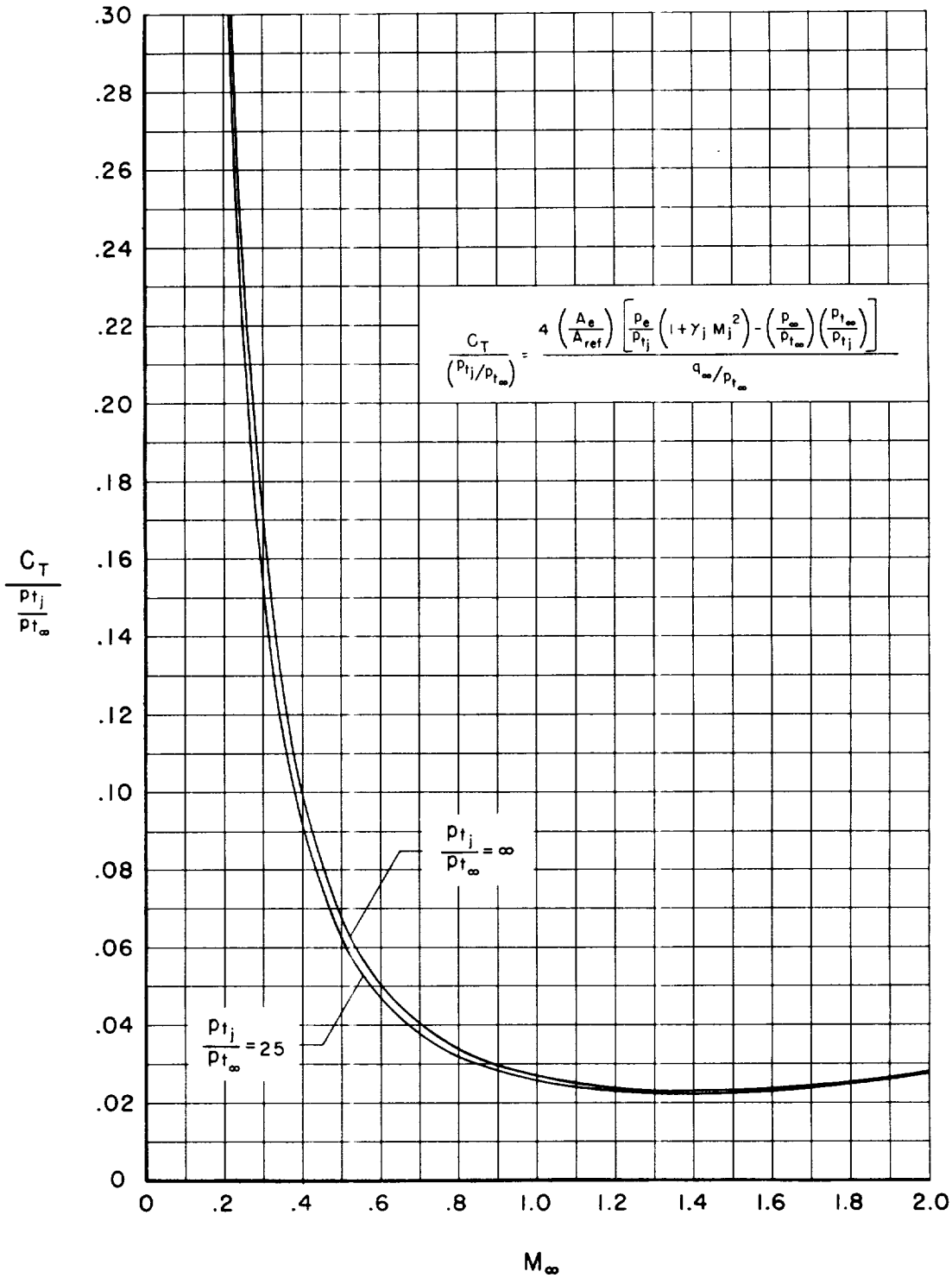

Figure 9.- Dependence of retrothrust coefficient on free-stream Mach number and ratio of jet to free-stream total pressures.

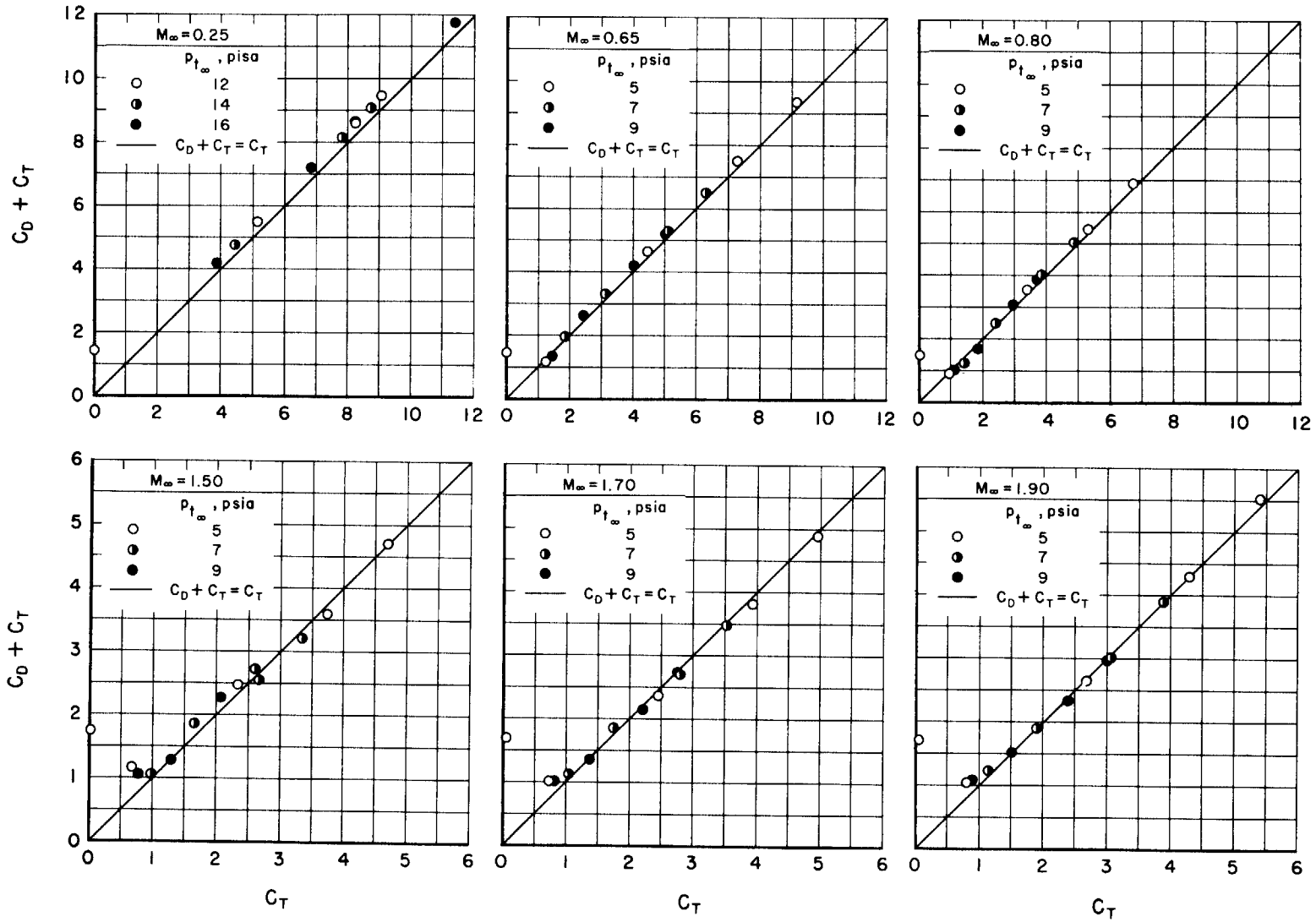

Figure 10.- Relation between total decelerating force coefficient and retrothrust coefficient; $\alpha = 0^\circ$.

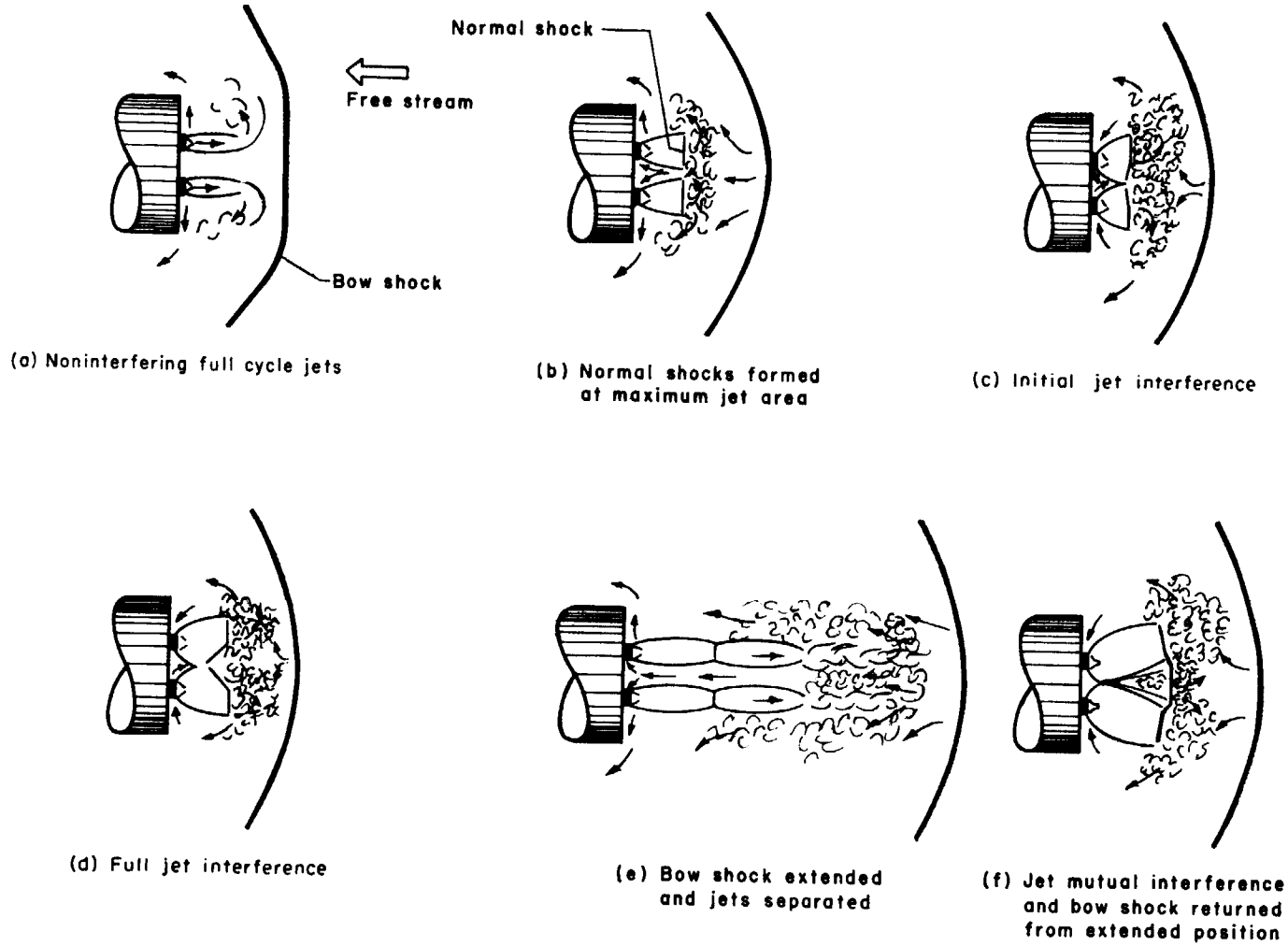

Figure 11.- Schematic representations (not to scale) of types of flows observed between the bow shock and model for progressively increasing ratio of jet to free-stream total pressures; $\alpha = 0^{\circ}$.

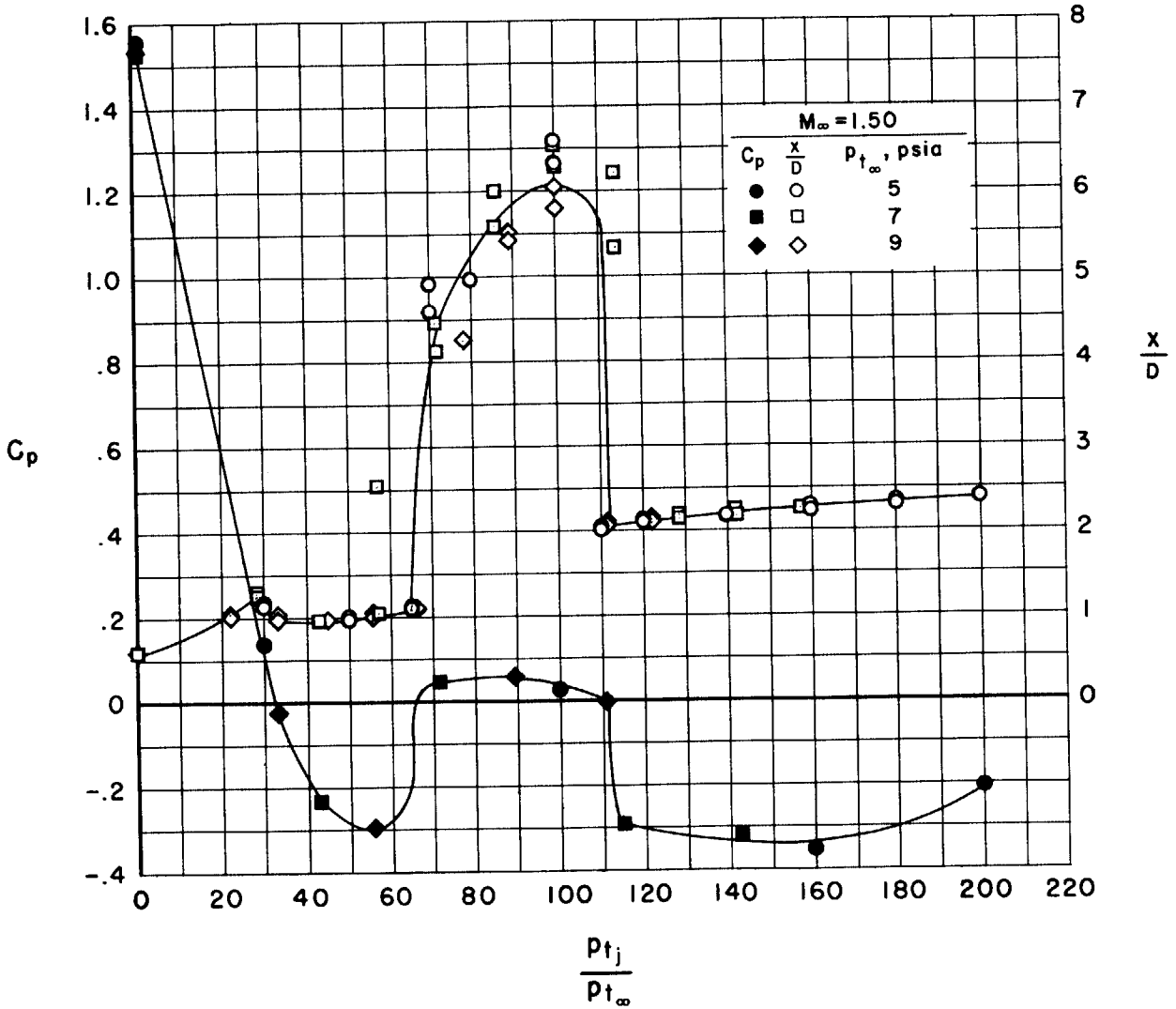

Figure 12.- Correlation of pressure coefficients on model face and bow shock standoff distance; $\alpha = 0^\circ$.

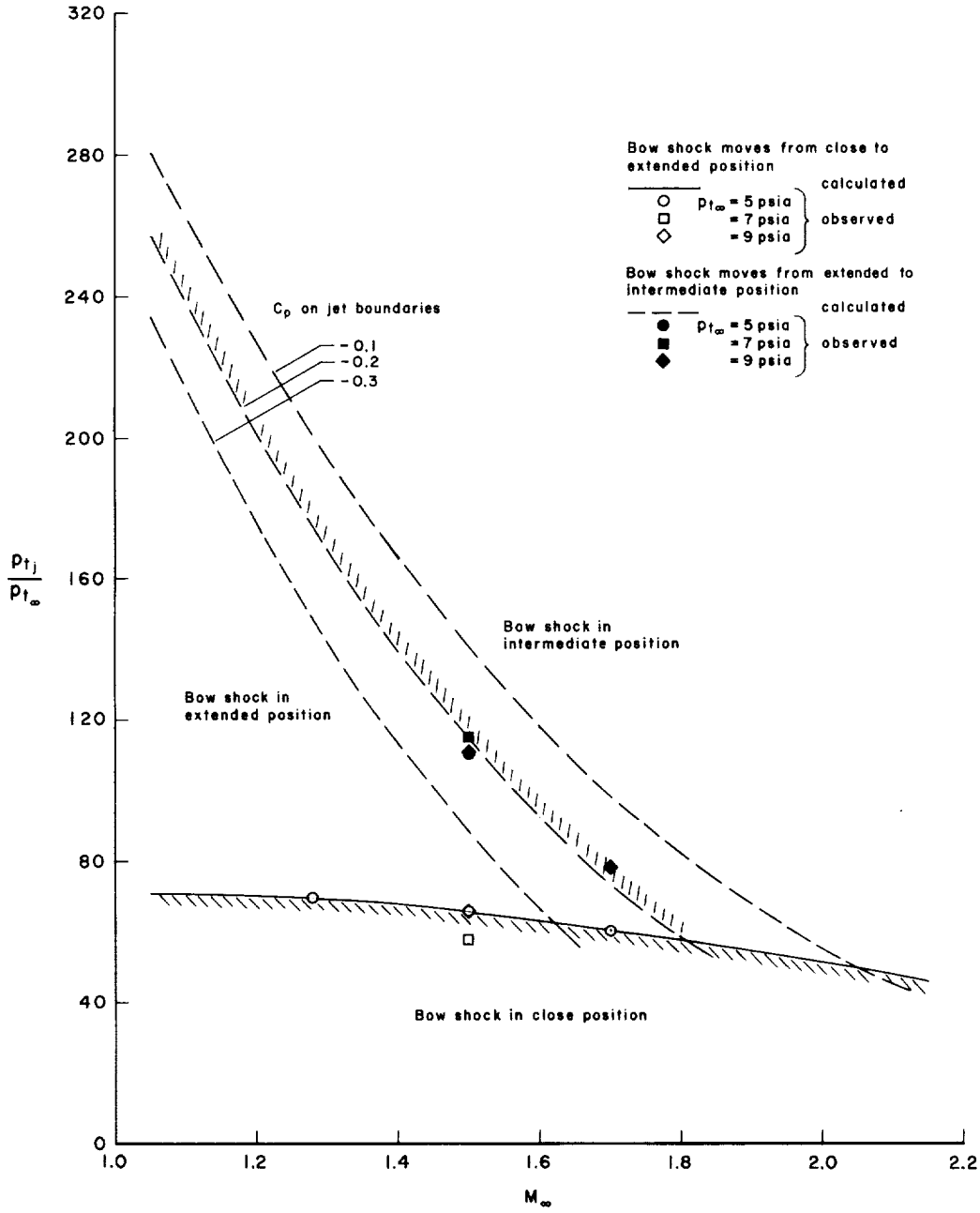

Figure 13.- Comparison of observed and calculated bow shock behavior; $\alpha = 0^\circ$.

NASA TN D-1300

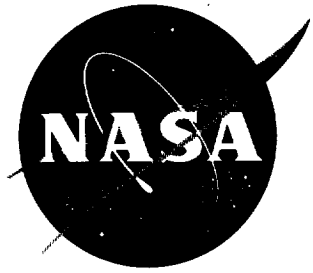

TECHNICAL NOTE
D-1300

EFFECTS OF SIMULATED RETROROCKETS ON THE AERODYNAMIC CHARACTERISTICS OF A BODY OF REVOLUTION AT MACH NUMBERS FROM 0.25 TO 1.90

By Victor L. Peterson and Robert L. McKenzie

Ames Research Center
Moffett Field, Calif.

NATIONAL AERONAUTICS AND SPACE ADMINISTRATION
WASHINGTON May 1962

NATIONAL AERONAUTICS AND SPACE ADMINISTRATION

TECHNICAL NOTE D-1300

EFFECTS OF SIMULATED RETROROCKETS ON THE AERODYNAMIC CHARACTERISTICS OF A BODY OF REVOLUTION AT MACH NUMBERS FROM 0.25 TO 1.90

By Victor L. Peterson and Robert L. McKenzie

SUMMARY

Force and moment coefficients are presented for a semiellipsoid body shape which had four simulated retrorockets on the forward flat face operating countercurrent to subsonic and supersonic airstreams. Experiments were performed at stream Mach numbers ranging from 0.25 to 1.90 and the retrorockets, which were simulated by expanding cold air through converging-diverging nozzles, were operated over a range of chamber pressures to 1000 psia. Model angle of attack was varied from 0° to 10°.

At all stream Mach numbers the force and moment coefficients exhibited a strong dependence on the ratio of jet to free-stream total pressures. The axial force, exclusive of retrothrust, was of considerably lower magnitude with the jets on than with the jets off. The large effect of the jets on the axial force caused the total decelerating force (drag plus retrothrust) to be nearly equal to the retrothrust alone. The pitching moments underwent erratic variations with changing ratio of jet to free-stream total pressures, but for a wide range of test conditions, they were of smaller magnitude with the jets on than with the jets off. At zero angle of attack and at low supersonic speeds the bow shock wave was observed to be in stable positions close to the model at low values of the jet to free-stream total pressure ratio, far upstream from the model at intermediate values of the pressure ratio, and in intermediate positions at high pressure ratios. The range of pressure ratios for which the bow shock was in the extended position decreased with increasing Mach number until at the highest Mach number the bow shock moved directly from the close position to the intermediate position. It appears that this bow shock phenomenon is peculiar to configurations having several nozzles in close proximity.

INTRODUCTION

The design of a vehicle required to execute a soft landing upon returning from a mission outside the atmosphere introduces a number of problems. Because of the large expenditure of energy required to overcome the earth's gravitational attraction in the launch phase of the

mission, it is imperative that the device used to decelerate and land the vehicle at the termination of a round-trip mission be as light in weight as possible. One such method would be to let aerodynamic drag reduce the velocity as much as possible and then use retrorockets to perform the terminal braking.

Some calculations were made to determine the interrelationships between various parameters of interest, such as fuel weight, velocity, drag coefficient, deceleration, and time of retrorocket operation. The analysis was simplified for this terminal phase by considering only vertical descents with continuous rocket motor operation; no consideration was given to stabilization or control of the vehicle. The vehicle chosen had a ratio of weight to reference area of 150 lb/sq ft prior to firing the retrorocket. The rocket motor had an area ratio corresponding to an exit Mach number of 3.5 and a chamber pressure of 500 psia, and was assumed to burn a fuel with a characteristic velocity of 5000 ft/sec. The results of this simplified analysis with these assumptions were quite sensitive to the value of drag coefficient assumed for the vehicle. For instance, the calculated fuel weights increased by as much as 40 percent as the drag coefficient was reduced from 0.8 to 0. Since the calculations indicated that the landing maneuver could be accomplished with fuel weights ranging from 10 to 20 percent of the initial vehicle weight for a variety of initial conditions, including velocities up to 1000 ft/sec, a further study of the aerodynamic forces and moments experienced by the vehicle during operation of the retrorocket would be of some interest.

A 5 6 8

The purpose of this report is to present measured forces and moments on a model having four simulated retrorockets operating countercurrent to subsonic and supersonic airstreams. The tests conducted in the Ames 6- by 6-Foot Supersonic Wind Tunnel were designed to be exploratory in nature; hence the selection of the configuration was somewhat arbitrary. The tests were performed at Mach numbers from 0.25 to 1.90 and the retrorockets, which were simulated by expanding cold air through converging-diverging nozzles, were operated over a range of chamber pressures to 1000 psia. Model angle of attack was varied from 0° to 10° to determine whether asymmetric flow could lead to stability and control problems when retrorockets are used.

Results of other investigations involving jet flow countercurrent to supersonic streams are presented in references 1 and 2.

SYMBOLS

A_e nozzle exit area

A_{ref} coefficient reference area, $\frac{\pi D^2}{4}$

C_A axial force coefficient, $\frac{\text{axial force}}{q_\infty A_{ref}}$

C_D drag coefficient, $\frac{\text{drag}}{q_\infty A_{ref}}$

C_m pitching-moment coefficient referred to center of model face, $\frac{\text{pitching-moment}}{q_\infty L A_{ref}}$

C_N normal-force coefficient, $\frac{\text{normal force}}{q_\infty A_{ref}}$

C_p pressure coefficient, $\frac{p - p_\infty}{q_\infty}$

C_T retrothrust coefficient, $\frac{\text{jet retrothrust}}{q_\infty A_{ref}}$

D model maximum diameter

L length of body including portion deleted by sting mounting

M Mach number

p static pressure

p_t total pressure

q dynamic pressure, $\frac{\gamma}{2} pM^2$

R radius of model face

x,r,θ cylindrical coordinates defined by figure 1(b)

α model angle of attack

γ ratio of specific heats

Subscripts

b model afterbody

e nozzle exit

f model face

j	jet
∞	free stream
2	pressure after exit from a normal shock

MODEL AND APPARATUS

Model Description

The model shape was a semiellipsoid with the 5.0-inch-diameter flat face forward. The semimajor axis of the model was 7.5 inches. Four nozzles in the model face were spaced 90° apart on a 2.12-inch-diameter circle. Each nozzle had a throat diameter of 0.20 inch, a conical converging section with a semivertex angle of 30°, and a conical diverging section with a semivertex angle of 15°. The exhaust cones were extended to a length sufficient for a nozzle-exit Mach number of 3.0 based upon one-dimensional flow considerations. All nozzles were connected to a common plenum chamber located within the model. The model was sting mounted in the wind tunnel in the manner shown in figure 1(a). A dimensional sketch of the complete model is presented in figure 1(b), and details of the nozzles are presented in figure 1(c).

Pressure orifices of 0.030-inch diameter were installed flush with the model surface at 87 positions on the model face and at 62 positions on the body. The exact locations of the orifices are tabulated in figure 1(b).

The model used in this investigation was intended to represent a reentry vehicle that would employ rocket braking for terminal recovery after aerodynamic braking had slowed the descent to low supersonic speeds. Rather arbitrary choices were made, however, regarding the details of the configuration. Multiple nozzles were used with a ratio of nozzle throat to vehicle reference area of 0.0064 which was considered representative of a possible full-scale vehicle. In terms of a vehicle weighing 10,000 pounds with a reference diameter of 8 feet, this area ratio corresponds to maximum values of retrothrust ranging from 35,000 to 70,000 pounds for motor chamber pressures ranging from 500 to 1,000 psia, respectively.

Apparatus and Instrumentation

The simulated retrorockets were supplied by a high-pressure source of dry air which was controlled by two remotely operated pneumatic valves. Air was piped to the model plenum chamber through a hollow streamlined strut and sting as shown in figure 1(a). Pressure in the plenum chamber was measured by a probe (see fig. 1(b)) connected to two high-accuracy

Bourdon-tube dial gages of different pressure ranges. Plenum chamber temperature was measured by an iron-constantan thermocouple (see fig. 1(b)) connected to an automatic recording potentiometer. Model surface pressure orifices were connected to manometer tubes filled with tetrabromoethane (specific gravity = 2.92 at 80° F). Liquid column heights were photographically recorded. Shadowgraph apparatus was used to provide photographs of the flow field in the vicinity of the model.

TESTS AND PROCEDURE

Ranges of Test Variables

Tests were conducted at free-stream Mach numbers of 0.25, 0.65, 0.80, 1.50, 1.70, and 1.90. Free-stream total pressure was set at 12, 14, and 16 psia for $M_\infty = 0.25$ and at 5, 7, and 9 psia for all other free-stream Mach numbers. Free-stream Reynolds numbers varied from 1.3 to 2.6 million per foot for these ranges of pressures and Mach numbers. At Mach numbers of 0.65 and 1.70 the model was positioned only at zero angle of attack but for all other Mach numbers the angles of attack were 0°, 5°, and 10°. For each set of free-stream conditions and model attitude the nozzle plenum chamber pressure was varied up to 1000 psia. Operation over this pressure range resulted in combined weight flows through the four nozzles of between 0 and about 3.1 pounds per second. Shadowgraphs were taken at every data point. A special series of shadowgraphs was made, without accompanying model pressure distribution data, at free-stream Mach numbers of 1.28, 1.50, and 1.70 to investigate more thoroughly the flow field around the model.

Data Reduction

Pressure coefficients were computed from the individual pressure measurements made on the model surface. Force and moment coefficients for the model face were obtained from integrations of the pressure coefficients over the model face excluding the nozzle exits. For the model body, the force and moment coefficients were obtained from integrations of the pressure coefficients over all the body except that portion deleted by the sting mounting (see fig. 1(b)). The total force and moment coefficients for the model were then obtained from a summation of the face and body contributions. To perform the various integrations it was necessary to extrapolate certain quantities; for example, because of physical limitations, no orifices could be located on the model face at values of $r_f/R = 1.0$. Therefore, to provide consistent results for the integrated coefficients, the necessary values of pressure coefficient were obtained mathematically by passing a second degree curve through the three experimental data points nearest the unknown value and extrapolating to the desired model location.

The retrothrust coefficient, C_T, was based on free-stream dynamic pressure and model reference area to allow direct magnitude comparisons with other force coefficients. Retrothrust coefficients were calculated by means of the following equation:

$$C_T = \frac{4\left(\frac{A_e}{A_{ref}}\right)\left[\left(\frac{p_{t_j}}{p_{t_\infty}}\right)\left(\frac{p_e}{p_{t_j}}\right)\left(1 + \gamma_j M_j^2\right) - \frac{p_\infty}{p_{t_\infty}}\right]}{\left(\frac{q_\infty}{p_{t_\infty}}\right)}$$

A 5 6 8

The ratio (p_e/p_{t_j}) and the jet Mach number M_j appearing in the above equation were determined from equations based on the assumption of one-dimensional isentropic flow.

Accuracy

The free-stream Mach numbers quoted are nominal values and are accurate within ± 0.04. However, each set of data at a given Mach number, angle of attack, and free-stream pressure is consistent in Mach number within ± 0.02. Pressure measurements on the model surface are accurate within ± 0.02 psia. With the jets off, a comparison of the pressure coefficients at the center of the model face with those calculated for free-stream stagnation conditions showed differences amounting to 8.0 percent at the lowest Mach number ($M_\infty = 1.25$) diminishing to 1.3 percent at the highest Mach number ($M_\infty = 1.90$). This relatively large error at the lower Mach numbers, where small differences between total and static pressures must be measured, was much greater than the scatter in values of local coefficient. The gage used to indicate the pressure measured by the probe within the nozzle plenum chamber was accurate to ± 1.5 percent throughout the pressure range. Nozzle exit Mach number was measured and found to vary between 3.04 and 3.06 across the exit planes. Boundary-layer thicknesses inside the nozzles at the exits were negligible compared to the exit diameter. No adjustments of model angle of attack or angle of sideslip were made for wind-tunnel stream inclinations which are known not to exceed $\pm 0.3^\circ$. Body force errors due to the presence of the sting were found from pressure measurements to be negligible compared to other model forces.

RESULTS AND DISCUSSION

A cursory examination of the force and moment coefficients for the model at zero angle of attack showed abrupt and seemingly erratic variations of these parameters with the ratio of jet to free-stream total pressure. This effect was particularly evident at supersonic free-stream Mach numbers. Further study showed that rapid changes in certain coefficients appeared to be linked with the behavior of the bow shock wave and mutual interactions of the jets observed in shadowgraphs taken throughout the tests. Therefore, since the flow over the model was dictated to some extent by interactions between the jets themselves and the jets and free stream, the flow phenomena ahead of the model are described prior to interpretation of the resulting pressure and integrated force and moment coefficients.

Bow Shock and Interference Phenomena

Tests of the model at zero angle of attack and at some supersonic Mach numbers revealed abrupt changes in the bow shock standoff distance at certain jet pressures. Shadowgraphs of this phenomenon are presented in figure 2 for the model at zero angle of attack and for a free-stream Mach number of 1.50. The photographs of figure 2 show that the bow shock assumed a position close to the model at low jet pressures, moved far upstream from the model at intermediate jet pressures, and then returned to an intermediate position at high jet pressures. For these particular free-stream conditions ($M_\infty = 1.50$, $p_{t_\infty} = 7$ psia) the ratio of jet to free-stream total pressures at which the bow shock moved abruptly away from the model was about 57.2 This is evidenced by figures 2(d) and 2(e) which show the bow shock at two different positions for this jet pressure. Measurements, obtained from shadowgraphs, of the variation of bow-shock position with jet to free-stream total pressure ratio are presented in figure 3 for free-stream Mach numbers of 1.50, 1.70, and 1.90. These results show that at the highest free-stream Mach number the bow shock moved directly from the close to the intermediate position. The results in figure 3 also indicate that bow shock standoff distance was a function of the total pressure ratio, p_{t_j}/p_{t_∞}, rather than individual pressure magnitudes.

A detailed analysis of the circumstances believed to be responsible for the unusual behavior of the bow shock wave is presented in the appendix. Also included therein are results of calculations made using theory for free jets exhausting into still air to obtain a correlation with the data of this investigation.

Pressures on the Model Surface

The force and moment coefficients obtained from integrations of the pressures on the model surface are of primary interest. For this reason, only representative samples of the distributions of pressure on the model with and without the simulated retrorockets operating are presented.

The effects of the retrojets on the model pressure coefficients at subsonic speeds are typically illustrated in figure 4 for a Mach number of 0.65 and an angle of attack of 0°. The data of figure 4 show a large difference between the jet-off and jet-on distributions of pressures, but the pressures on the model were relatively independent of jet total pressure for total pressures between 300 and 1000 psia. The results of figure 4(a) show that the jets prevented attainment of free-stream stagnation pressure on the model face; in fact, the pressures on the model face with the jets on were quite near free-stream static pressure. For the model body (fig. 4(b)), with the jets off, the pressure distributions were indicative of separated flow. This observation was substantiated by shadowgraphs. With the jets on, however, the pressures at the rear of the body recovered to near free-stream static pressure and there was no evidence of flow separation in the shadowgraphs. It might be conjectured that the highly turbulent mixture of tunnel flow and turned jet flow was attached over the rearward portion of the body.

Typical effects of the retrojets on the model pressure coefficients at supersonic speeds are illustrated in figure 5 for a Mach number of 1.70 and an angle of attack of 0°. The data of figure 5 show dependence on jet total pressure, over a wider range, than did the subsonic results of figure 4. The dependence of model face pressure distributions on jet total pressure shown in figure 5(a) results primarily from the effects of total pressure ratio p_{t_j}/p_{t_∞} on the position of the bow shock wave which are discussed in the appendix. On the model body, effects of the jets on the pressure distributions at supersonic speeds (fig. 5(b)) were encountered with the bow shock wave in the extended position. The flow over the model body apparently was quite similar with the jets on or off, though, since the pressures were nearly the same in magnitude and distribution. Shadowgraphs for these conditions indicated attached flow over most of the body.

Force and Moment Coefficients

All of the force and moment coefficients were obtained from integrations of the pressure coefficients and thus exclude effects due to frictional forces acting on the model surface. It should also be remembered that retrothrust from the simulated rockets contributed to these coefficients only to the extent that the presence of the jets altered the pressures over the model surface.

The coefficients of axial force are presented in figure 6 as a function of the jet to free-stream total pressure ratio. The contributions of the model face and model body are presented separately in figures 6(a) and 6(b), respectively, and the sum of the two contributing model components is presented in figure 6(c). The results of figure 6(a) for the model face show the values of the coefficient obtained with the nozzles operating to be considerably lower than those obtained with no nozzle flow. In fact, negative values of C_{A_f} prevailed for a wide range of test conditions. Values of this coefficient were somewhat higher over the ranges of total pressure ratio for which the bow shock wave was in the extended position; for example, at $M_\infty = 1.50$, $\alpha = 0^\circ$, $65 < p_{t_j}/p_{t_\infty} < 110$. The component of axial force coefficient contributed by the model body showed more dependence on jet operation at subsonic Mach numbers than at supersonic Mach numbers (see fig. 6(b)). Also, it is shown that movement of the bow shock to the extended position caused the body axial force coefficient to be reduced. This contrasts with the increase in axial force coefficient of the model face measured for the same conditions; for example, compare results of figures 6(a) and 6(b) for $M_\infty = 1.50$. The axial force coefficients for the complete model (fig. 6(c)) generally follow the trends with pressure ratio established by the model face.

The normal-force coefficients, which are simply the pressure loads on the model body, are presented in figure 7 as a function of the jet to free-stream total pressure ratio. These coefficients displayed erratic variations with pressure ratio and angle of attack. However, it is noted that while the normal forces were positive at positive angles of attack for $M_\infty = 0.80$, they were predominantly negative at supersonic Mach numbers. It is believed that the negative normal forces at supersonic speeds probably resulted from longer runs of attached flow on the lower surface of the body than on the upper surface when the model was at angle of attack. Shadowgraphs for the jet-off conditions substantiate this.

The pitching-moment coefficients resulting from pressure loads on the model are presented in figure 8 as a function of the jet to free-stream total pressure ratio. The pitching-moment coefficients for the model face (fig. 8(a)) arise from asymmetric axial loading. Thus, they are independent of the model moment reference center, provided it lies on the longitudinal axis of the model. A measure of the symmetry of the model face and of the nozzle flows is afforded by the insignificant pitching moments of the model face at zero angle of attack. The variation of pitching moment of the model face with angle of attack was positive (static instability) at all Mach numbers with the jets both off and on. Turning the jets on to low values of the pressure ratio p_{t_j}/p_{t_∞} resulted in large destabilizing effects. At subsonic speeds, these large effects persisted throughout the entire range of pressure ratios. However, at supersonic speeds they diminished with increasing pressure ratio until at the highest pressure ratios small stabilizing effects existed. The pitching-moment coefficients for the model body are presented in figure 8(b). In most cases these pitching-moment results reflected trends consistent with the normal-force results; however, in some cases the

asymmetric axial loading predominated. The total pitching-moment coefficients for the model are presented in figure 8(c). The variations of this parameter with pressure ratio were quite erratic but were repeatable at any given set of conditions. In general, these results show that the nozzles could be operated over a wide range of pressure ratios without the pitching-moment coefficients exceeding values for jets-off conditions.

The total decelerating force consists of model drag plus retrothrust. This quantity could not be measured directly but an indication of its magnitude, exclusive of skin-friction drag, was obtained by adding drag coefficients due to integrated pressure loads to calculated retrothrust coefficients based on free-stream dynamic pressure and model reference area. Curves showing the dependence of the calculated retrothrust coefficient on free-stream Mach number and jet to free-stream total pressure ratio are presented in figure 9 for the model of this investigation. Of note is the fact that for a given total pressure ratio the retrothrust coefficient is very large at low subsonic speeds and relatively small at supersonic speeds. The total decelerating force coefficients are presented as a function of retrothrust coefficient in figure 10 for zero angle of attack. The total decelerating force was nearly always less than the jets-off drag of the model for values of retrothrust coefficient smaller than the jets-off drag coefficient. Thus, if the purpose of the retrorockets were to slow the descent of the vehicle it would not be practical to operate the rockets at these low retrothrust coefficients. For values of retrothrust coefficient above the jets-off drag coefficient the results of figure 10 indicate that the total retarding force was very nearly equal to the retrothrust itself. This trend was to be expected because of the previously discussed effects of the jets on the axial force coefficients.

CONCLUSIONS

An experimental investigation directed toward the determination of the effects of simulated retrorockets on the aerodynamic characteristics of a body of revolution showed that:

1. Force and moment coefficients exhibited a dependence on the ratio of jet to free-stream total pressures.

2. The axial forces, exclusive of retrothrust, were of considerably lower magnitude when the jets were on than when they were off; in fact, they were negative for some test conditions. Thus, the total decelerating force (drag plus retrothrust) was generally less than the jets-off drag for values of retrothrust less than the jets-off drag and approximately equal to the thrust for higher values.

3. The pitching moments underwent erratic variations with changing ratio of jet to free-stream total pressures, but for a wide range of test conditions, they were of smaller magnitude with the jets on than with the jets off.

4. At zero angle of attack and at some supersonic speeds the bow shock wave was observed to be in stable positions close to the model at low values of the jet to free-stream total pressure ratio, far upstream from the model at intermediate values of the pressure ratio, and in intermediate positions at high pressure ratios. It appears that this bow shock phenomenon is peculiar to configurations that have several nozzles in close proximity.

Ames Research Center
National Aeronautics and Space Administration
Moffett Field, Calif., Feb. 2, 1962

APPENDIX

ANALYSIS OF BOW SHOCK AND JET INTERFERENCE PHENOMENA

For the purpose of directing attention to pertinent circumstances affecting the flow field between the bow shock and model, a series of sketches made from a study of enlargements of the shadowgraphs of figure 2 is presented in figure 11. These sketches illustrate the sequence of events that gave rise to the unusual behavior of the bow shock. With the nozzles operating at relatively low total pressure the initial portions of the jets were separated, were free of normal shocks, and displayed an expansion and contraction cycle similar to the first of multiple cycles common to free jets. This type of flow field, which is sketched in figure 11(a), was observed to occur for values of the pressure ratio p_{t_j}/p_{t_∞} between 22, the lowest at which the jets were operated, and 28 at $M_\infty = 1.50$. Within this range the total pressures of the jet and free-stream flows were apparently matched by viscous losses and a series of weak shock waves in the jets. Increasing the pressure ratio from 22 to 28 caused the bow shock to move from about 1.0 to 1.3 model diameters ahead of the model face as shown by the results of figure 3.

Concurrent with the upstream movement of the bow shock was an expansion of the boundaries of each jet. The maximum cross-sectional area of each jet increased as a result of this expansion and reached a value for which the local Mach number at the maximum area, in combination with existing pressures, was sufficient to support a normal shock in the first cycle of each jet. The flow field then took the form sketched in figure 11(b). This type of flow field occurred for total pressure ratios between 28 and 57 to 65, depending upon free-stream pressure, at $M_\infty = 1.50$. The presence of the normal shock in each jet nearly arrested the movement of the bow shock with changing total pressure ratio in this range as shown in figure 3. The continued expansion of the jet boundaries with increasing jet pressure in this range caused the boundaries of the jet from each nozzle to interfere physically with one another as shown in figure 11(c). The jet interference became more pronounced as pressure ratio continued to increase until no further inward expansion was possible. At this point the flow field was observed to appear like that sketched in figure 11(d).

Raising total pressure ratio above about 60 at $M_\infty = 1.50$ increased the difference between $p_{t_{\infty_2}}$ and p_{t_j} to the extent that normal shocks in the jets in conjunction with viscous losses could no longer match $p_{t_{\infty_2}}$ and p_{t_j}. The normal shock disappeared and jet interference abruptly terminated. Each jet then developed at least one full expansion-contraction cycle which extended the high pressure region of the jets further upstream

from the model and thereby moved the bow shock upstream. Further increase in total pressure ratio increased the number of expansion-contraction cycles in the jets and caused the bow shock to move even farther upstream. A qualitative sketch of this type of flow field is shown in figure 11(e). The flow field in which the bow-shock position was extended existed between the values of p_{t_j}/p_{t_∞} of about 60 and 110 for $M_\infty = 1.50$ as shown by figure 3.

At the onset of the fully developed cyclic jet flow the jets were distinctly separated but as the ratio of jet to free-stream total pressure was further increased, the jets were forced to expand again and finally interfere for the second time. This time an oblique shock wave formed in the jets at the contact point and deflected them away from the center line of the model. The extended high pressure region ahead of the model was destroyed and the bow shock moved abruptly to a position several model diameters closer to the model face. A sketch of this flow condition is shown in figure 11(f). Further increase in pressure ratio only enlarged the flow pattern shown in figure 11(f) which, in turn, resulted in the gradual upstream movement of the bow shock shown for $p_{t_j}/p_{t_\infty} > 112$ in figure 3. It is conceivable that the entire cycle of normal shocks forming in the jets, jet mutual interference, and bow shock extension and return could repeat itself at higher jet pressures with retention of the oblique shock at the point of mutual jet interference. However, pressure ratios of a higher magnitude were not obtainable to substantiate this.

The abrupt upstream movement of the bow shock and its subsequent movement back toward the model might be expected to be accompanied by similarly abrupt variations in the pressure coefficient on the model, especially the model face. A typical comparison of pressure coefficient on the model face and bow shock standoff distance as a function of the total pressure ratio is made in figure 12 for a free-stream Mach number of 1.50. The pressure coefficients measured at r_f/R of 0.5 and four values of θ_f, $\pm 22.5^\circ$ and $\pm 67.5^\circ$, were averaged to provide a mean value of pressure coefficient between the nozzle exits for this comparison. This comparison shows that as the total pressure ratio was increased to about 60 the pressure coefficient varied smoothly from stagnation to a negative value. Then, as the bow shock moved upstream, pressure coefficient jumped to a small positive value. At total pressure ratio above about 112 the pressure coefficient became negative.

In an attempt to gain further insight into the flow phenomena, an interesting correlation was found to exist between the data of this investigation and calculations made using theory for free jets exhausting into still air. As noted previously, the apparent sequence of events based on shadowgraphs lead to the conclusion that just prior to the movement of the bow shock to the extended position, the jets were expanded to the longitudinal center line of the model and each jet contained a normal shock at its maximum area. The assumptions that (a) a normal shock exists at the maximum area of the first cycle of a free jet, (b) the

maximum jet radius is equal to the distance between the nozzle center line and the model longitudinal center line, and (c) the jet total pressure behind the jet normal shock is equal to the free-stream total pressure behind a normal bow shock (i.e., $p_{t_{j_2}} = p_{t_{\infty_2}}$), made it possible to use the results of reference 3 to calculate the total pressure ratio necessary to satisfy the given conditions. These calculations describe the ratios of total pressures as a function of free-stream Mach number at which the bow shock would move abruptly upstream.

The total pressure ratios, as a function of M_∞, for which the bow shock should move back toward the model were also calculated. A correlation of the shadowgraphs and the pressure coefficients measured on the model face near the nozzle exits showed that after the bow shock returned from its extended position, the pressure coefficient was between about -0.1 and -0.3. Also, as pointed out previously, at the time of the bow shock return the jets had again expanded sufficiently to interfere mutually. Thus, the assumptions that the pressure coefficient measured on the model face near the nozzle exits was indicative of the pressure coefficient along the jet boundaries and that the maximum jet radius was equal to the distance between the nozzle center line and the model center line, made it possible again to use the results of reference 3 to obtain the ratio of total pressure necessary to satisfy these conditions.

A 5 6 8

The results of both of the aforementioned calculations are presented in figure 13 wherein the experimental data are also shown for comparison. The experimental and calculated pressure ratios for which the bow shock moves to the extended position are in nearly perfect agreement. The experimentally measured trend showing the range of total pressure ratios for which the bow shock was in the extended position to diminish and disappear with increasing free-stream Mach number is also predicted by the calculations.

It should be emphasized that even though the calculations agree quite well with the experimental measurements, it remains to be proven whether or not this semiempirical analysis would apply to other multijet configurations.

REFERENCES

1. Charczenko, Nickolai, and Hennessey, Katherine W.: Investigation of a Retrorocket Exhausting From the Nose of a Blunt Body into a Supersonic Free Stream. NASA TN D-751, 1961.

2. Hayman, Lovick O., Jr., and McDearmon, Russell W.: Jet Effects on Cylindrical Afterbodies Housing Sonic and Supersonic Nozzles Which Exhaust Against a Supersonic Stream at Angles of Attack From 90° to 180°. NASA TN D-1016, 1962.

3. Love, Eugene S., Grigsby, Carl E., Lee, Louise P., and Woodling, Mildred J.: Experimental and Theoretical Studies of Axisymmetric Free Jets. NASA TR R-6, 1959.

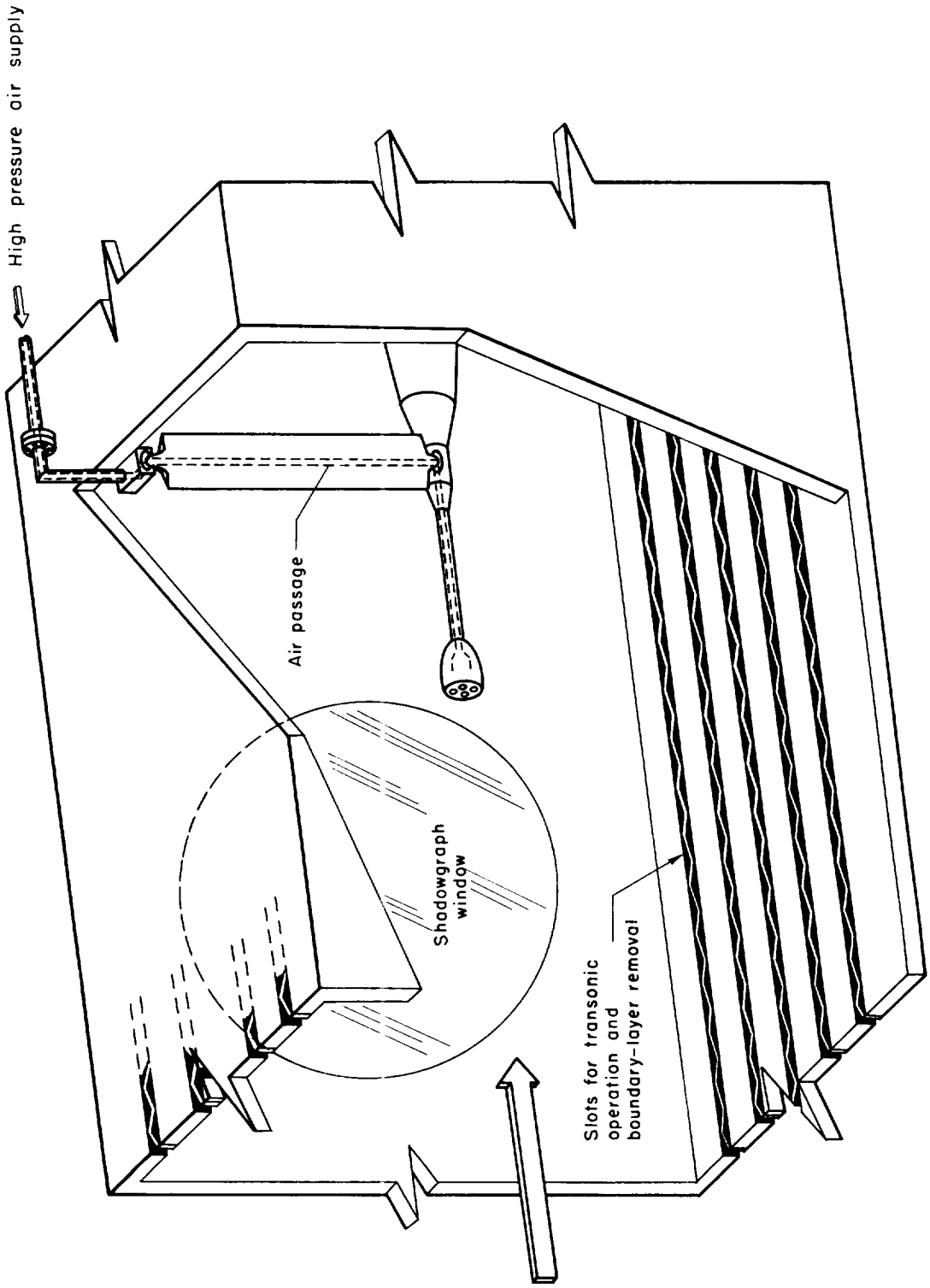

(a) Schematic drawing of model installed in wind tunnel.

Figure 1.- Wind-tunnel installation and model sketches.

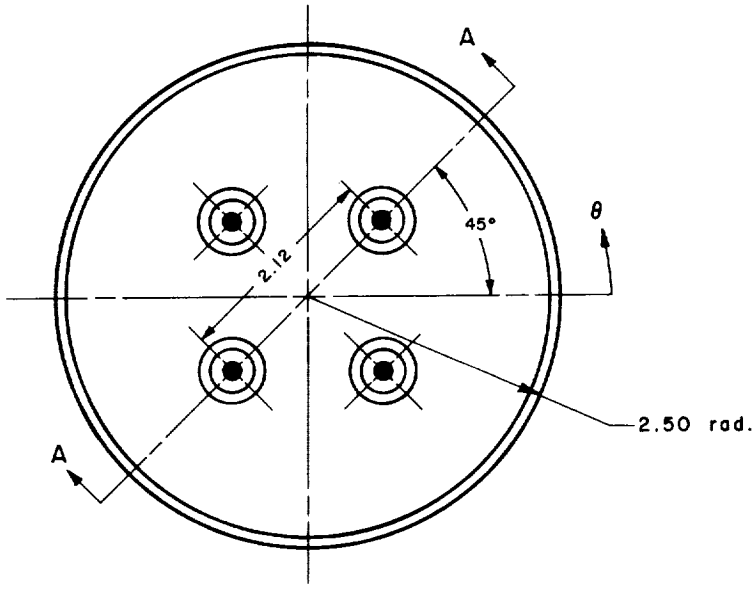

MODEL FACE

Body orifice locations								
	θ_b, deg							
	-90.0	-60.0	-30.0	0	30.0	60.0	90.0	180.0
$-\frac{x}{L}$	0.05	0.05	0.05	0.05	0.05	0.05	0.05	0.05
	.10	.10	.10	.10	.10	.10	.10	.10
	.20	.20	.20	.20	.20	.20	.20	.20
	.40	.40	.40	.40	.40	.40	.40	.40
	.60	.60	.60	.60	.60	.60	.60	.60
	.70	.70	.70	.70	.70	.70	.70	.70
	.80	.80	.80	.80	.80	.80	.80	.80
		.90	.90	.90		.90	.90	.90

Face orifice locations										
	θ_f, deg									
	-90.0	-67.5	-45.0	-22.5	0	22.5	45.0	67.5	90.0	180.0
$\frac{r_f}{R}$	0.	0.	0.	0.	0.	0.	0.	0.	0.	0.
	.10	.10	.10	.10	.10	.10	.10	.10	.10	.10
	.20	.20	.20	.20	.20	.20	.20	.20	.20	.20
	.30	.30	.25	.30	.30	.30	.25	.30	.30	.30
	.40	.40	.60	.40	.40	.40	.60	.40	.40	.40
	.50	.50	.70	.50	.50	.50	.70	.50	.50	.50
	.60	.60	.80	.60	.60	.60	.80	.60	.60	.60
	.70	.70	.90	.70	.70	.70	.90	.70	.70	.70
	.80	.80		.80	.80	.80		.80	.80	.80
	.90	.90		.90	.90	.90		.90	.90	.90

(b) Model details and dimensions.

Figure 1.- Continued.

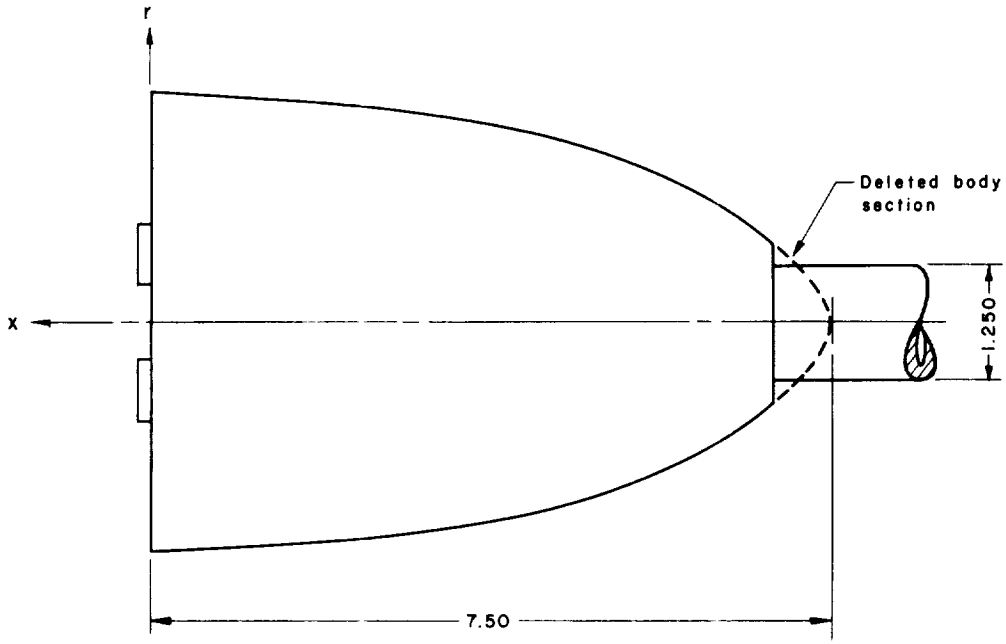

MODEL AFTERBODY AND STING

Note: all dimensions in inches unless otherwise noted

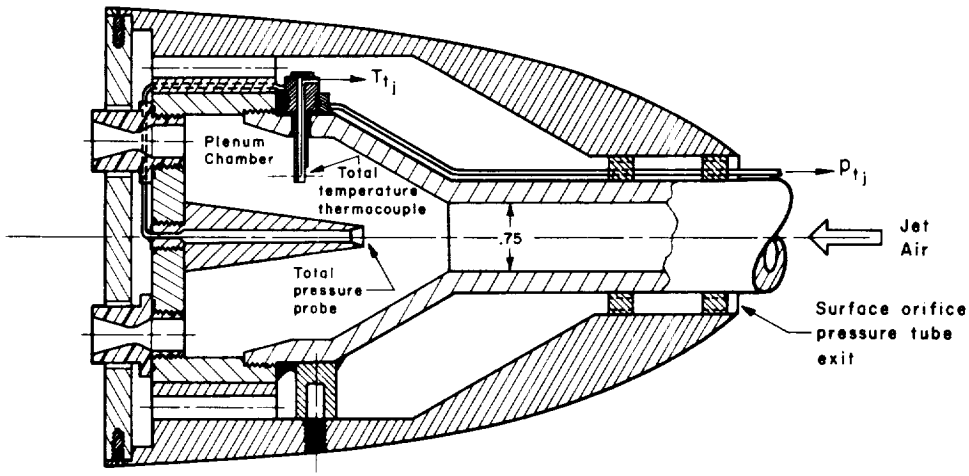

SECTION A-A

MODEL INTERNAL CONFIGURATION

(Surface pressure orifices not shown)

(b) Model details and dimensions - Concluded.

Figure 1.- Continued.

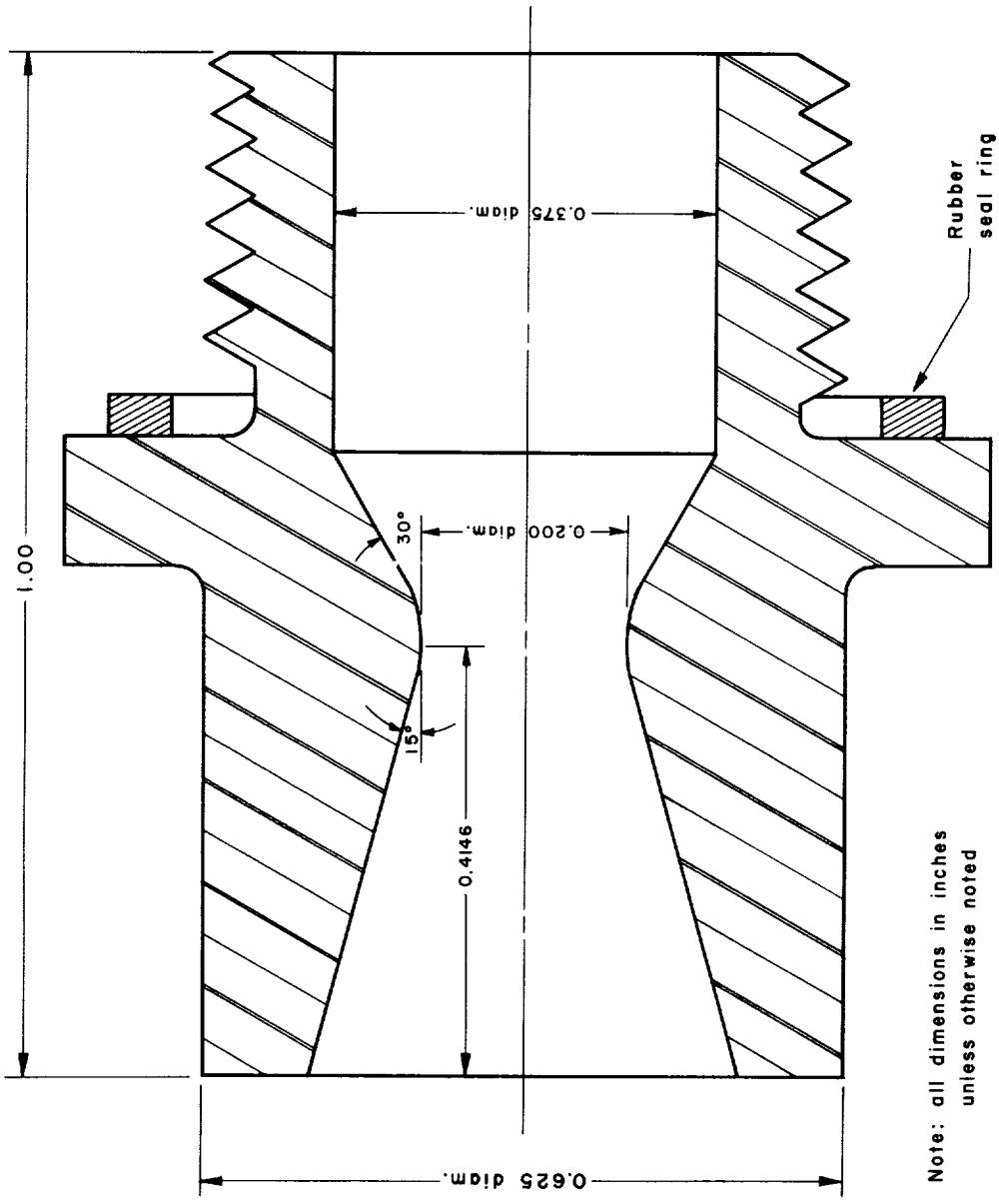

(c) Details of jet nozzles.

Figure 1.- Concluded.

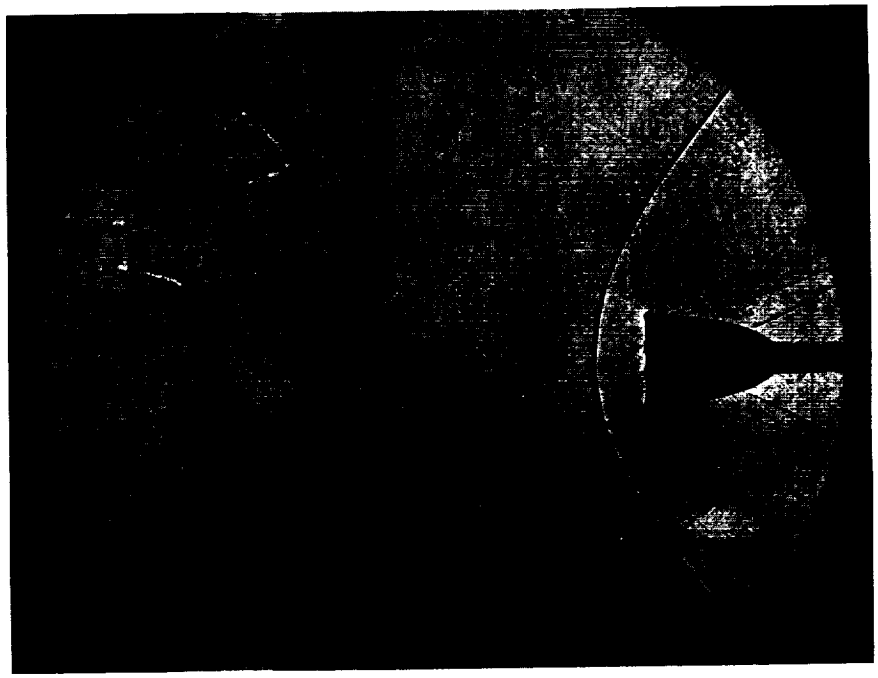

(a) Jets off.

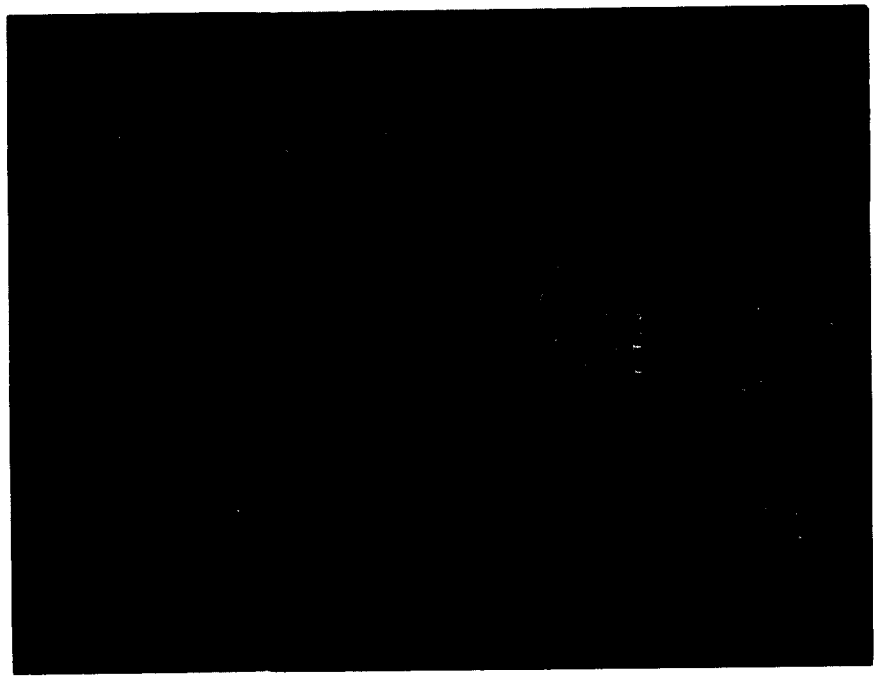

(b) $p_{t_j}/p_{t_\infty} = 28.6$

Figure 2.- Shadowgraphs illustrating effect of jet to free-stream total pressure ratio on bow shock position; M = 1.50, p_{t_∞} = 7 psia, $\alpha = 0^\circ$.

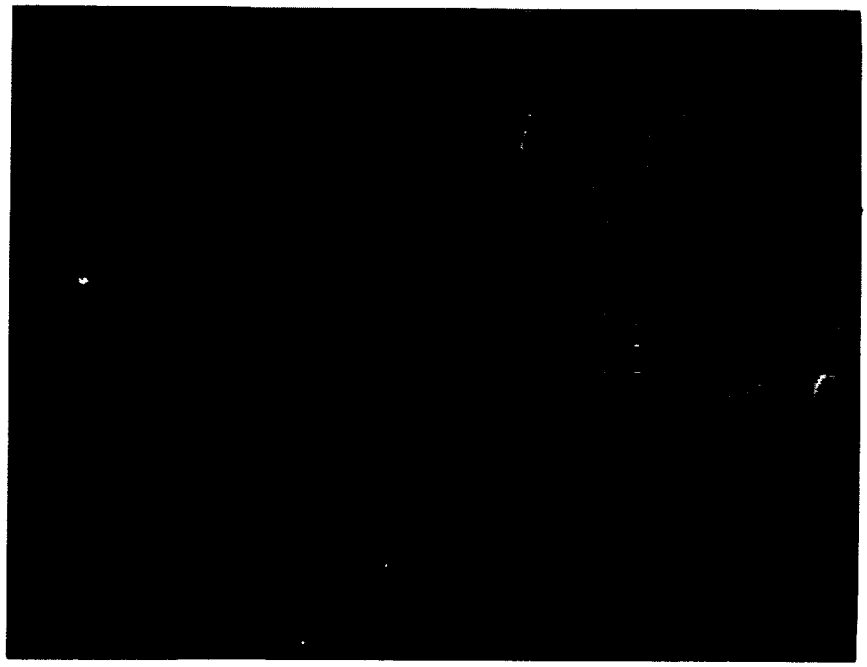

(c) $p_{t_j}/p_{t_\infty} = 42.9$

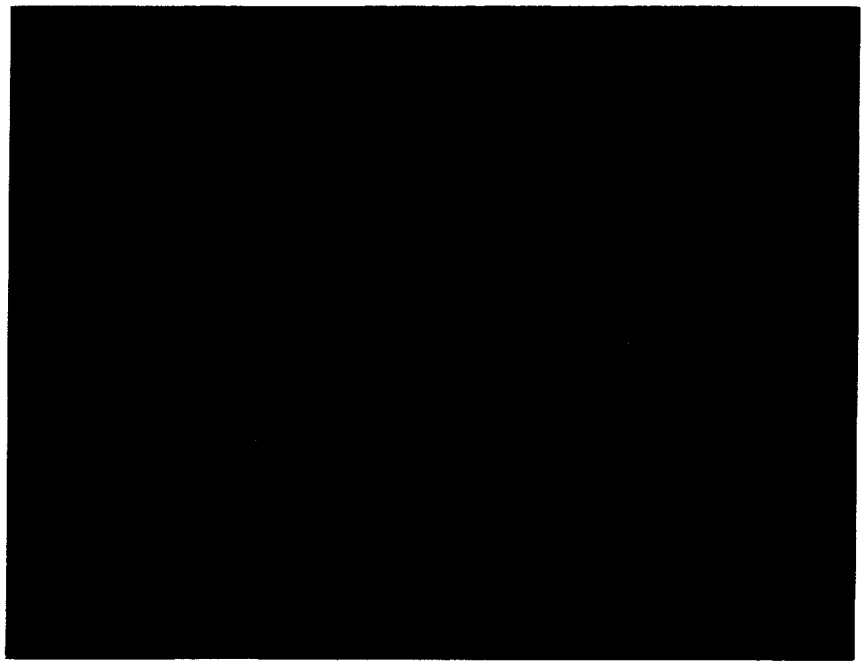

(d) $p_{t_j}/p_{t_\infty} = 57.2$

Figure 2.- Continued.

(e) $p_{t_j}/p_{t_\infty} = 57.2$

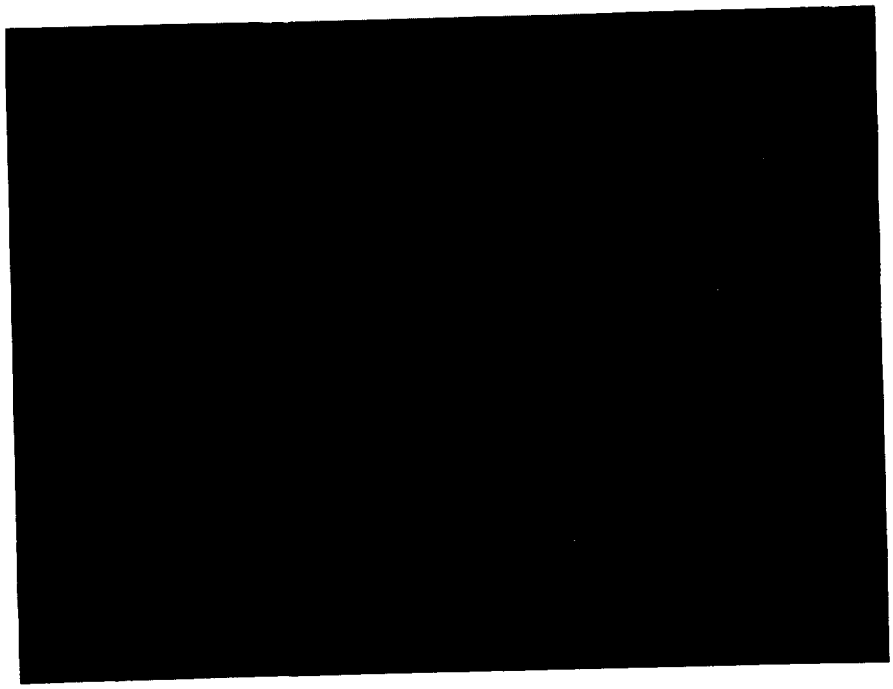

(f) $p_{t_j}/p_{t_\infty} = 71.4$

Figure 2.- Continued.

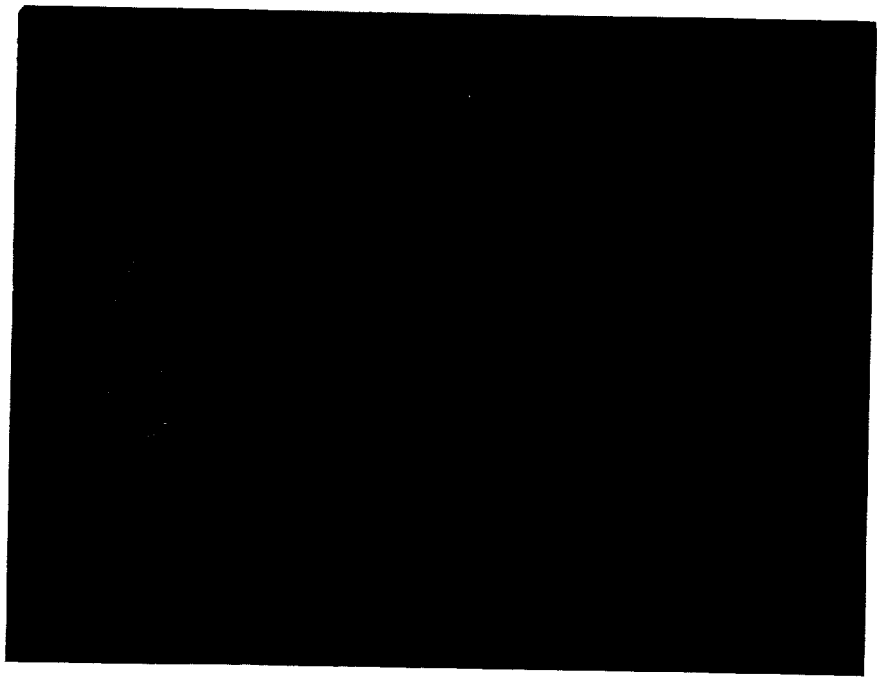

(g) $p_{t_j}/p_{t_\infty} = 85.7$

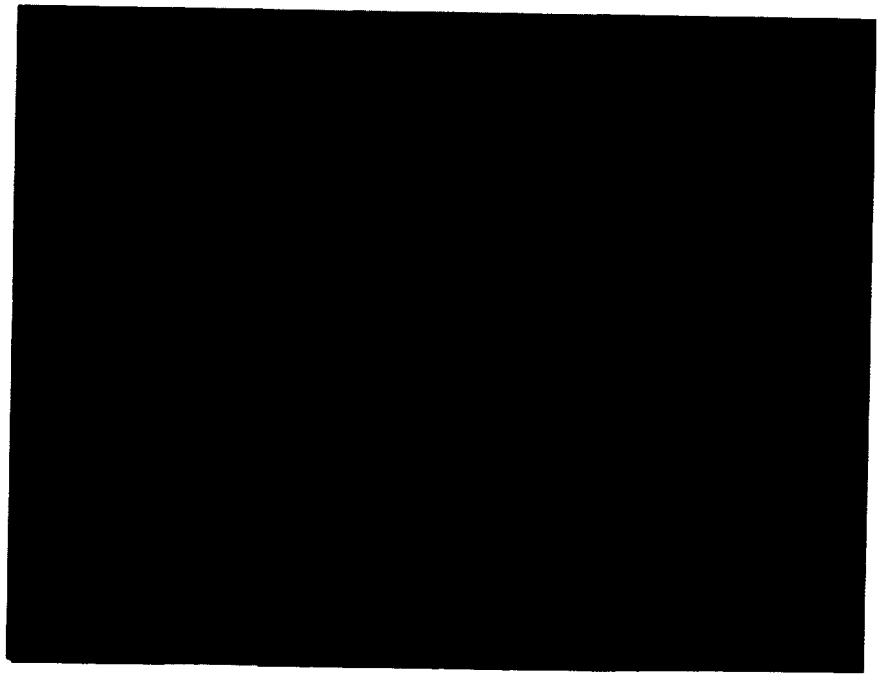

(h) $p_{t_j}/p_{t_\infty} = 100.0$

Figure 2.- Continued.

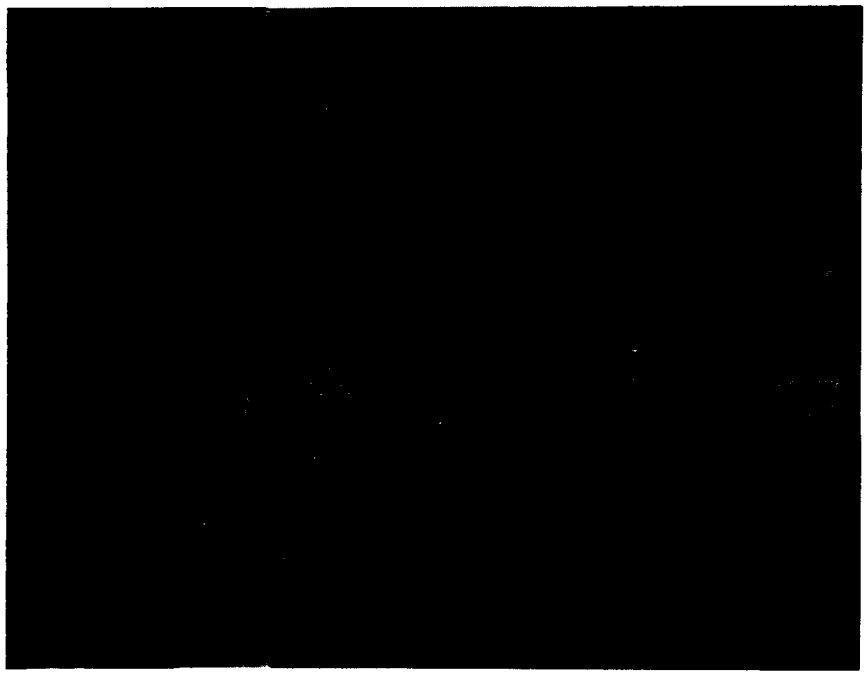

(i) $p_{t_j}/p_{t_\infty} = 114.3$

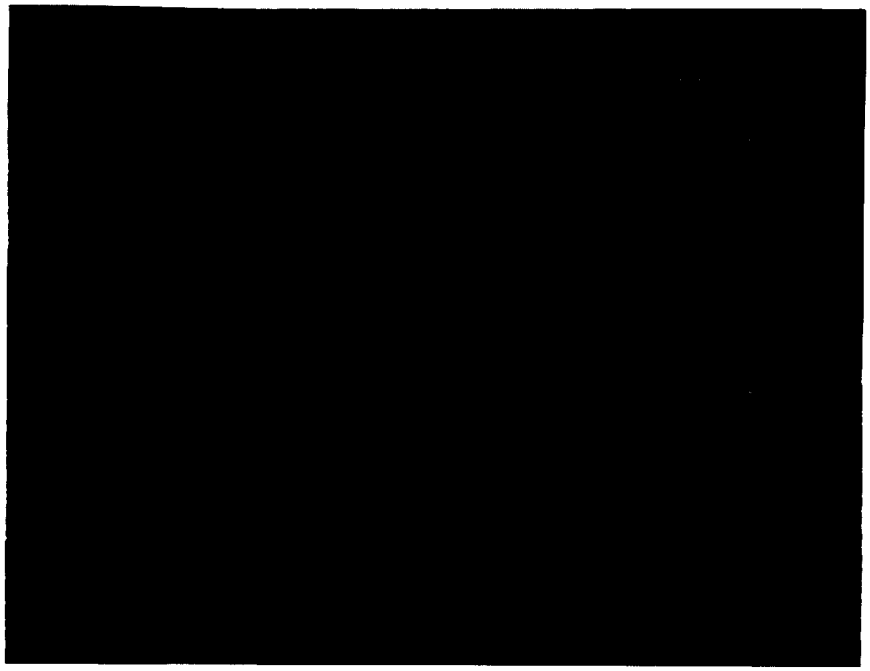

(j) $p_{t_j}/p_{t_\infty} = 128.6$

Figure 2.- Continued.

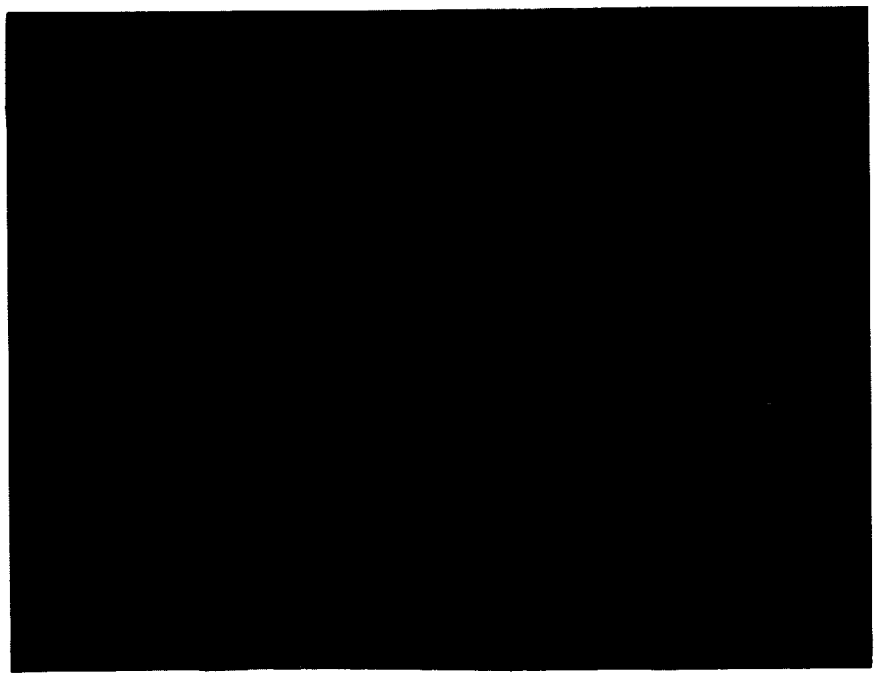

(k) $p_{t_j}/p_{t_\infty} = 142.9$

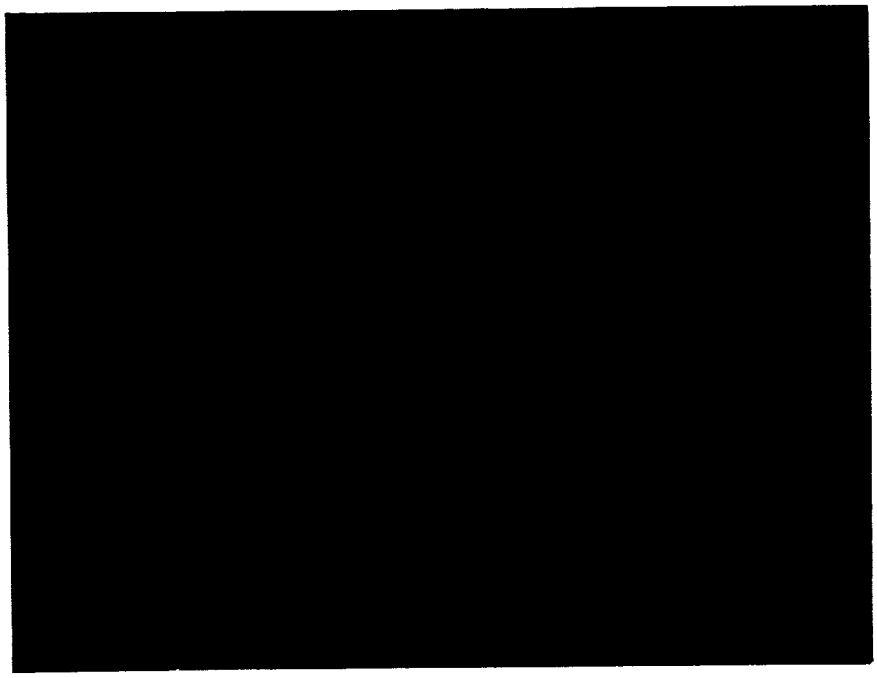

(l) $p_{t_j}/p_{t_\infty} = 157.3$

Figure 2.- Concluded.

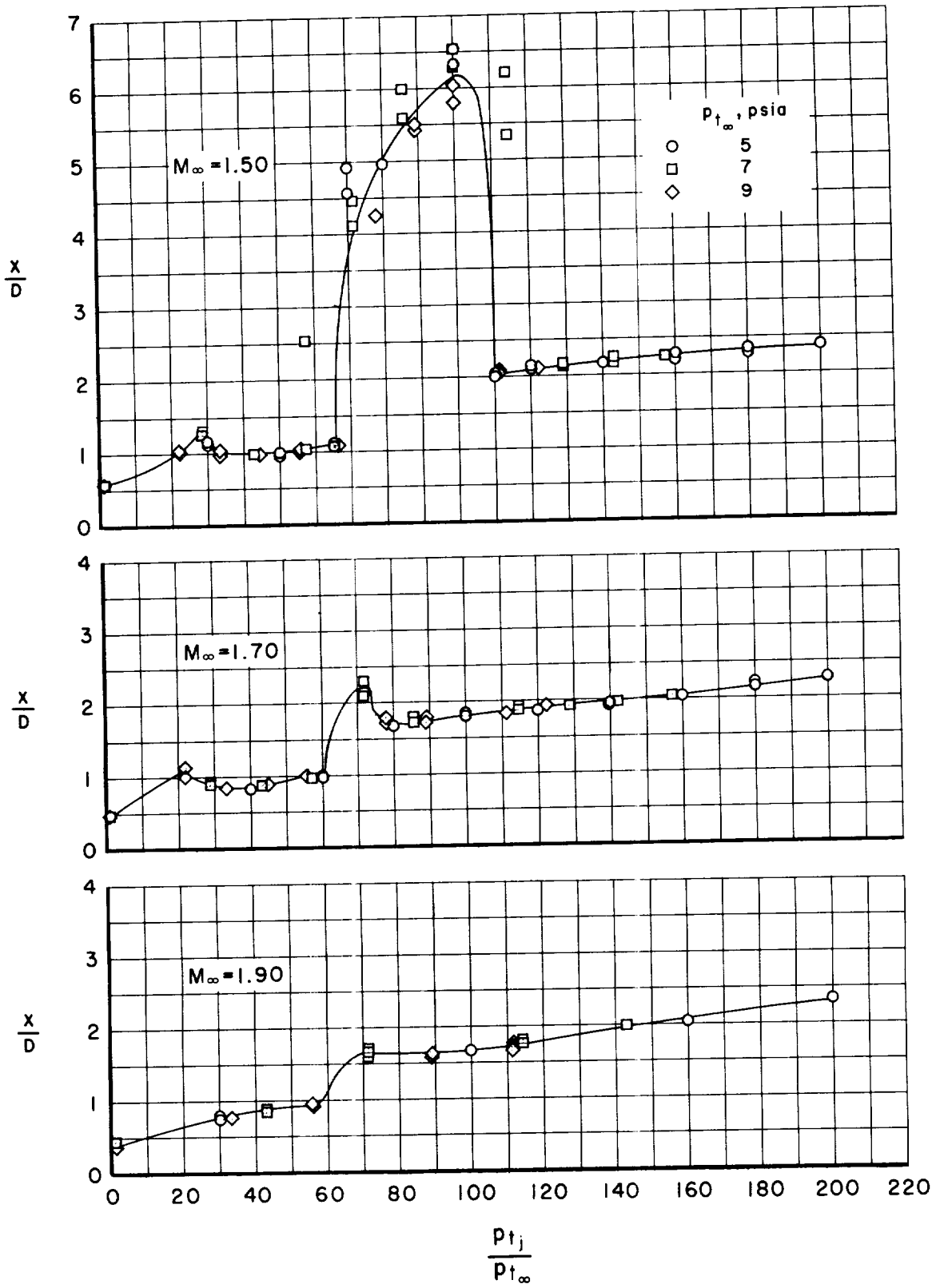

Figure 3.- Effects of jet to free-stream total pressure ratio on bow shock standoff distance; $\alpha = 0^\circ$.

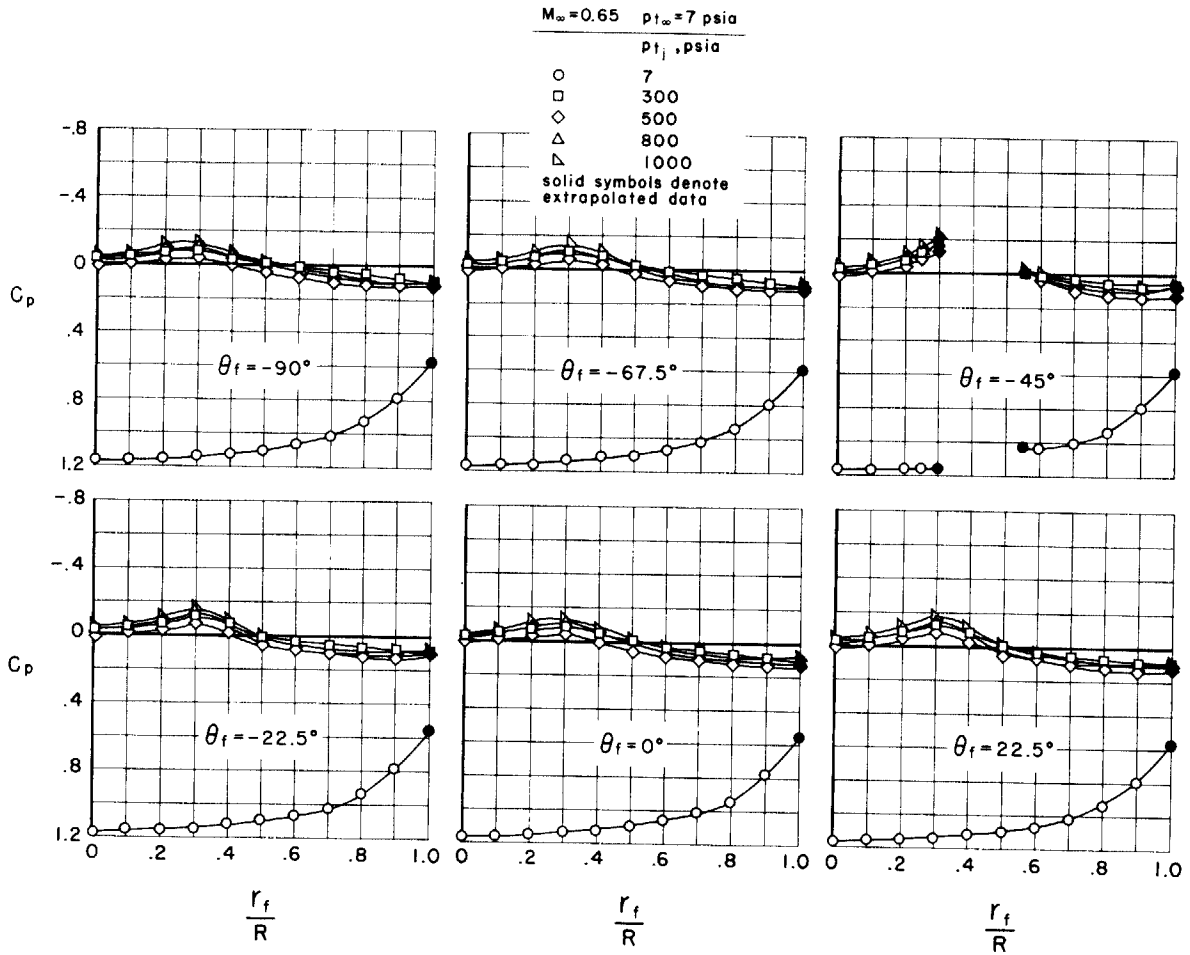

(a) Pressure coefficients on model face.

Figure 4.- Typical effects of the retrojets on the model pressure distributions at subsonic free-stream Mach numbers; $\alpha = 0^\circ$.

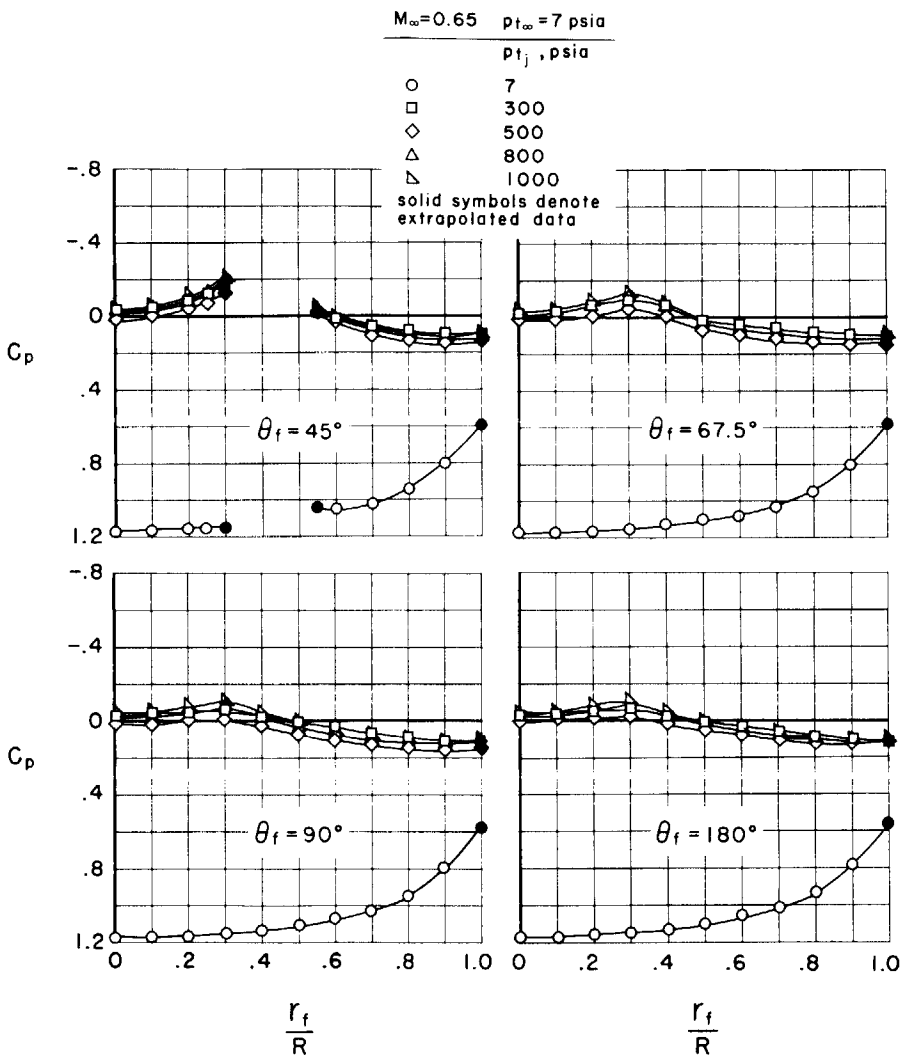

(a) Pressure coefficients on model face - Concluded.

Figure 4.- Continued.

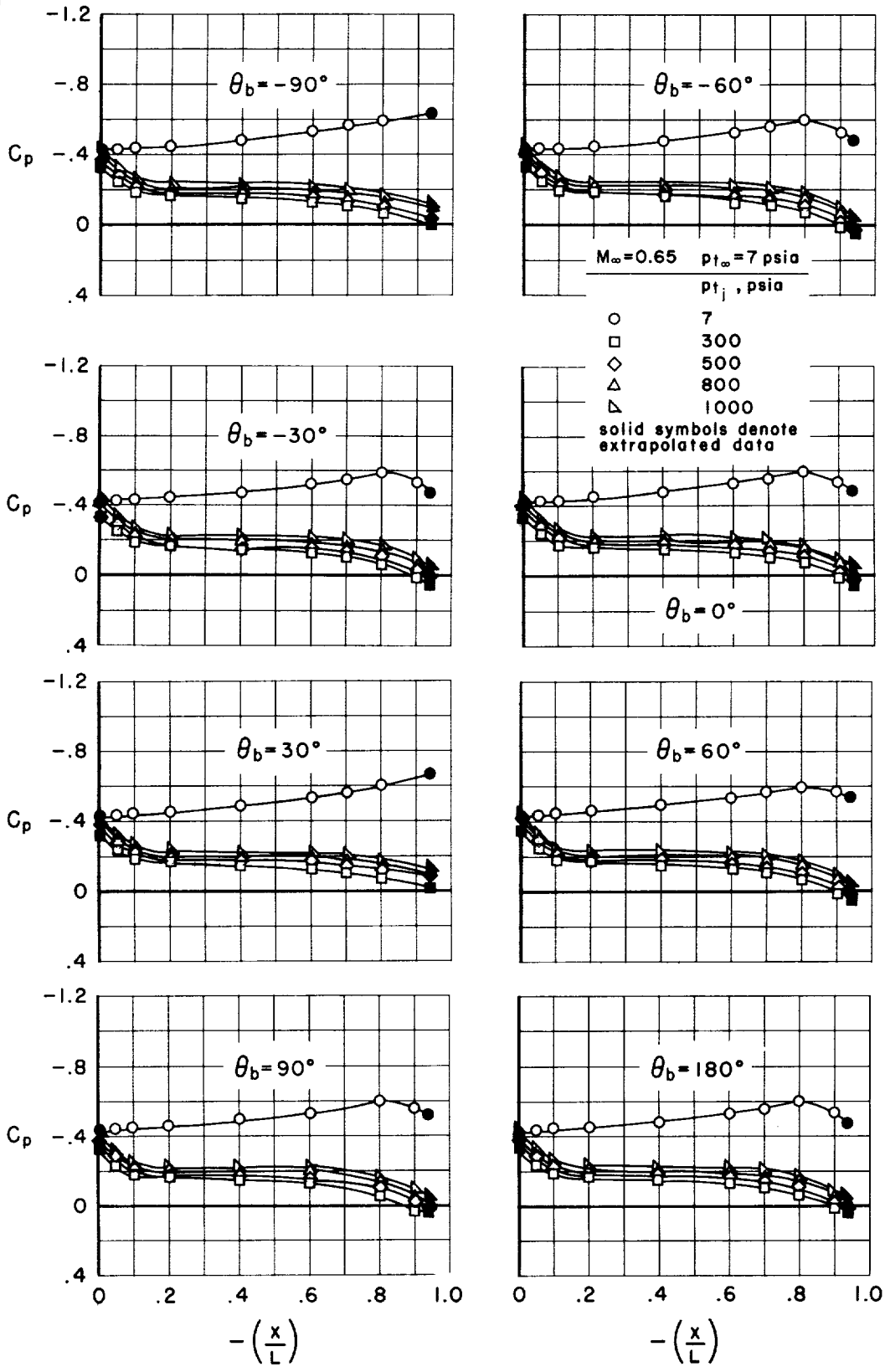

(b) Pressure coefficients on model body.

Figure 4.- Concluded.

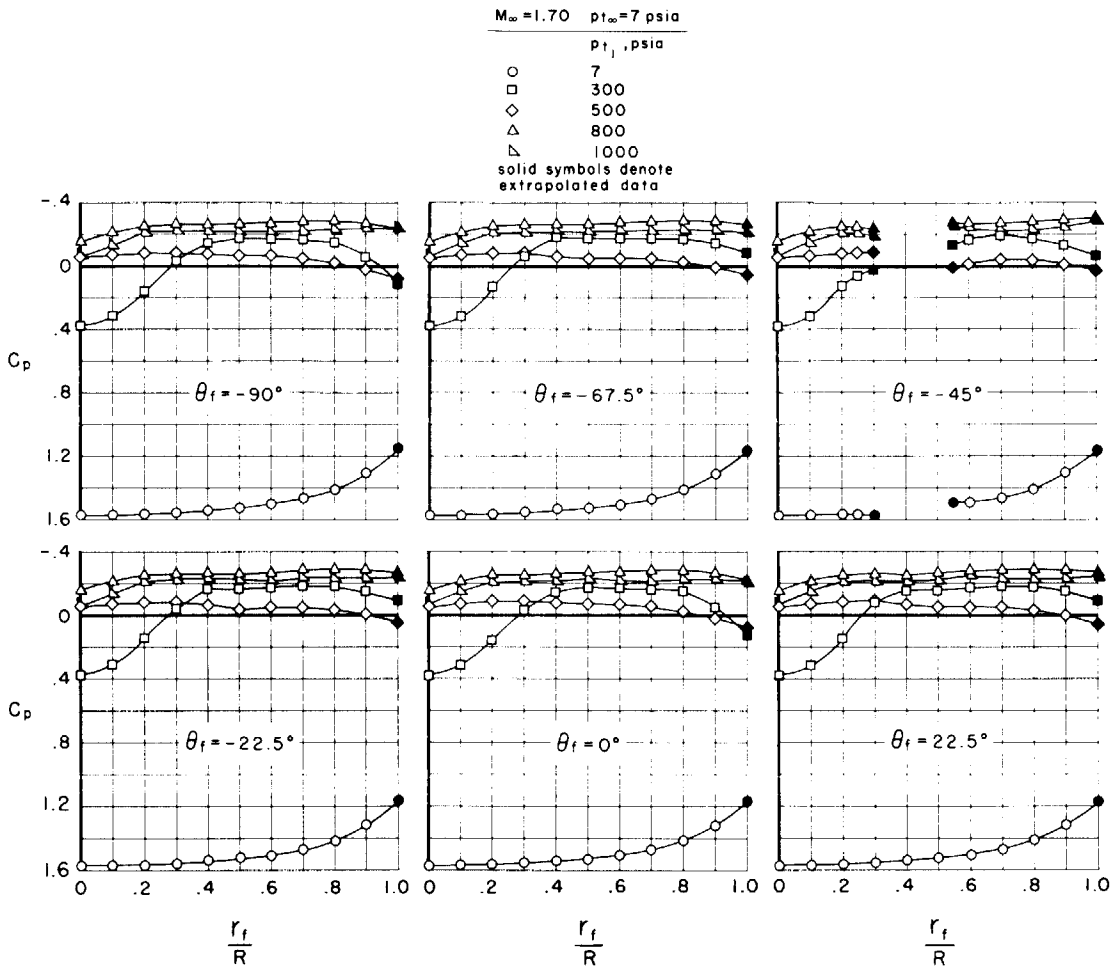

(a) Pressure coefficients on model face.

Figure 5.- Typical effects of the retrojets on the model pressure distributions at supersonic free-stream Mach numbers; $\alpha = 0^\circ$.

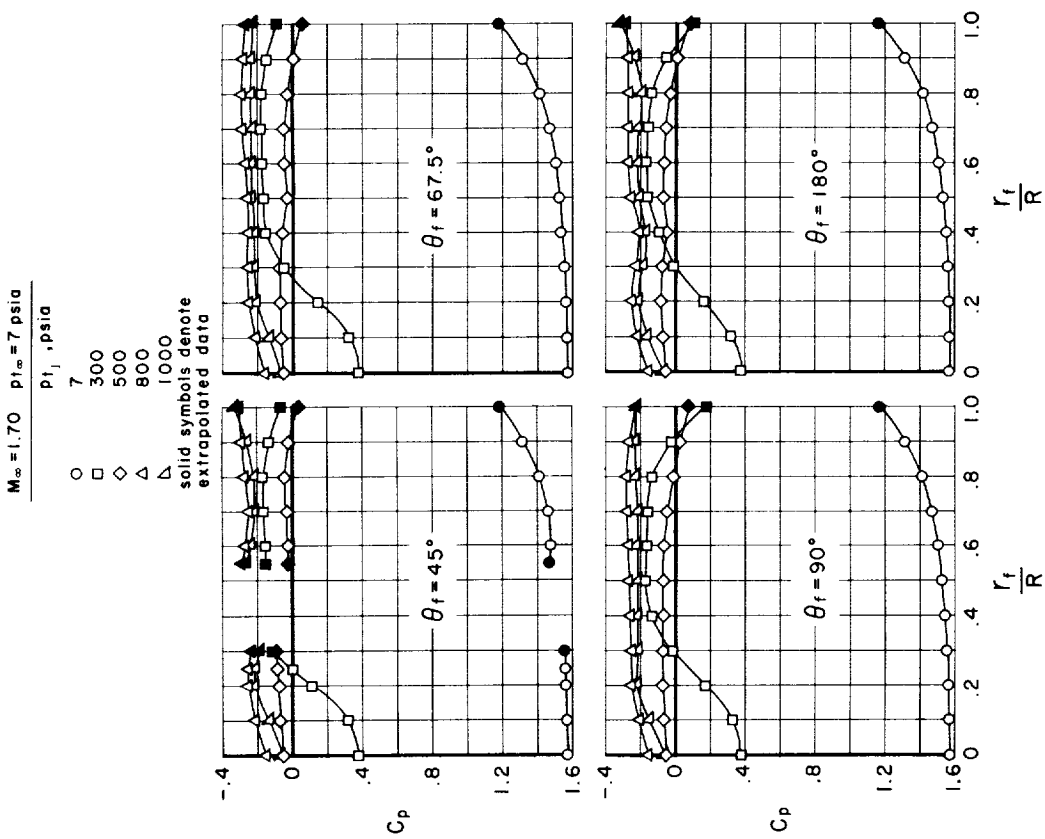

(a) Pressure coefficients on model face - Concluded.

Figure 5.- Continued.

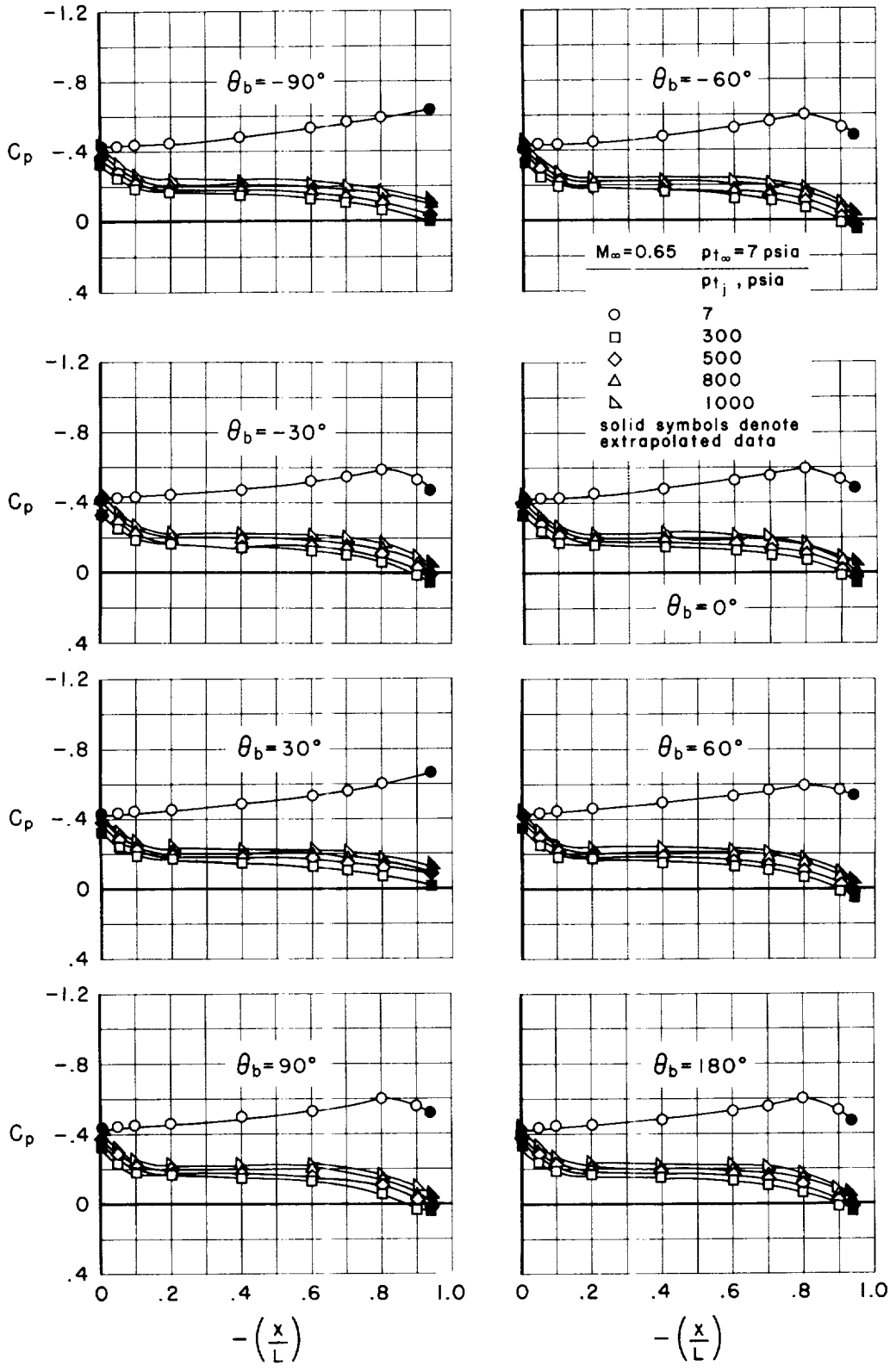

(b) Pressure coefficients on model body.

Figure 5.- Concluded.

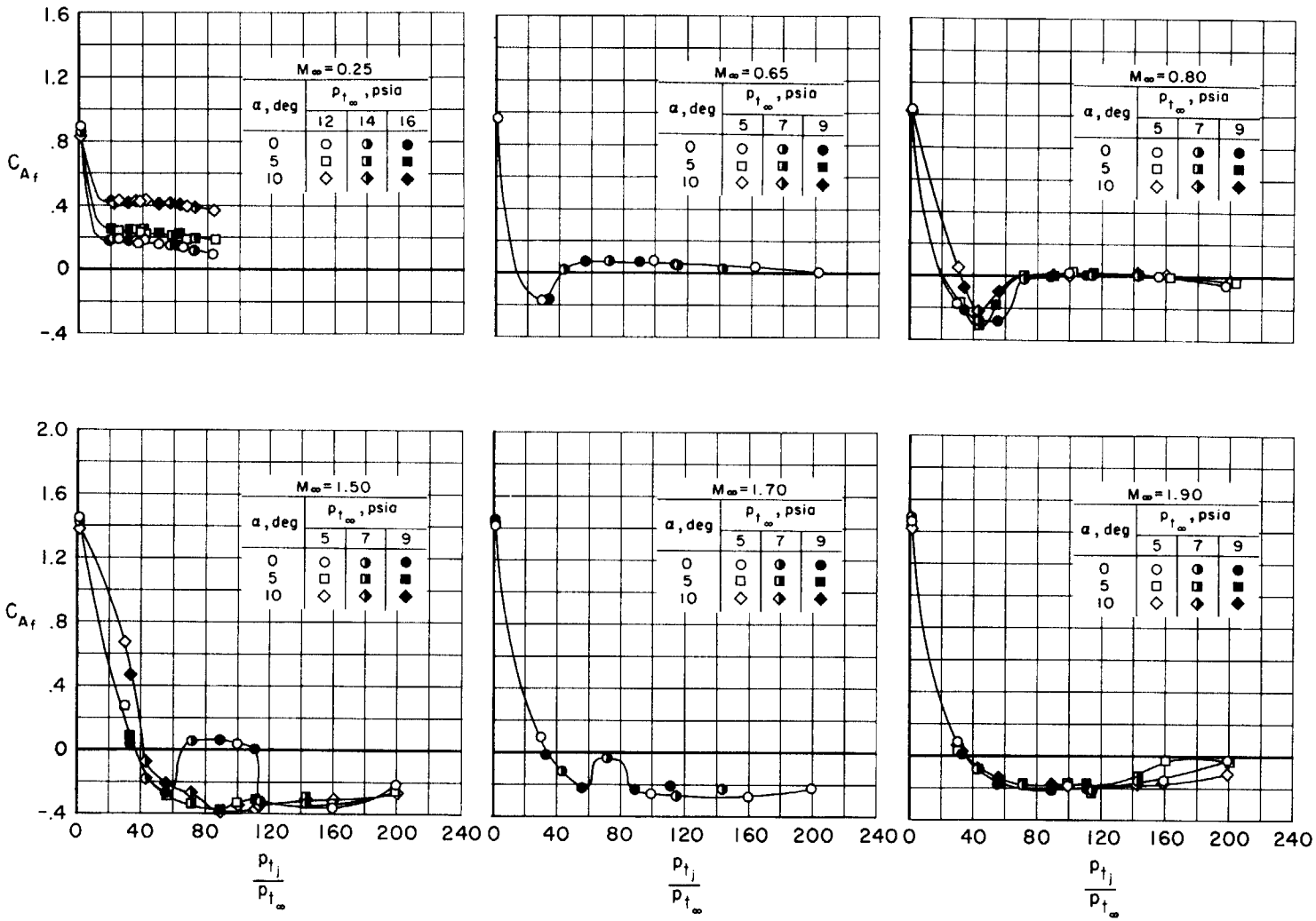

(a) Model face.

Figure 6.- Effects of the retrojets on coefficients of axial force exclusive of retrothrust.

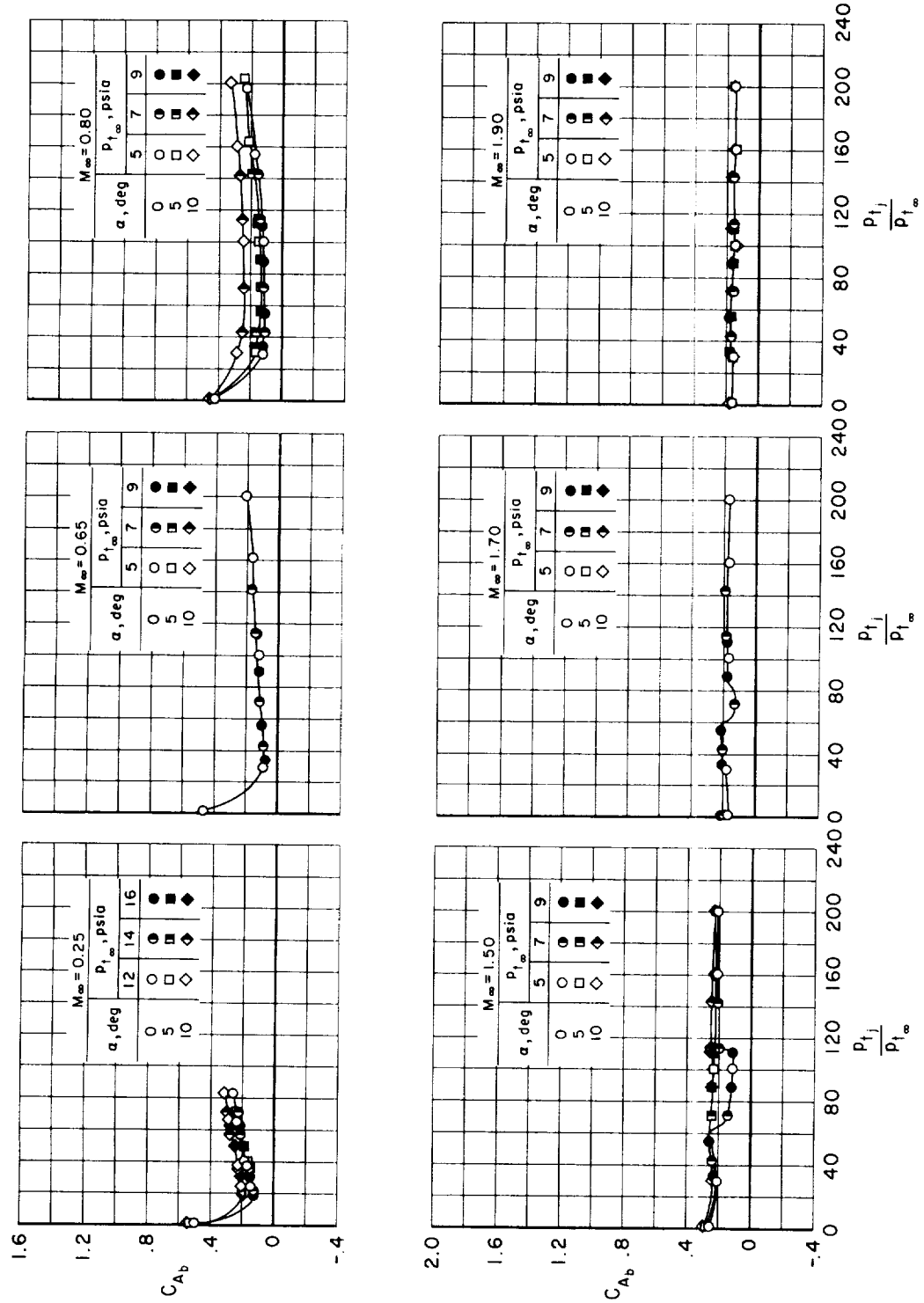

(b) Model body.

Figure 6.- Continued.

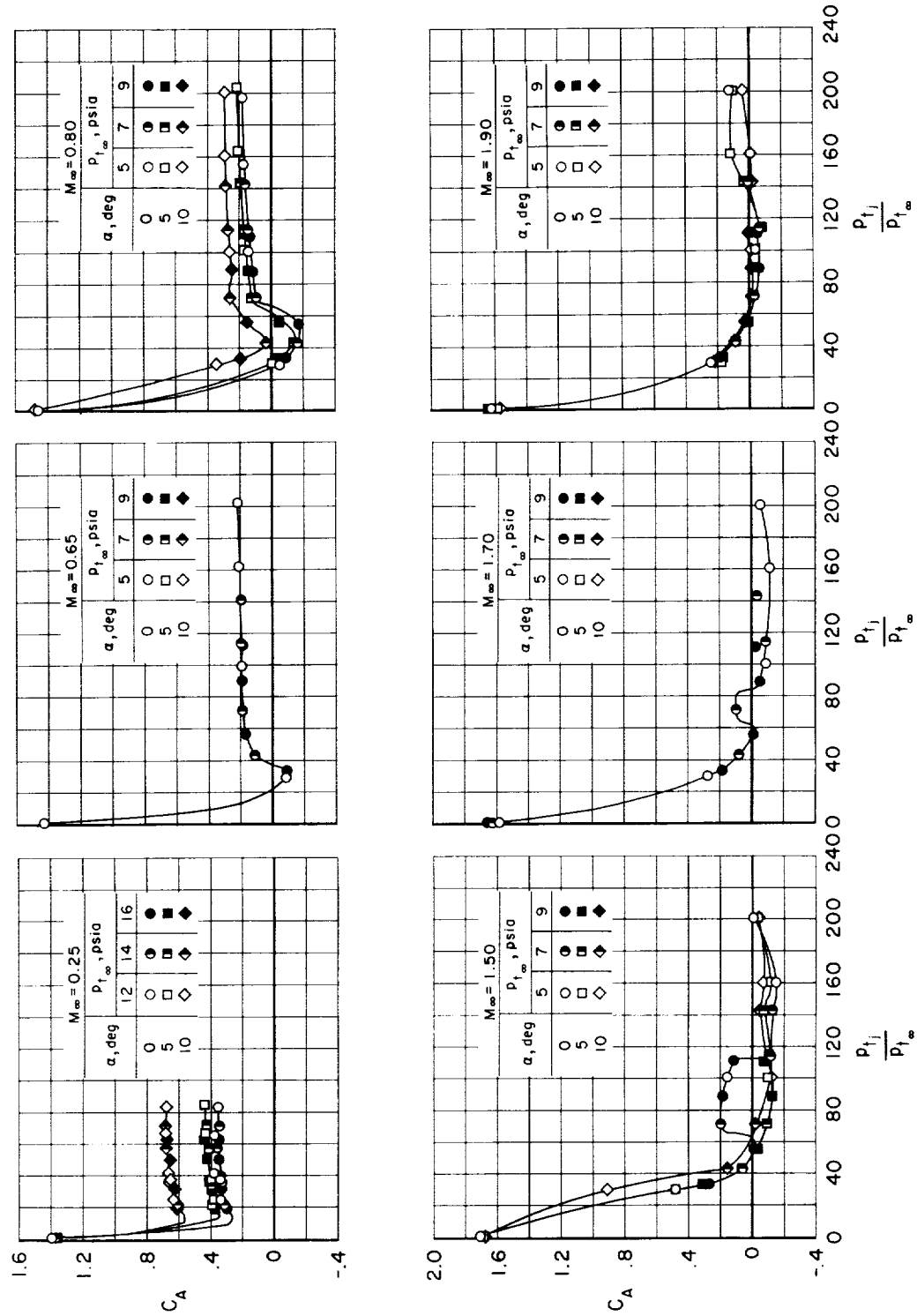

(c) Complete model.

Figure 6.- Concluded.

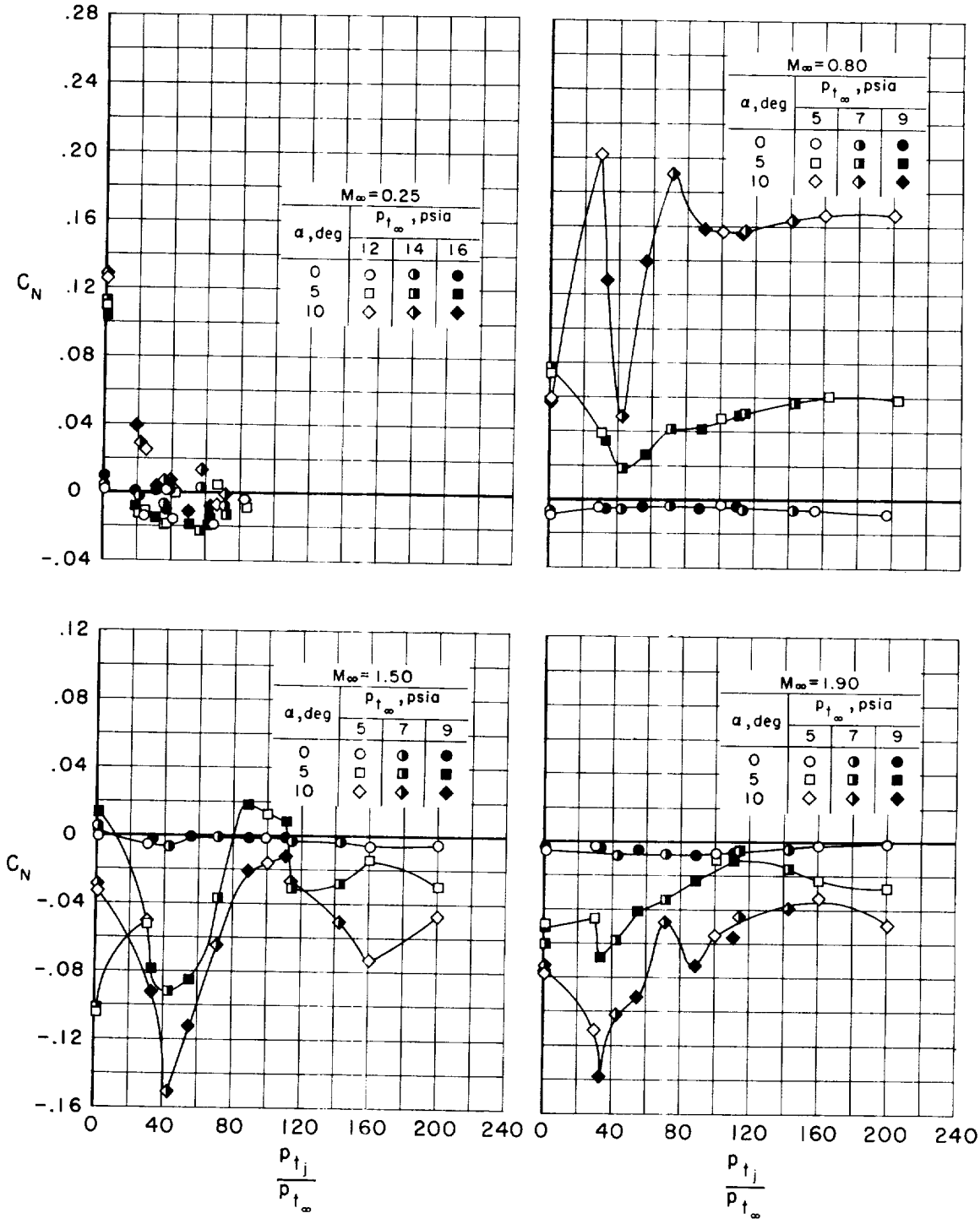

Figure 7.- Effects of the retrojets on coefficients of normal force.

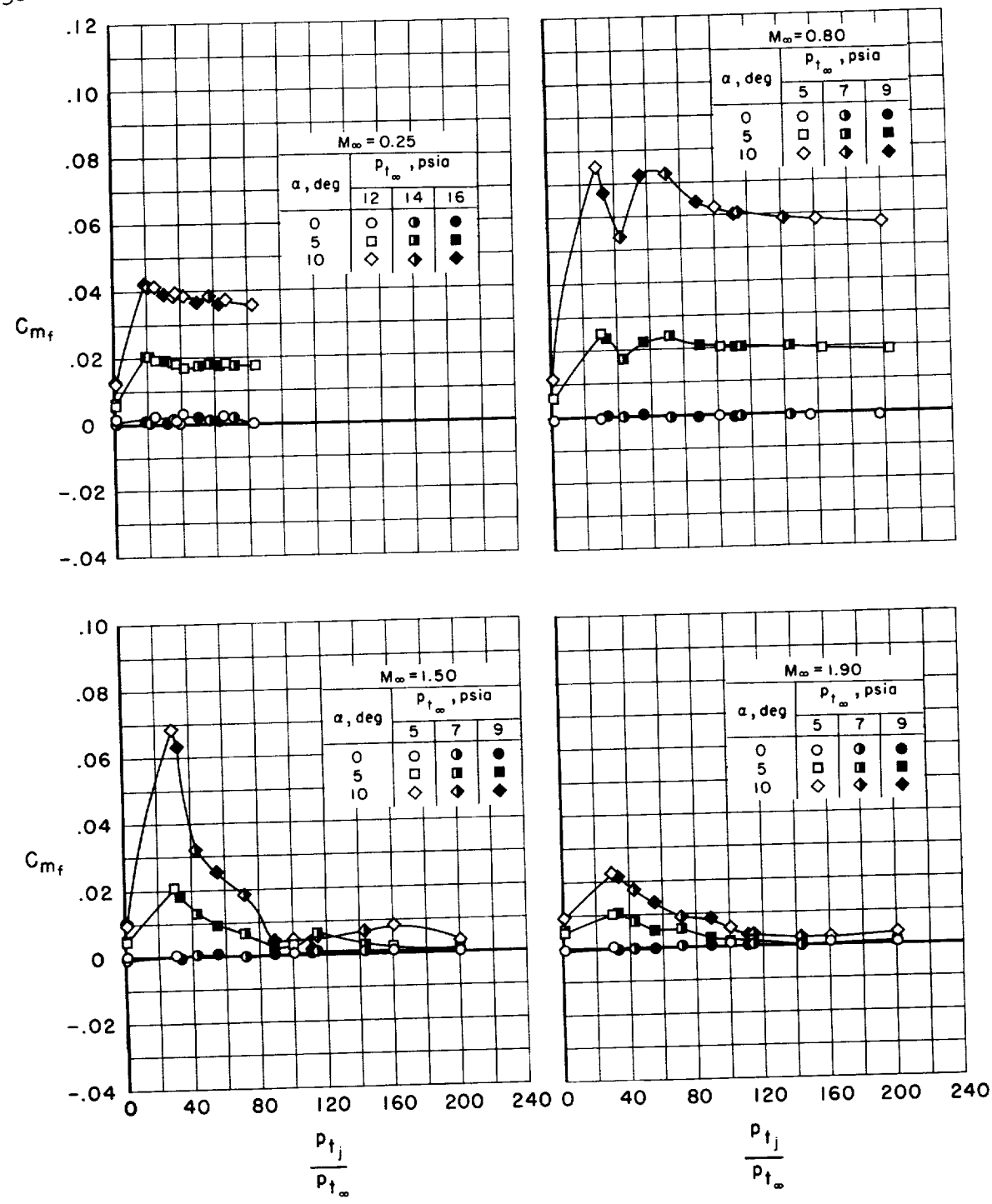

(a) Model face.

Figure 8.- Effects of the retrojets on pitching-moment coefficients.

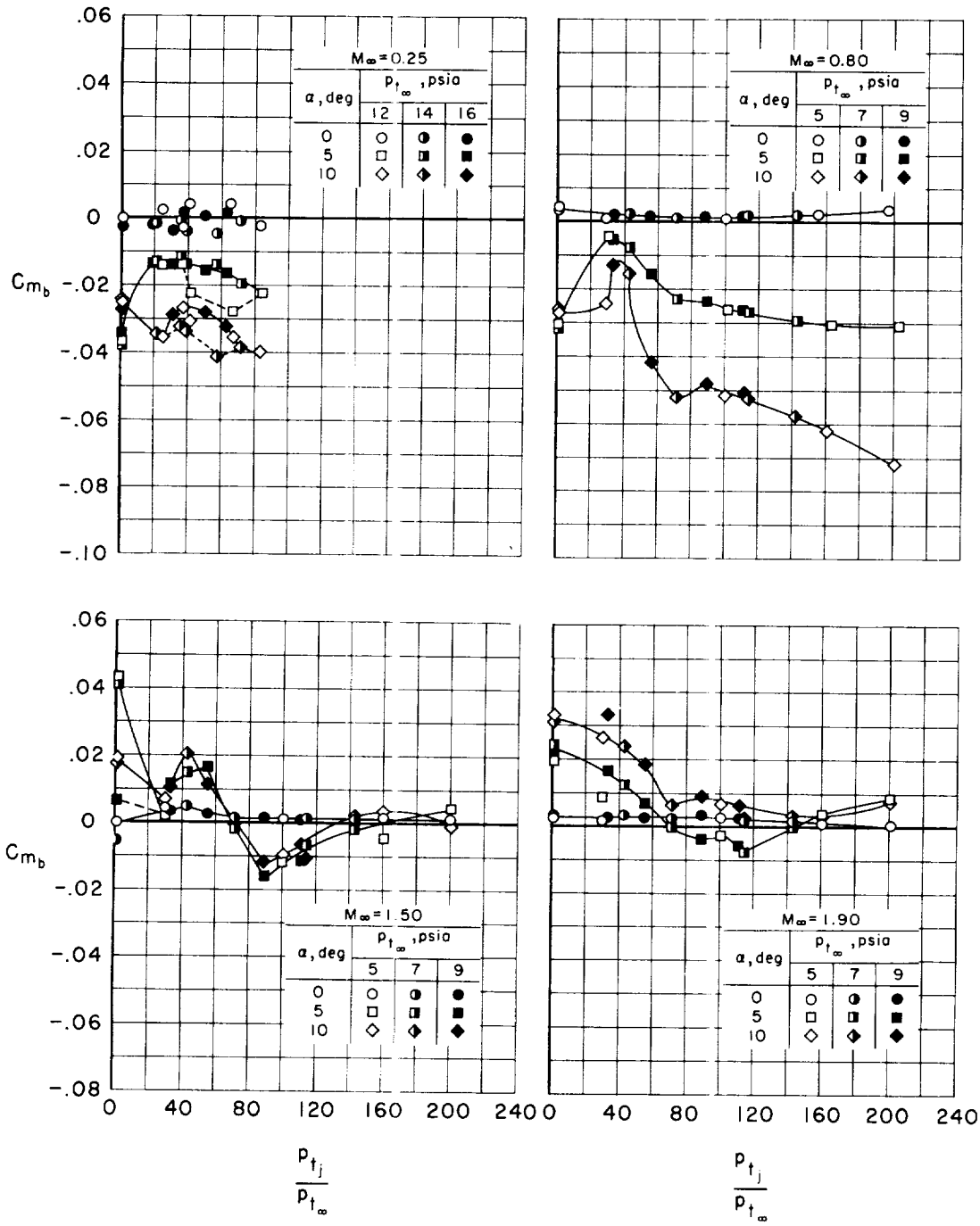

(b) Model body.

Figure 8.- Continued.

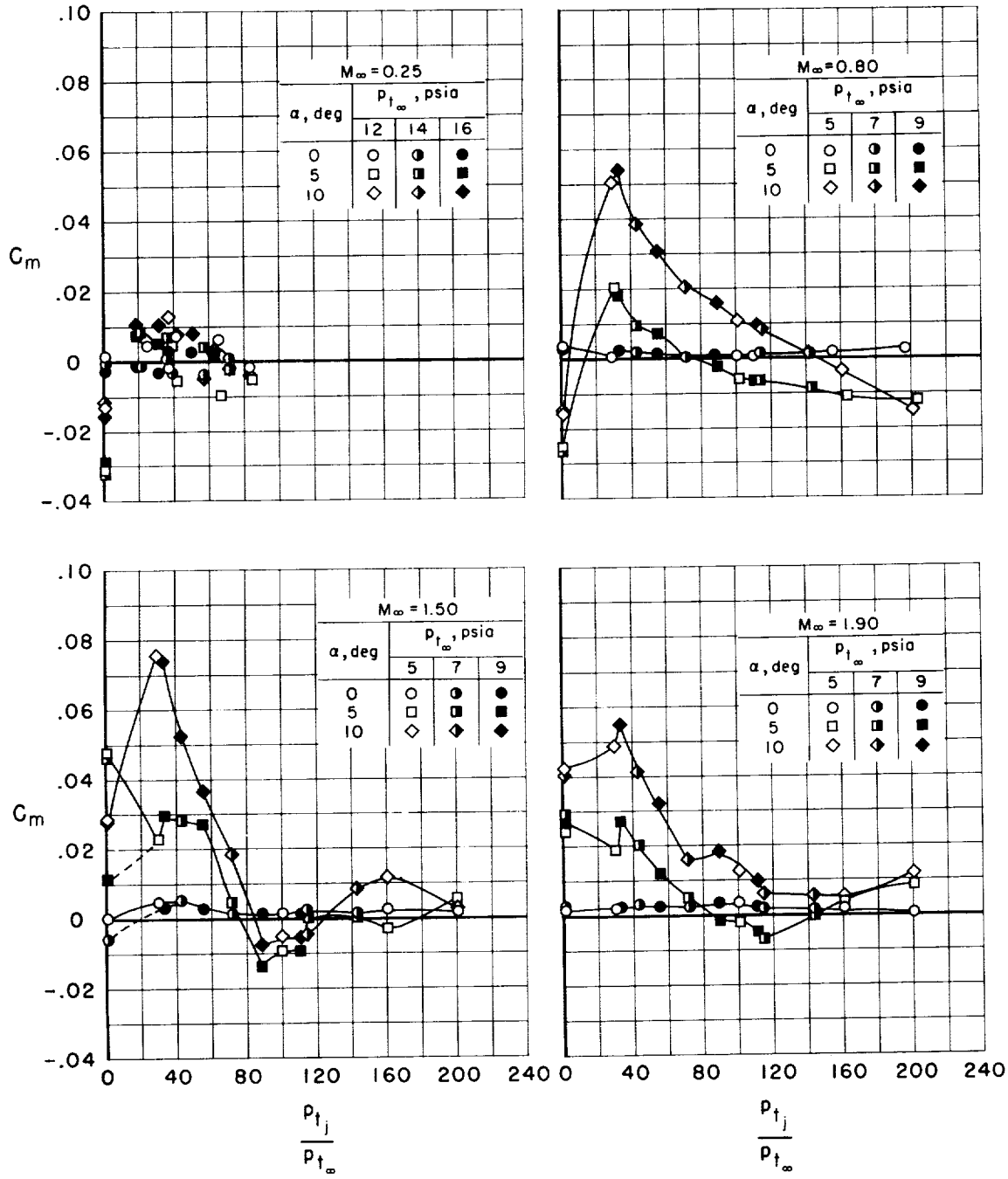

(c) Complete model.

Figure 8.- Concluded.

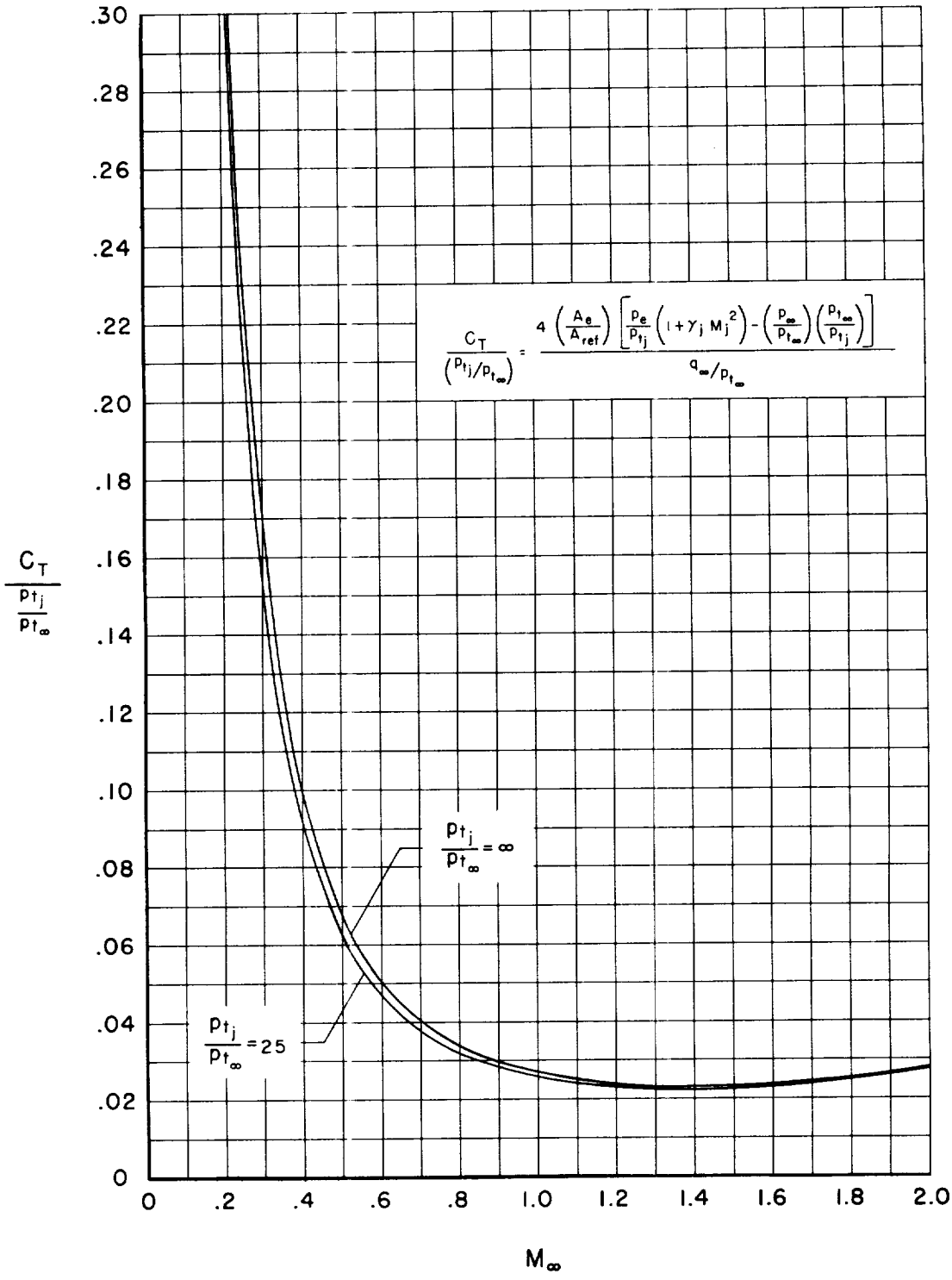

Figure 9.- Dependence of retrothrust coefficient on free-stream Mach number and ratio of jet to free-stream total pressures.

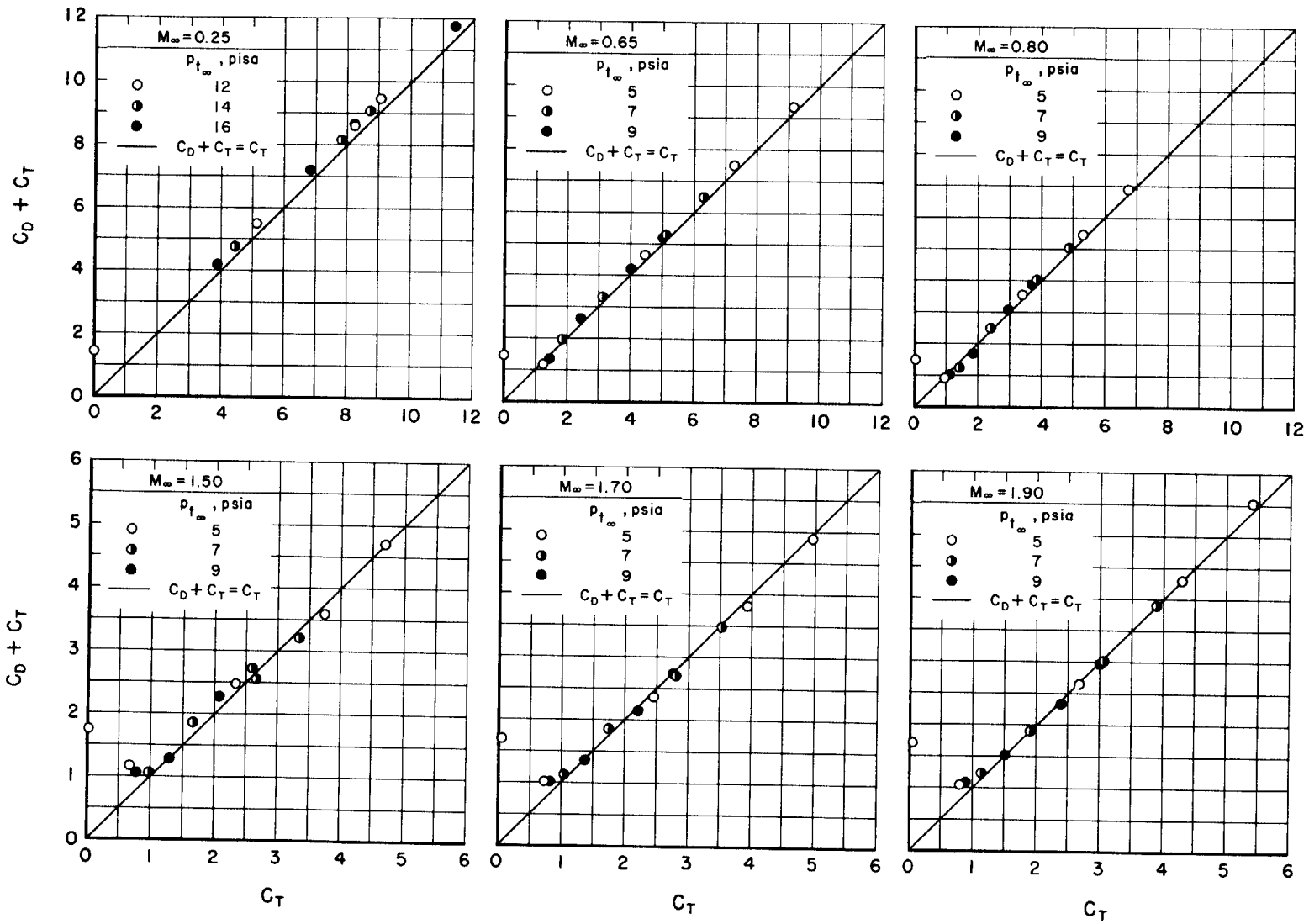

Figure 10.- Relation between total decelerating force coefficient and retrothrust coefficient; $\alpha = 0^\circ$.

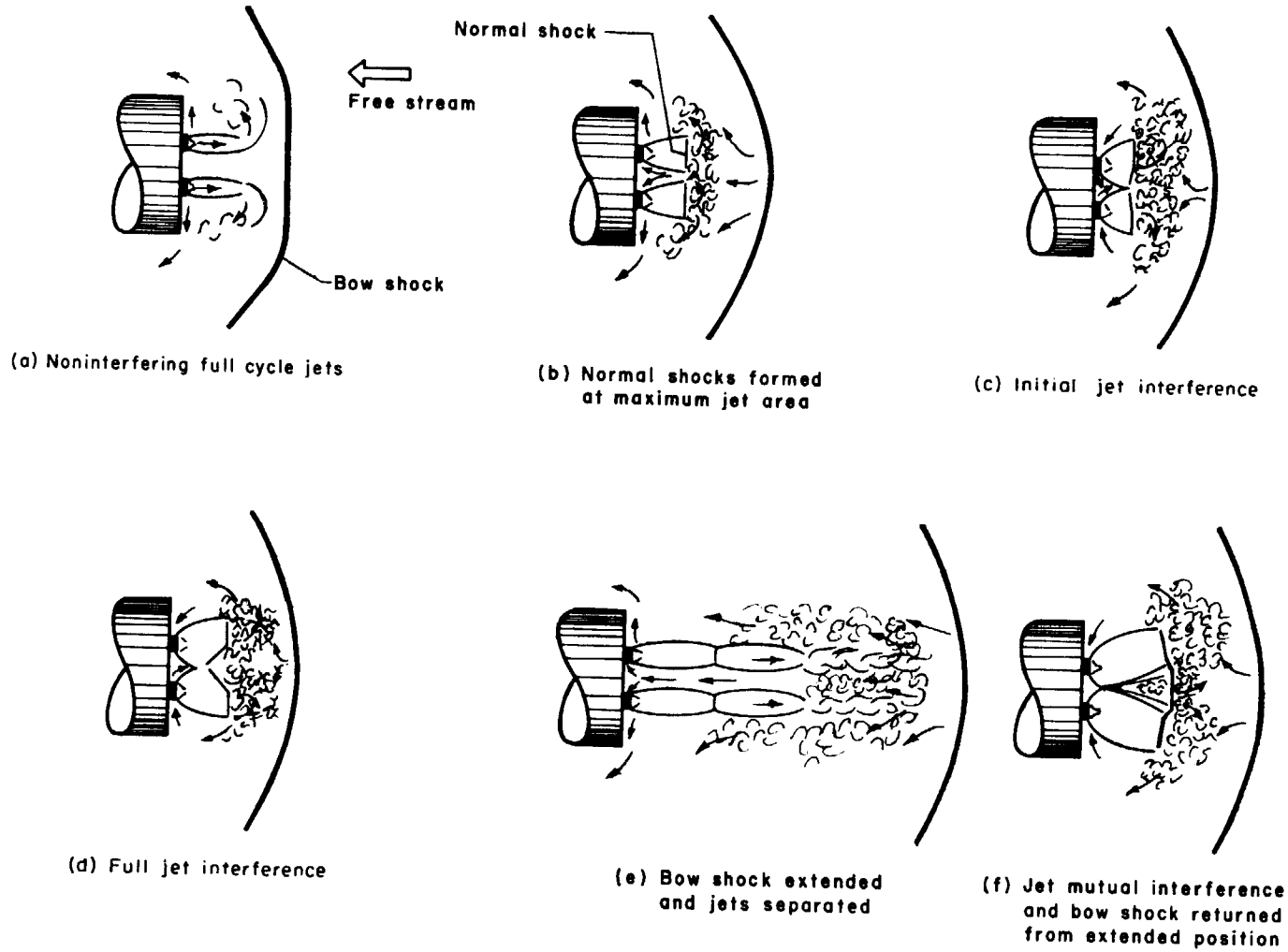

Figure 11.- Schematic representations (not to scale) of types of flows observed between the bow shock and model for progressively increasing ratio of jet to free-stream total pressures; $\alpha = 0^{\circ}$.

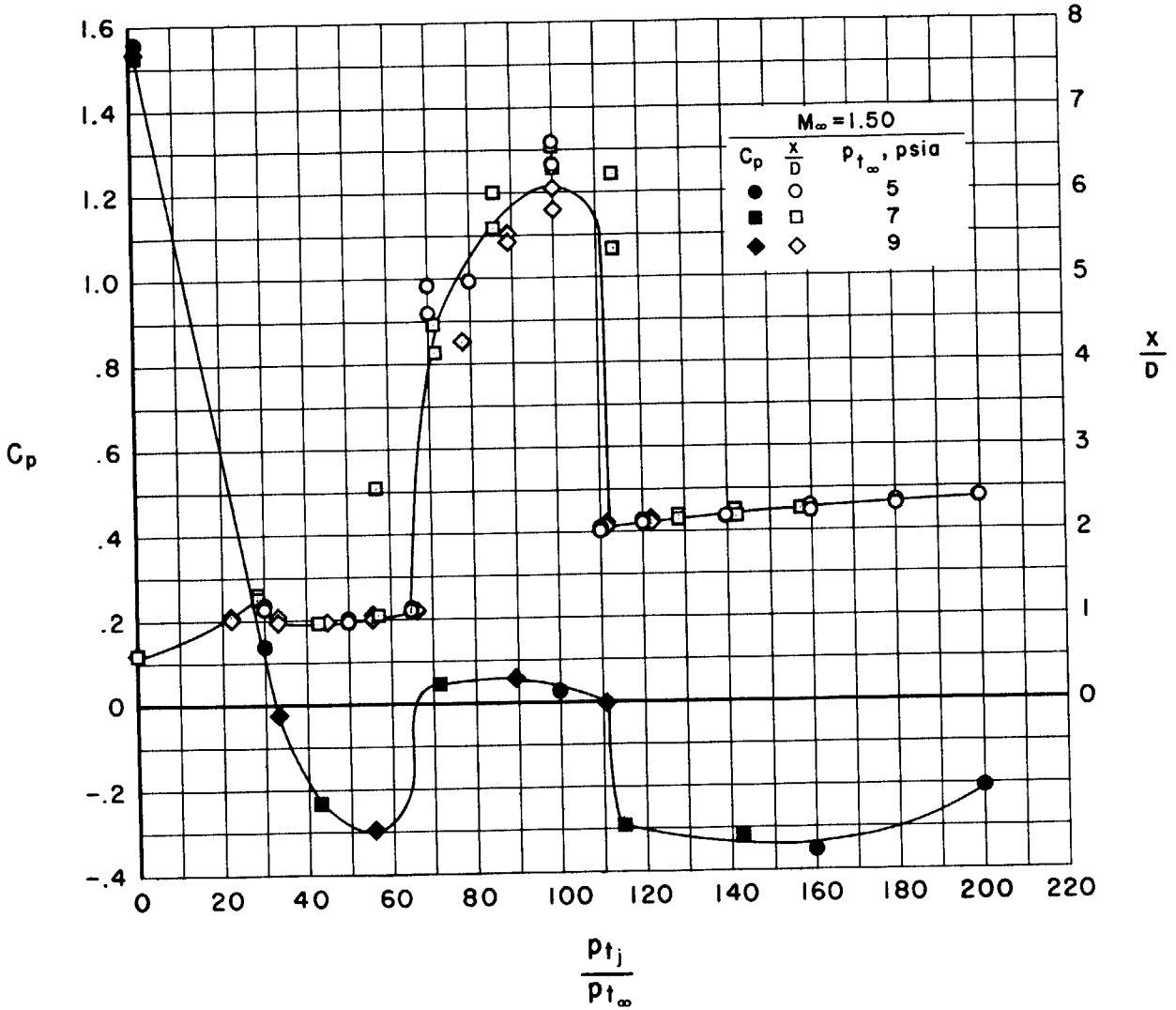

Figure 12.- Correlation of pressure coefficients on model face and bow shock standoff distance; $\alpha = 0^{\circ}$.

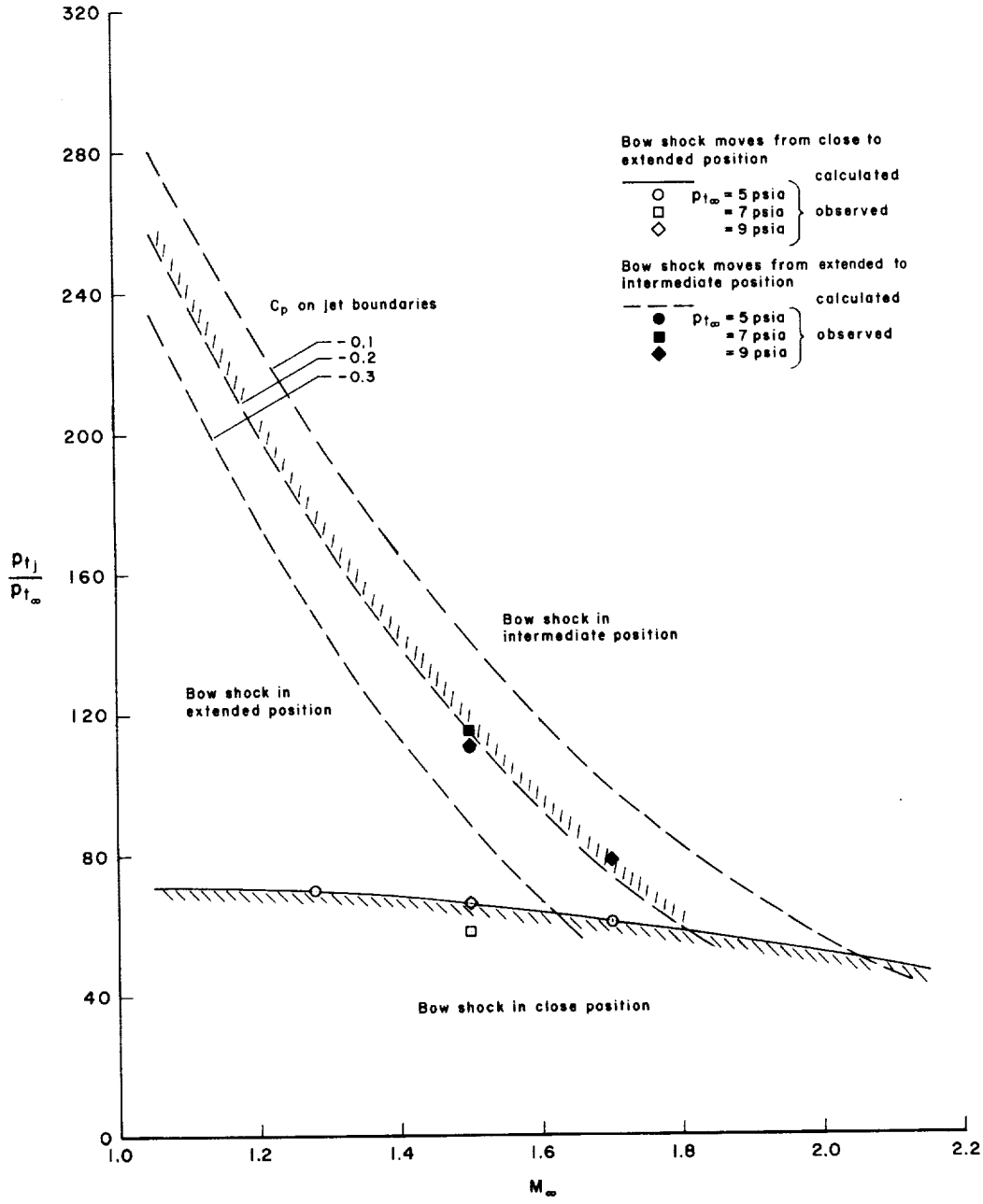

Figure 13.- Comparison of observed and calculated bow shock behavior; $\alpha = 0^\circ$.